DESIGN AND CHARACTERIZATION OF ZEOLITE SUPPORTED COBALT CARBONYL CATALYSTS

by

Melissa Clare Connaway

Dissertation submitted to the Faculty of the
Virginia Polytechnic Institute and State University
in partial fulfillment of the requirements for the degree of

DOCTOR OF PHILOSOPHY

in

Chemistry

APPROVED:

B. E. Hanson, Chairman

J. G. Dillard

J. P. Wightman

J. M. Tanko

M. E. Davis

July, 1987

Blacksburg, Virginia

DESIGN AND CHARACTERIZATION OF ZEOLITE SUPPORTED COBALT CARBONYL CATALYSTS

by

Melissa Clare Connaway

Committee Chairman: Brian E. Hanson
Chemistry

(ABSTRACT)

Transition metal compounds such as $Co_2(CO)_8$ have often been used to catalyze various organic reactions. Severe difficulties may be encountered when attempts are made to recover and separate the soluble catalysts. A heterogeneous system consisting of $Co_2(CO)_8$ impregnated on zeolites with faujasitic structure has been designed and investigated using a variety of techniques. In situ FTIR spectroscopy and carbon monoxide evolution were used to identify the major products generated, namely $Co_4(CO)_{12}$ and $Co(CO)_4^-$. Disproportionation may be induced thus forming $Co(CO)_4^-$ and an associated cation from the supported subcarbonyls by addition of various ligands such as methanol. The location of the supported cobalt carbonyls is determined by their reactivity toward various phosphines with various kinetic diameters.

The materials prepared in this manner were found to be active in catalyzing the methanol carbonylation reaction and following thermolysis were also found to be active Fischer-Tropsch catalysts. Major products observed in the carbonylation of methanol were methyl acetate and an

acetaldehyde dimethyl acetal. The supported cobalt catalyst displays greater activity than $Co_2(CO)_8$ in solution for the carbonylation reaction when conducted under similar conditions. In the Fischer-Tropsch process, selectivity is seen for the production of linear, short-chain hydrocarbons.

ACKNOWLEDGEMENTS

I am grateful to my research adviser, Dr. Brian E. Hanson, for his guidance, patience and encouragement during the course of this project. I would also like to thank Dr. Mark Davis for his general knowledge and contribution to this work.

Funding from the National Science Foundation and a tuition waiver from the chemistry department of VPI & SU are gratefully acknowledged.

A very special appreciation must be awarded to my parents for their love, faith and support.

TABLE OF CONTENTS

LIST OF FIGURES

LIST OF TABLES

CHAPTER I.

INTRODUCTION

1.1 INTENT OF THESIS

Homogeneous transition metal catalysts find utility in many organic reactions such as hydroformylation of alkenes[1,2] and carbonylation of alcohols.[3] These materials are often difficult to recover and recycle and may deteriorate under the severe conditions used to conduct the catalytic reaction. Immobilzation of such homogeneous catalysts on a solid, insoluble support is one technique which may be used to alleviate such problems. Use of a supported catalyst may aid in preventing molecular aggregation and stabilize the supported complex thus inhibiting deactivation. The aim is to design a supported catalyst which retains the typically high activity and selectivity of the homogeneous counterpart. One system which may be utilized toward developing this goal is offered by zeolite encapsulated catalyst molecules. A catalyst synthesized within a zeolite cage such that it is entrapped due to its physical size would be expected to exhibit advantageous properties such as dispersity with concurrent immobilization while retaining the activity and selectivity of the homogeneous parent catalyst. The zeolite support may also increase the intrinsic selectivity of the catalyst by way of its molecular sieving effect. The size and shape of reactant molecules is restricted by their ability to diffuse through the pores to encounter the active sites and likewise, species formed within the zeolite must be able to diffuse out of the channels to be observed as products. The dimensions of the zeolite pores may also impose

unusual coordination configurations or coordinative unsaturation upon the encaged catalytic complex such that unique reactivities and selectivities result.[4]

The intent of the research discussed herein is concerned with designing heterogeneous catalysts synthesized from cobalt carbonyl compounds on a zeolite support. The catalysts contain cobalt in a low oxidation state necessary for activating carbon monoxide and hydrogen for various chemical reactions. The identification and characterization of the species present on the zeolite is also given much attention. Specifically $Co_2(CO)_8$ and derivatives of this complex are adsorbed onto synthetic zeolites with faujasite structure. Techniques used to elucidate the nature of the supported species include infrared spectroscopy, gas evolution, gas adsorption, x-ray powder diffraction, x-ray photoelectron spectroscopy and scanning electron microscopy. The activity and selectivity of these materials when applied to the catalysis of various chemical reactions including methanol carbonylation and Fischer-Tropsch synthesis of hydrocarbons is also a major focus of this research

1.2 ZEOLITES[5,6]

Zeolites are crystalline aluminosilicates consisting of SiO_4 and AlO_4 tetrahedra. The tetrahedra are linked via oxygen bridges thus forming various polyhedral structures. Zeolite classification is based on the polyhedra found as repeating units, the polyhedral linkages and the silicon to aluminum ratio ($Si/Al \geq 1$). The crystalline nature of zeolites and the manner in which the polyhedra are linked results in the formation of channels and sometimes cages at the junction of two or more

channels within the framework of the lattice. The external surface area of the crystallites accounts for only a small fraction of the total surface area of the particles due to the extensive channel network within the structure. The general empirical formula of zeolites is given by $M_{x/n}[(AlO_2)_x(SiO_2)_y]\cdot wH_2O$ where M is a cation of valence n. The negative charge on the AlO_4 tetrahedra is compensated for by the inclusion of cations within the structure thus maintaining electroneutrality. The cation exchange capability associated with zeolites results from the included ions. The zeolites containing a significant quanitity of aluminum have a great affinity for water. Dehydration of the crystals is reversible unless conducted at very high temperature where collapse of the structure will result in irreversible changes in the system.

Two synthetic analogs of the naturally-occurring mineral faujasite are zeolites X and Y. The structure of these zeolites is given in Figure 1.1. The aluminum and silicon tetrahedra join to form truncated octehedra, referred to as sodalite cages, which are the basic repeating polyhedral units. The sodalite cages join to four other sodalite units via six membered faces thus forming hexagonal prismatic bridges between the cages. This results in a tehahedra of sodalite units. Two types of cages exist within the faujasite structure. The void within a sodalite octehedra is referred to as a β-cage which has a diameter of 6.6 Å and entrance to the void is through a six-membered ring with an aperture of 2.2 Å. The α-cage or supercage is derived by the bridging of 10 sodalite units and has a diameter of 13Å. Access occurs via a 12-membered ring with a crystallographic diameter of 7.4Å. Molecules

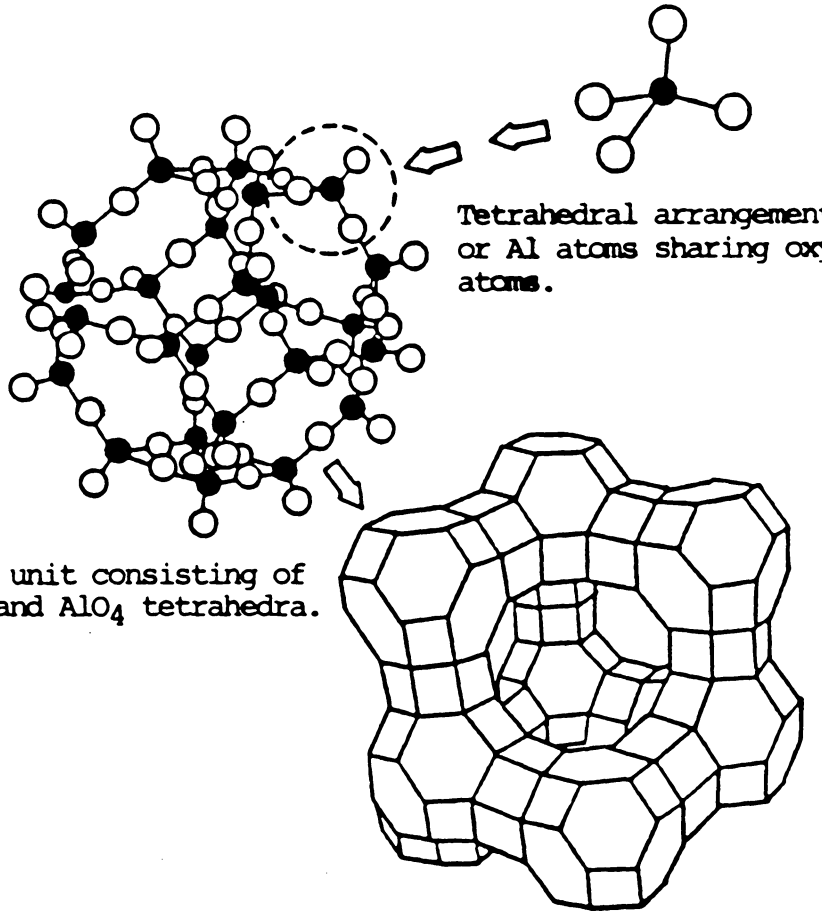

Figure 1.1. Framework structure of zeolites X and Y. (Adapted from ref.6.)

having dimensions greater than 7.4Å have been observed to diffuse through the pores and a quantity referred to as the kinetic pore diameter is a preferable method of measuring the channel proportions. The kinetic pore diameter is obtained by quantifying the adsorption of molecules having various dimensions by zeolites. The α-cage is observed to have a pore opening of 8.4Å by this technique.

1.3 ADDITION OF TRANSITION METALS TO ZEOLITES

There are various methods available for the addition of transition metals to zeolites. Cationic complexes of transition metal salts may be introduced to zeolites through techniques such as cation exchange or incipient wetness. Cation exchange involves the substitution of transition metal ions for the occluded ions. In the incipient wetness method, aqueous solutions of transition metal salt solutions are introduced to the zeolite in a manner such that pore filling of the voids by the metal salt solutions will result. Techniques which incorporate the addition of transition metals in a high oxidation state must be followed by reduction of the metal generally by heating in a reducing atmosphere such as hydrogen or in the presence of alkali metal to form a catalyst capable of activating CO and H_2 for various chemical reactions.

To avoid the necessity of reducing the transition metal, addition of the metal in a zero or low oxidation state through the introduction of organometallic complexes may be employed. Techniques used to load the support with organometallic complexes include dry-mixing, sublimation and adsorption from solution.[7] The organometallic compound

may be intimately mixed with the support and then activated by heating. Molecular interaction between the complex and support will occur only during the activation process. For dry-mixing to be effective, it is essential that the organometallic becomes volatile before it decomposes when thermal treatment occurs. The exact metal loading and uniformity is difficult to control since much of the complex may be lost through evaporation during activation.

Organometallic complexes may be introduced to zeolites via sublimation. Metal loading and homogeneity are troublesome to regulate. It has been observed that zeolites will extract organometallic materials such as metal carbonyls from non-aqueous solutions in a spontaneous fashion. Use of this technique allows impregnation of the zeolite support with transition metals in a low oxidation state in a manner which is readily controllable, uniform and reproducible. It is for these reasons that adsorption of $Co_2(CO)_8$ from pentane has been selected as the method of choice for impregnation of zeolite supports. $Co_2(CO)_8$ exists in solution as an equilibrium mixture of two isomers.[91,92] A bridged structure with C_{2v} symmetry corresponds to the structure observed in the solid state while its isomer with D_{3d} symmetry contains no bridging carbonyls and is seen only in solution. The strucures [93] of both forms are given in Figure 1.2.

1.4 METHANOL CARBONYLATION[8]

For more than 100 years, acetic acid has been produced in relatively large quantities. Originally it was produced via fermentation. The hydrolysis of acetylene to acetaldehyde catalyzed by

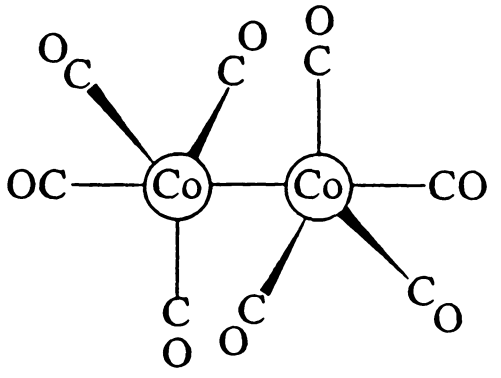

$Co_2(CO)_8$ in solution

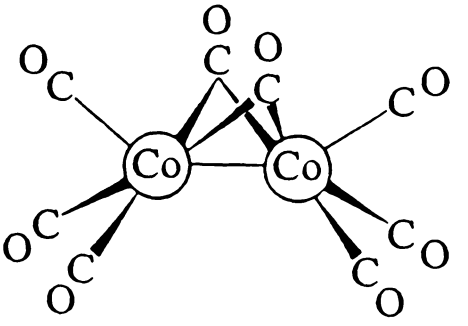

$Co_2(CO)_8$ in the solid state

Figure 1.2. Structure of $Co_2(CO)_8$. (Adapted from ref. 93)

mercuric ion was the basis of the first major synthetic process used to produce acetic acid. This process was the dominant route for acetic acid manufacture until two new processes were developed around 1955-1960. A short-chain paraffin oxidation catalyzed by manganese or cobalt salts was introduced by Celanese in the United States and British Petroleum in Europe. Wacker Chemie developed a palladium-copper-catalyzed oxidative hydration of ethylene to acetaldehyde.

Shortly after this time the methanol carbonylation process was developed using a soluble catalyst. Methanol carbonylation is the addition of carbon monoxide to methanol to yield acetic acid and other oxygenated products such as methyl acetate. In 1965, BASF described a high-pressure process for the carbonylation of methanol to acetic acid using an iodide-promoted cobalt catalyst[9,10] and in 1968, Monsanto Company announced the discovery of a low-pressure carbonylation of methanol using an iodide promoted rhodium or iridium catalyst.[11] Monsanto commercialized this process in 1970 using the rhodium-based system.

The cobalt and rhodium processes demonstrate several marked differences in their reactivity. Table 1.1 gives a comparison of the cobalt and rhodium based systems.[8,12] The low reactivity of the cobalt system requires high reaction temperatures and very high partial pressures of carbon monoxide are required to stabilize the cobalt carbonyl.[13] Also, the rhodium system is insensitive to hydrogen while the cobalt system produces increased amounts of hydrogenated side products with increased hydrogen partial pressure.

TABLE 1.1.

COMPARISON OF COBALT AND RHODIUM CATALYZED METHANOL CARBONYLATION REACTIONS (Adapted from ref.8)

	Cobalt process	Rhodium process
Metal concentration	$\sim 10^{-1}\,M$	$\sim 10^{-3}\,M$
Reaction temperature	~ 230°C	~ 180°C
Reaction pressure	500–700 atm	30–40 atm
Selectivity (on methanol)	90%	> 99%
Hydrogen effect	CH_4, CH_3CHO, C_2H_5OH formed as by-products	No effect

Spectroscopic investigations have indicated that the carbonylation of rhodium(III) halides in alcoholic[14] and aqueous media[15] gives the dicarbonyldihalorhodate(I) anion according to reaction 1.1.

$$RhX_3 + 3CO + H_2O \rightarrow [Rh(CO)_2X_2]^- + CO_2 + 2H^+ + X^- \qquad (1.1)$$

Using the $[Rh(CO)_2I_2]^-$ ion as an active species, a catalytic cycle may be proposed[8] which is depicted in Figure 1.3 The generation of the initial metal-carbon bond by reaction of methyl iodide with a metal carbonyl moiety has been proposed as a necessary step in both the cobalt[10] and rhodium[12] catalyzed systems. The mechanism involves the oxidative addition of CH_3I to the metal followed by a migratory insertion step where CO is inserted into the $M-CH_3$ bond. Carbon monoxide is assumed to coordinate to the metal with elimination of the carbonylated product thus regenerating the active species. It is quite probable that the cobalt and rhodium-catalyzed systems proceed by different mechanisms since the two systems display different reaction kinetics.[16]

A great deal of effort has been directed toward developing a heterogeneous rhodium catalyst for the carbonylation of methanol.[17-20] A vapor-phase reaction using a rhodium carbonyl halide deposited on activated carbon catalyst was investigated by Robinson at Monsanto.[18] The kinectics displayed by the vapor-phase reaction were analogous to the homogeneous reaction thus indicating that similar mechanisms were operative in both cases.

Phosphinated polymers exchanged with rhodium complexes such as $[Rh(Ph_3P)_2(CO)Cl]$ used in liquid phase methanol carbonylation have received much attention.[19,20] Low reactivity, rhodium leaching from the

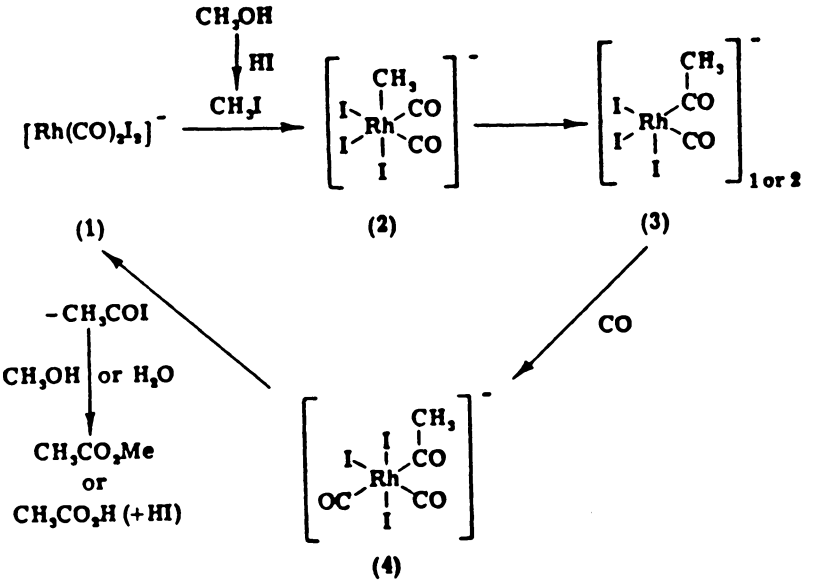

Figure 1.3. Proposed reaction mechanism for Rh-catalyzed methanol carbonylation. (Adapted from ref. 8)

support and deactivation often occur in these systems.

1.5 FISCHER-TROPSCH SYNTHESIS[21]

The increase in oil prices since the end of 1973 and concern regarding the rapid depletion of oil and natural gas reserves have led to a reassessment of the role of coal as a major energy source. Success in utilizing coal reserves depends on developing technology to convert coal into liquid products and gas.[22] One method of accomplishing this goal is via the Fischer-Tropsch (F-T) process in which synthesis gas, a mixture of CO and H_2, produced by burning coal in the presence of oxygen and steam, is converted into a wide range of hydrocarbon products.

The F-T synthesis may be viewed as a reductive polymerization of carbon monoxide. The synthesis of hydrocarbons involves stepwise incorporation of one carbon atom at a time with simultaneous formation of water according to the overall equation (eq. 1.2):

$$nCO + 2nH_2 \rightarrow (CH_2)_n + nH_2O \qquad \text{(eq. 1.2)}$$

Methane and straight chain alkanes are the major products obtained with most heterogeneous catalysts while secondary products include branched-chain hydrocarbons, alkenes, alcohols and carboxylic acids. The distribution of the various products depends on both the type of catalyst and reaction conditions used.

The F-T process can be traced back to 1902 when it was reported that heterogeneous nickel systems were able to catalyze the reduction of CO to methane.[23] In 1913 Badische Anilin and Soda Fabrik (BASF) disclosed that in the presence of alkali-activated cobalt and osmium oxides supported on asbestos, CO and H_2 react at 100-200 bar and 300-

400°C to give a liquid product containing alkanes, alkenes, alcohols, aldehydes, ketones and acids.[24] Fischer and Tropsch reported an analogous high-pressure reaction using alkalized iron turnings as the catalyst.[25] The first catalyst to produce higher hydrocarbons from CO and H_2 at atmospheric pressure was reported in 1925 using an iron oxide/zinc oxide blend.[26] Research over the next ten years led to the development of the Co-ThO_2-MgO-kieselguhr catalyst and the first commercial F-T plant was commissioned by Ruhrchemie in 1936. Several plants went into production over the next 5 years in Germany, Japan, France and Manchuria. At the height of production in 1943, the German plants were manufacturing 585,000 metric tons of products consisting of 46% gasoline, 23% diesel oil, 3% lubricating oil and 28% waxes, detergents, synthetic fat and oil.[27] All of these used the cobalt-based catalysts since the process was developed to operate at atmospheric pressure and in this regard cobalt is superior to iron.

Iron-based catalysts were employed in all plants put into operation after WWII since iron is less expensive than cobalt. Generally iron systems are more stable and the product distribution can be varied more readily. The largest complex conducting the F-T process today is SASOL operated in South Africa. The low temperature (220°-240°C) reactor uses an iron-based catalyst operating at 25 bar with an H_2/CO ratio of 1.7 and produces a C_5^+ product consisting of 32% gasoline, 21% diesel fuel, and 47% higher paraffins. A second type of reactor operates at 320°-340°C with an H_2/CO ratio of 3.5 and produces almost 70% gasoline.[28]

The product distribution obtained with most heterogeneous catalysts in the F-T process for C_3 and higher hydrocarbons can generally be

described by the Schulz-Flory[29,30] equation (eq. 1.3) given by:

$$W = n\,\alpha^{(n-1)}\,(1-\alpha)^2 \qquad \text{(eq. 1.3)}$$

where W represents the weight fraction of the oligomers having carbon number, n and α is the probability of chain growth. The chain propagation factor, α, varies for different metals. An α of 0.7-0.8 is generally observed for cobalt while iron displays an α value of 0.5-0.7.[31] Deviations from the Schulz-Flory distribution occur for C_1 and C_2 products. The weight fraction of methane is generally higher while the weight fraction of C_2 products is usually lower than predicted by the Schulz-Flory distribution.

A great deal of effort has been directed toward illucidating the mechanism of the F-T process. Three main types of mechanisms have been proposed including metal-carbide formation, hydroxyl carbene condensation and a CO insertion mechanism.[21] There is no general consensus as to which mechanism is the preferred route.

Fischer and Tropsch[32] proposed the earliest mechanism which was later extended by Craxford and Rideal[33] for cobalt-based catalyst which proceeded via formation of a metal carbide intermediate. The carbide reacts to form a methylene group which may polymerize to form hydryocarbon chains. The mechanism is proposed to follow the reaction sequence:

$$\underset{}{Co} + \underset{}{CO} \rightarrow \underset{\text{chemisorbed CO}}{Co\text{-}CO} \xrightarrow{H_2} \underset{\text{surface carbide}}{Co\text{-}C} + H_2O$$

$$Co\text{-}C + H_2 \rightarrow \underset{\text{surface methylene}}{Co\text{-}CH_2} \xrightarrow{\text{polymerization}} \text{hydrocarbon products}$$

Storch[34] proposed the second mechanism via formation of a hydroxyl carbene intermediate formed by chemisorption of CO followed by hydrogenation. Chain growth is proposed to result by condensation of these groups with elimination of water and addition of hydrogen. The sequence postulated for the mechanism[21] is indicated in Figure 1.4. The third type of mechanism was advanced by Pichler and Schulz[35] which is suggested to occur by insertion of CO into a metal-carbon bond produced by hydrogenation of a surface carbonyl. The portion of the mechanism[21] resulting in hydrocarbon formation is given in Figure 1.5. This mechanism incorporates concepts which have been substantiated experimentally in organometallic chemistry.

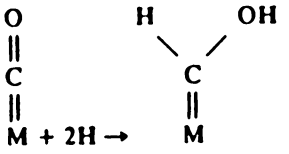

Chain growth

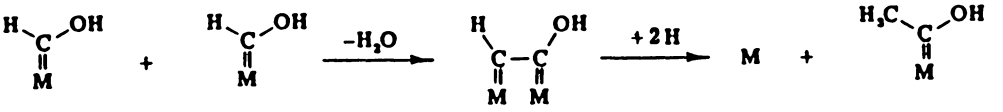

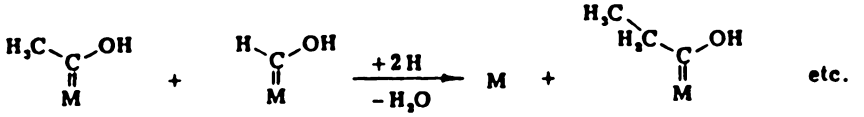

and termination

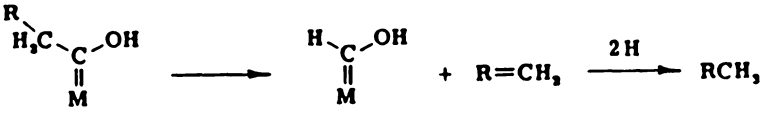

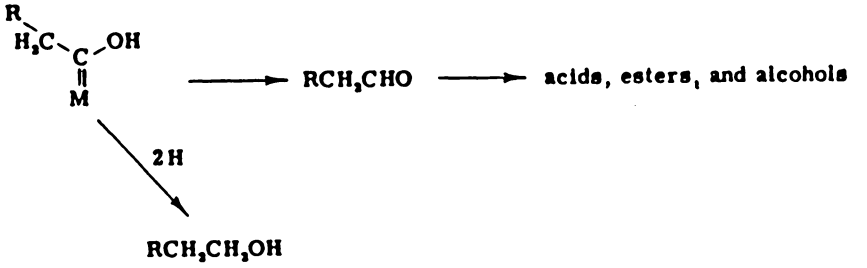

Figure 1.4. Proposed hydroxyl carbene reaction mechanism for the Fischer-Tropsch synthesis. (Adapted from ref. 21)

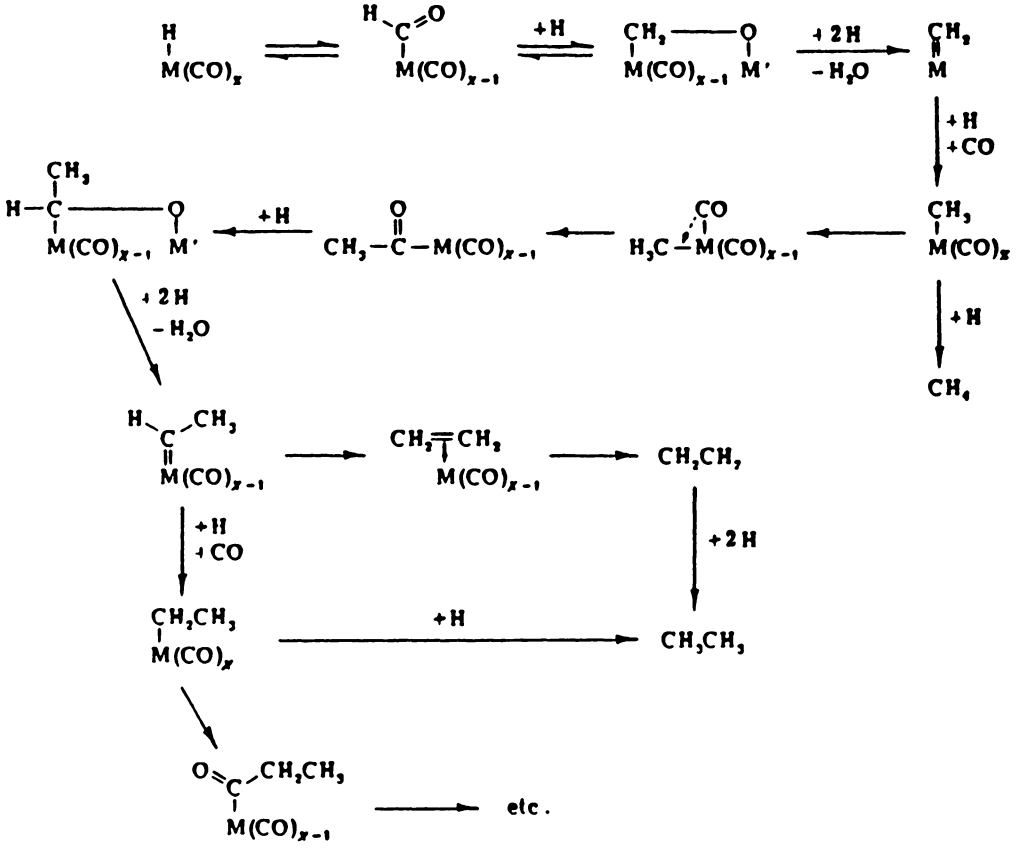

Figure 1.5. Proposed CO insertion reaction mechanism for the Fischer-Tropsch synthesis. (Adapted from ref. 21)

CHAPTER II.

EXPERIMENTAL

2.1 ZEOLITE PREPARATION

Powdered NaY and NaX zeolites purchased from Strem Chemicals, Inc., were the support materials used throughout this study. To standardize the supports, lots of approximately 7 g of zeolite powder were stirred in 150 ml 1 M NaCl for one hour, suction filtered, and washed with distilled water until the wash was free of chloride. The moist zeolite cake was then oven dried at 150°C, powdered and stored at room temperature.

A glass vessel, Figure 2.1, was charged with a weighed quantity of the zeolite powder, generally between 1.5 and 2.0 g, for preparation of a single batch of catalyst. The vessel was connected with swagelok fittings in line with a gas flow system similar in design to that of Burwell and Brenner.[36,37] The design and operation of the flow system are discussed in Appendix 1. The zeolite was calcined in oxygen with a flow rate of approximately 8 ml/min at 375°C for 30 min, followed by evacuation. The vessel was purged with helium (grade 5, 99.999%, Industrial Gas and Supply) flowing at 30 ml/min for 20 min while the temperature was maintained at 375°C. The vessel was allowed to cool to room temperature under continuous helium flow.

HY zeolite was prepared by heating the ammonium form of zeolite Y (Strem Chemical Co.) to 375°C for 4.0 hr in flowing helium to remove ammonia and generate the acid form of the zeolite. The powder was cooled to room temperature in helium and stored in the same manner as zeolites NaX and NaY.

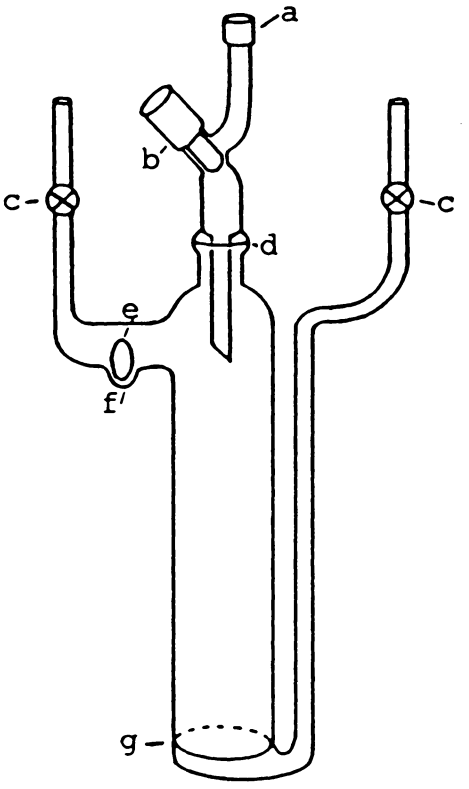

a) septum on syringe port b) rotoflow stopcock c) high vacuum stopcock d) o-ring seal e) stirbar f) stirbar well g) glass frit

Figure 2.1. Glass reaction vessel for use on gas flow system.

2.2 ADDITION OF COBALT CARBONYL COMPOUNDS TO SUPPORT

Dicobaltoctacarbonyl, obtained from Pressure Chemical Co., Inc., was sublimed under vacuum at ambient temperature and stored in a nitrogen atmosphere glove box. When required, tetracobaltdodecacarbonyl was synthesized from $Co_2(CO)_8$ by refluxing in a minimum of dry, oxygen-free tetrahydrofuran overnight according to literature methods.[38] The black crystals of $Co_4(CO)_{12}$ were filtered under nitrogen, washed free of unreacted $Co_2(CO)_8$ with dry, degassed pentane, dried in vacuum and stored in a nitrogen atmosphere glove box. The purity of the synthesized $Co_4(CO)_{12}$ was confirmed by its IR spectrum.

To load the zeolite with cobalt, a weighed quantity of freshly sublimed $Co_2(CO)_8$ was dissolved in pentane distilled from NaK alloy/benzophenone under a nitrogen atmosphere. An alliquot of the solution was syringed into the glass vessel containing the zeolite to give the desired metal loading, generally 1.0-2.5 weight % cobalt for catalytic studies. The initially deep reddish-brown solution was immediately decolorized with concurrent evolution of carbon monoxide as the zeolite adsorbed the cobalt carbonyl. The stopcocks were closed on the vessel and the slurry was stirred for 20 min to allow adsorption to occur. Flowing helium removed the excess pentane and dried the light brown zeolite impregnated with cobalt. When dry, the glass vessel was removed from the flow system and stored in a nitrogen atmosphere glove box unless a Fischer-Tropsch catalyst was to be generated. To generate the Fischer-Tropsch catalyst, an additional thermal treatment at 200°C was performed on the dry sample before the vessel was removed from the flow line.

2.3 GAS EVOLUTION

Experiments were conducted to quantify the evolution of carbon monoxide which occurred during the adsorption of $Co_2(CO)_8$. A typical experiment was carried out as follows. A pentane solution of $Co_2(CO)_8$ was syringed onto the zeolite in the glass reaction vessel with stirring while on the gas flow system described in Appendix 1. The stopcocks on the reactor were then closed and at various time intervals would be reopened to allow a helium purge to flush evolved CO from the reactor. A dewar of liquid nitrogen was placed on the silica gel trap where evolved CO from the reactor would condense. Often a dewar containing a slush of ethylene glycol and CO_2 would be placed around the reactor to inhibit further CO evolution while previously evolved CO was being removed from the reaction vessel. When the vessel had been thoroughly flushed (approximately 20 min with a 30 ml/min helium flow), the dewar was removed from the silica gel trap to allow the condensed CO to be carried in flowing helium to the 5A molecular sieve column where it was separated from residual atmospheric gases and then analyzed on the thermal conductivity detector. The evolved CO was quantified by comparison with standard 150 µl pulses of CO at an accurately known pressure from the gas sampling valve.

The CO evolution experiments were conducted during the $Co_2(CO)_8$ adsorption process after various intervals of stirring in the closed vessel, under conditions of helium flow, while heating with helium flow and during the thermal decarbonylation procedure. The experiments were conducted to ascertain the stoichiometry of the cobalt carbonyl moieties present on the zeolite.

A similar procedure was used to determine whether hydrogen was evolved during the thermal decarbonylation procedure through oxidation of cobalt by Bronsted acid sites on the zeolite. The glass vessel containing the zeolite was purged with the effluent being directed through the 5A molecular sieve trap held at -196°C. The dewar was removed from the 5A trap at the end of the decarbonylation sending the trapped gas through the CuO tube at 500°C where the H_2 was converted to H_2O. The columns were bypassed sending the gas directly to the TCD through copper tubing heated to 120°C. Hydrogen was quantified as water by comparison with standard pulses of hydrogen from the gas sampling valve.

2.4 GAS ADSORPTION

Gas adsorption experiments were conducted on the decarbonylated cobalt zeolite samples in an effort to ascertain the degree of dispersion and the average oxidation state of the cobalt. The gases used in the pulsed gas adsorption experiments included CO, O_2 and H_2 and were conducted on the gas flow system described in Appendix 1. A typical experiment was carried out as follows. A 500 µl pulse of the gas to be adsorbed at a known pressure was sent from the gas sampling valve through the cobalt zeolite and was then conducted with flowing helium to a trap at -196°C, an SiO_2 trap for CO and O_2 and a 5A molecular sieve trap for H_2, to condense any non-adsorbed gas. After each pulse, gas chromatography was used to measure the quantity of nonadsorbed gas in a manner analogous to that discussed in the Gas Evolution section. Pulses were continued in this fashion until they

integrated to the value of a standard pulse not directed through the catalyst.

Hydrogen adsorption was also performed under a static pressure of hydrogen by manometric methods in a manner similar to that of Bartholomew.[39,40] Decarbonylated samples were evacuated with an oil diffusion pump to less than 2×10^{-4} Torr. Isotherms were measured for H_2 at 150°C, 25°C and at -196°C by the adsorption method (increasing pressure) allowing 45 min to attain equilibrium before each pressure reading. Hydrogen adsorption was also measured on the clean zeolite support so that adsorption due to cobalt could be quantified.

2.5 IN SITU INFRARED SPECTROSCOPY

Powdered NaX and NaY zeolites which had been slurried with NaCl, washed and dried were formed into self-supporting wafers by compressing 10-20 mg of powder at 1500 psi in a standard infrared pellet die. The pellets were 8 mm in diameter and approximately 0.1 mm thick. Generally the pellets transmitted 50 to 60% of the IR beam intensity.

The zeolite pellet could be mounted in the quartz sample holder illustrated in Figure 2.2. A typical experiment was performed in the following manner. The pellet was calcined in flowing oxygen at 375°C for 30 min. The glass tube was then purged with helium and allowed to cool to room temperature with continuous helium flow. A pentane solution of $Co_2(CO)_8$ was added by syringe to the well at the bottom of the apparatus. The zeolite was loaded with cobalt by immersing the pellet into the pentane solution. The first IR spectrum in a series was recorded immediately after lifting the pellet into the IR beam. The

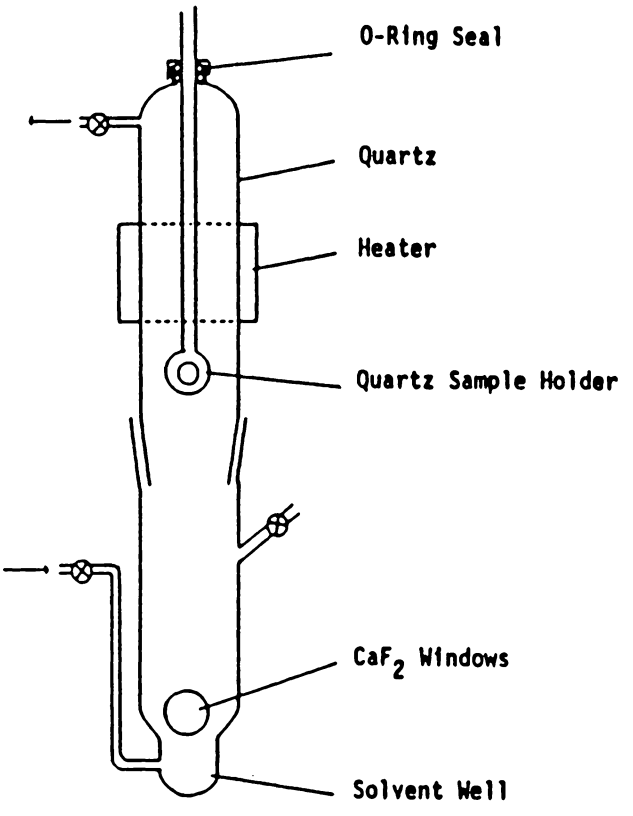

Figure 2.2. In situ IR cell.

pellet could be reimmersed until the desired loading of cobalt carbonyl was achieved such that the intensity of the strongest peak in the carbonyl region was between 0.4 and 1.0 absorbance units. Additional reagents were syringed directly on the zeolite pellet. All in situ IR spectra were recorded on a Nicolet 5DX Fourier transform spectrometer.

2.6. XPS, X-RAY POWDER DIFFRACTION AND SEM

Thermally decomposed samples of cobalt supported on NaY zeolite were mounted either on indium metal or double-stick tape in a N_2 atmosphere glove box for x-ray photoelectron spectroscopy measurements. The XPS measurements were performed with a Perkin-Elmer 5300 spectrophotometer using a magnesium x-ray source. Argon ion sputtering at 3KeV was used to obtain spectra from various portions of the samples. X-ray powder diffraction measurements were made using a Nicolet powder diffractometer.

Similar samples of cobalt/zeolite powders were mounted on double-stick tape and sputtered with gold-palladium for scanning electron microscopy. Magnifications of 2500x and 5000x were obtained on a Philips 420T STEM using a secondary electron detector and operating the electron gun at 40KeV.

2.7. METHANOL CARBONYLATION

The carbonylation of methanol was conducted in a batch process by loading a 300 ml Parr bomb with approximately 1.5 g cobalt carbonyl/zeolite (1.7 weight% cobalt) in a nitrogen atmosphere glove box. Once loaded with catalyst, 25 ml of methanol (spectral grade)

distilled under nitrogen from barium oxide and 80 µl of methyliodide were siphoned into the bomb through the solvent port. The bomb was pressurized with 700 psi CO and when included, 200 psi H_2. The reaction was carried out at either 100°C or 200°C. Routine product analysis was conducted on a Varian 3300 gas chromatograph equipped with 30m SPB-5 capillary column and a flame ionization detector. Product identification was carried out using a Hewlett Packard HP5890 gas chromatograph equipped with a 50m DB-5 capillary column in line with a Hewlett Packard 5970 mass selective detector utilizing 70eV electron impact for ionization. To measure the cobalt concentration in the reaction products, samples were analyzed on a Spectraspan IIIB direct current plasma spectrophotometer focusing on the 345.35 nm line of cobalt.

2.8 FISCHER-TROPSCH SYNTHESIS

To prepare the Fischer-Tropsch (F-T) catalyst, the zeolite supported cobalt carbonyl was thermally decomposed at 200°C in flowing helium for one hour before removing the reactor from the gas flow system. The decarbonylation was complete as indicated by the absence of any carbonyl bands in the IR spectrum of the material. The thermal treatment was necessary to generate cobalt metal on the zeolite support. Various dry alkali halide salts including NaCl, KCl, KBr and KI were intimately mixed or ball-milled with the cobalt zeolite to examine whether those salts could modify the activity of the catalyst. To conduct the F-T synthesis in a batch process, a 300 ml Parr bomb was charged with 0.4 g of cobalt zeolite catalyst in a nitrogen atmosphere

glove box. The bomb was pressurized with 400 psi H_2 and 200 psi CO at room temperature. The reaction was conducted at 200°C for 16 to 18 hours. Upon completion of the run, the gas stream from the bomb was vented through a gas sampling tube and the products were quantified using a Varion 3300 gas chromatograph equipped with a flame ionization detector. The catalyst was washed with pentane to extract heavy hydrocarbons and the wash was analyzed by gas chromatography.

A differential reactor in line with a high pressure flow system was constructed, Figure 2.3, to study the activity of the F-T catalyst. The differential reactor was charged with a quartz wool plug and approximately 1.0g of cobalt metal/zeolite in a nitrogen atmosphere glove box. The system was purged with research purity synthesis gas, 1:1 hydrogen to carbon monoxide, obtained from Matheson Gas Products and was then pressurized to 480 psi maintaining a flow of 5 to 10 ml/min. The reaction was carried out at 250°C. Gaseous products were analyzed by gas chromatography using an FID.

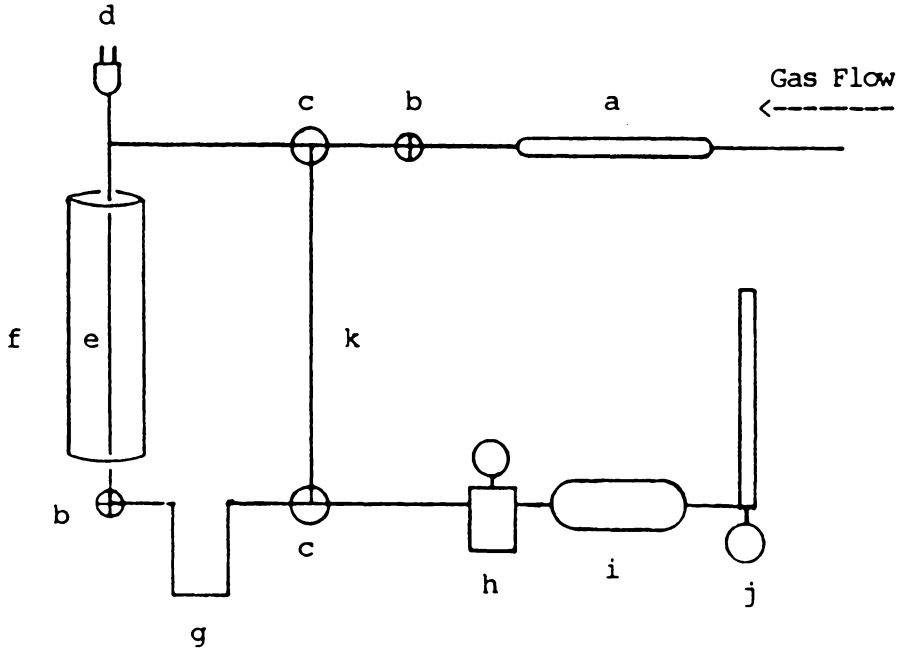

(a) stainless steel tube containing MnO_2 on SiO_2 (b) 2-way valve (c) 3-way valve (d) thermocouple (e) ¼" stainless steel reactor tube (f) tube furnace (g) ¼" stainless steel condenser (h) back pressure regulator (i) gas sampling tube (j) soap bubble flowmeter (k) reactor bypass for purging system

Figure 2.3. High pressure flow system used in conducting Fischer-Tropsch synthesis.

CHAPTER III.

IN SITU IR SPECTROSCOPY AND GAS EVOLUTION STUDIES OF INTRAZEOLITE COBALT CARBONYLS

3.1 INTRODUCTION AND LITERATURE SURVEY ON IR SPECTROSCOPY OF SUPPORTED COBALT CARBONYLS

Many techniques are available to study transition metal complexes supported on metal oxide carriers such as in situ IR spectroscopy,[4,41-52] magic-angle-spinning NMR,[53-55] temperature programmed decomposition,[56] ESR,[42,57] magnetic susceptibility[42] and catalytic activity.[58-60] In situ IR spectrosocpy is one of the preferred techniques used to study the adsorption of cobalt carbonyl compounds on zeolite supports for a variety of reasons. The carbonyl ligands of metal carbonyls have a strong absorptivity coefficient and even when very dilute, metal carbonyls may be observed on oxide supports. Many carbonyl compounds have been well characterized by IR spectroscopy such that analogies can be inferred between known compounds and the identity of the species supported on an oxide surface. Also, the carbonyl ligands are sensitive to the environment of the complex such that shifts in the carbonyl stretching frequencies may be utilized to interpret the surrounding interactions between the carbonyl compound and the support. IR spectroscopy is a non-destructive technique and will induce few or no perturbations in the system under investigation by its application. This technique is useful with air-sensitive materials since the samples may be protected under an inert atmosphere while IR spectra are being recorded.

Several investigators have employed IR spectroscopy to study cobalt carbonyl compounds supported on zeolites. Ballivet-Tkatchenko[41,45] and Watters[43] studied $Co_2(CO)_8$ sublimed onto various zeolite supports. Their results indicate that $Co_2(CO)_8$ reacts to form $Co_4(CO)_{12}$ and $[CoL_6][Co(CO)_4]_2$ when sublimed on NaY, NaX and HY zeolites. Similar findings were obtained and will be discussed in detail in the following sections for zeolites impregnated with $Co_2(CO)_8$ adsorbed from pentane solution. In addition, the reactivity of the zeolite supported cobalt carbonyl moieties with various ligands including phosphines, methanol, water and pyridine and during thermal decarbonylation has been elucidated by following this chemistry with in situ IR spectroscopy. This study was useful in providing information concerning the reactivity of the carbonyl species present, the location of the subcarbonyls in the zeolite and the chemistry which may occur under catalytic conditions.

3.2 ADSORPTION OF BINUCLEAR AND TETRANUCLEAR COBALT CARBONYLS ON NaY AND NaX ZEOLITES

A typical set of infrared spectra resulting from the adsorption of $Co_2(CO)_8$ on NaY are shown in Figure 3.1. Trace a was recorded immediately after a 30 sec immersion of the wafer in the pentane solution. A complex series of absorption bands are generated as the intrazeolite chemistry of $Co_2(CO)_8$ is followed with time. The most dramatic changes occur in the first 15 min after immersion and after 60 min, no further changes in the spectrum are observed. One of the most intense bands in the terminal region of trace c, 2063 cm^{-1}, is assignable to $Co_2(CO)_8$. In the bridging region there is a band of

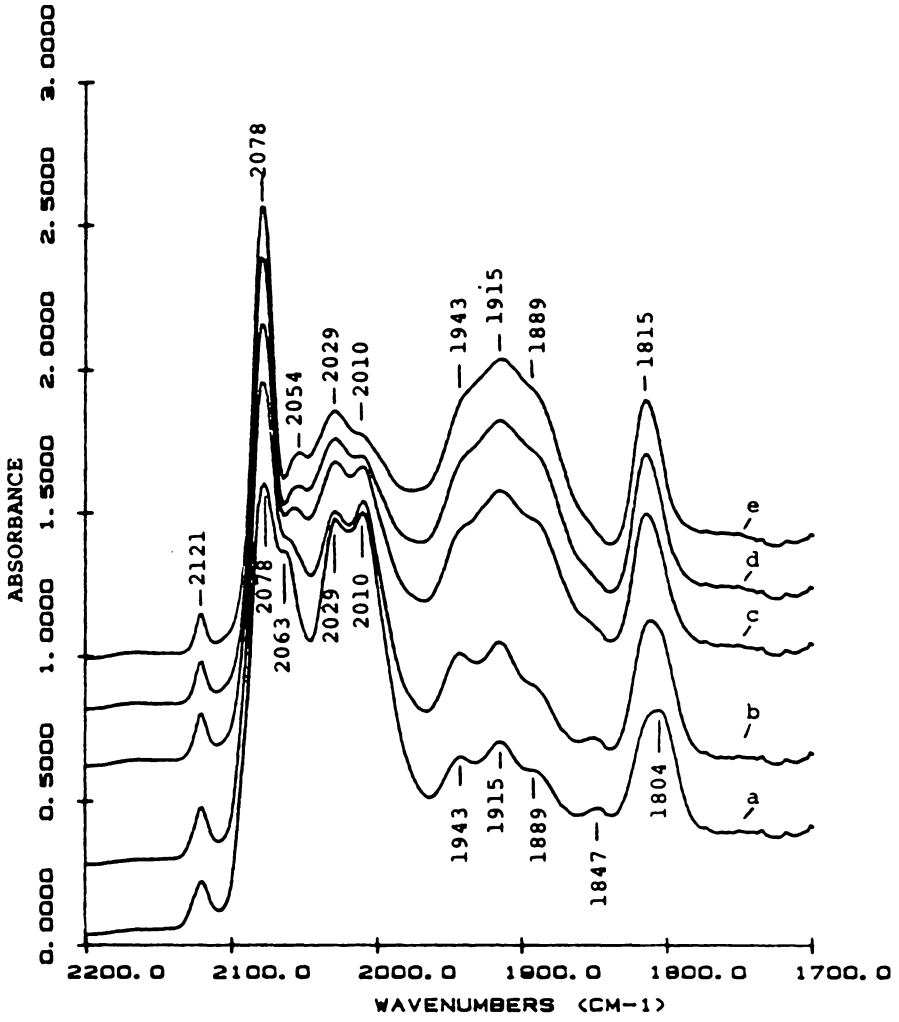

Figure 3.1. Adsorption of $Co_2(CO)_8$ on NaY zeolite; (a) immediately after immersion of pellet into $Co_2(CO)_8$/pentane solution; (b) 3 min after immersion; (c) 6 min after immersion; (d) 9 min after immersion; (e) 15 min. after immersion.

medium intensity at 1804 cm^{-1} and a weak band at 1847 cm^{-1}. The intensity of these correlate with the terminal bands at 2063 and 2029 cm^{-1} and are assigned to $Co_2(CO)_8$.

The bands assigned to $Co_2(CO)_8$ diminish rapidly with time and after 15 min (trace e) have virtually disappeared from the spectrum. In the terminal region the most intense peak is at 2078 cm^{-1} and in the bridging region the band at 1815 cm^{-1} are assigned to $Co_4(CO)_{12}$. This is consistent with the assignment made by Watters et.al.[43] However the shifts observed between the spectra for adsorbed $Co_4(CO)_{12}$ and $Co_4(CO)_{12}$ in solution should not be interpreted as evidence for the cluster residing within the zeolite.

There are several places in the spectrum where near isobestic behavior is observed, for example at ca. 1980 cm^{-1}. However the match is not exact. This is consistent with some loss of carbon monoxide during the experiments. As the terminal bands decrease in intensity, three peaks are seen to grow in intensity at 1943, 1915 and 1889 cm^{-1}. The 1889 cm^{-1} peak may be assigned directly to $Co(CO)_4^-$ (vide infra). In the terminal region two remaining bands are unassigned in spectrum e, namely those at 2029 and 2010 cm^{-1}. These may, in part be due to species of the type $Co(CO)_3L_2^+$ where L is a framework oxide. The 2029 and 2010 cm^{-1} bands may also result from a trimeric cobalt complex of the type, $Co_3(CO)_9$ CY where Y may be a lattice oxide.

Figure 3.2 shows the infrared spectra obtained upon adsorption of $Co_2(CO)_8$ on NaX zeolite. Trace c shows the spectrum 5 min after immersion of the pellet. The band at 1893 cm^{-1} continues to grow slowly after this time. The most intense band is seen at 1893 cm^{-1} and as on

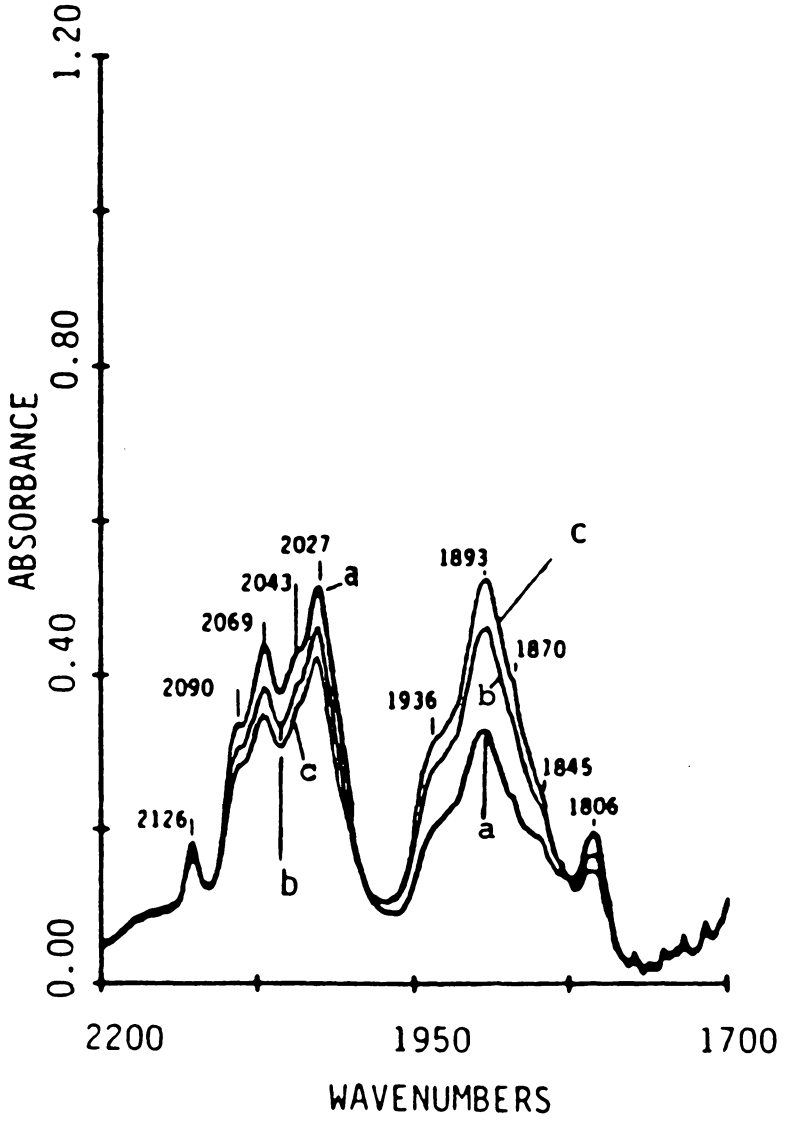

Figure 3.2. Adsorption of $Co_2(CO)_8$ on NaX zeolite; immediately after immersion of pellet into $Co_2(CO)_8$/pentane solution; (b) 3 min after immersion; (c) 6 min after immersion.

NaY, this is assigned to $Co(CO)_4^-$. Thus NaX zeolite favors formation of $Co(CO)_4^-$ compared to NaY zeolite. A similar result was observed by Watters et.al.[43] In the terminal region of the infrared spectrum bands are seen at 2126, 2090, 2043 and 2027 cm^{-1}. These are shifted to higher wavenumber compared to those for NaY zeolite. Also, these decrease in intensity as the 1893 cm^{-1} band increases. A bridging band is observed at 1806 cm^{-1}. By analogy with the results on NaY zeolite, the bridging band at 1806 cm^{-1} is assigned to $Co_4(CO)_{12}$ (adsorbed); however, the corresponding terminal bands cannot be clearly assigned.

Confirmation of the bands at 2121, 2078, 2054 and 1814 cm^{-1} assigned to $Co_4(CO)_{12}$ on NaY zeolite is obtained by direct adsorption of this cluster on NaY. The results of this experiment are shown in Figure 3.3. Traces 1-4 in Figure 3.3 represent four successive immersions of the NaY wafer into a pentane solution of $Co_4(CO)_{12}$. The spectra do not change with time. With each immersion all infrared adsorptions simply increase in intensity. At heavy loadings (traces 3 and 4) a bridging carbonyl band appears at 1870 cm^{-1}, which is assigned to physisorbed $Co_4(CO)_{12}$. This band however is extremely weak; the principal bands are observed at 2121, 2078, 2056 and 1811 cm^{-1}. These are very close to bands in the spectrum of $Co_2(CO)_8$ on NaY and are assigned to $Co_4(CO)_{12}$ strongly physisorbed or weakly chemisorbed.

From Table 3.1 it can be seen that the bands assigned to adsorbed $Co_4(CO)_{12}$ are shifted significantly from $Co_4(CO)_{12}$ in solution. The terminal bands move to higher wavenumber while the bridging band is shifted to lower wavenumber. This has previously been taken as evidence

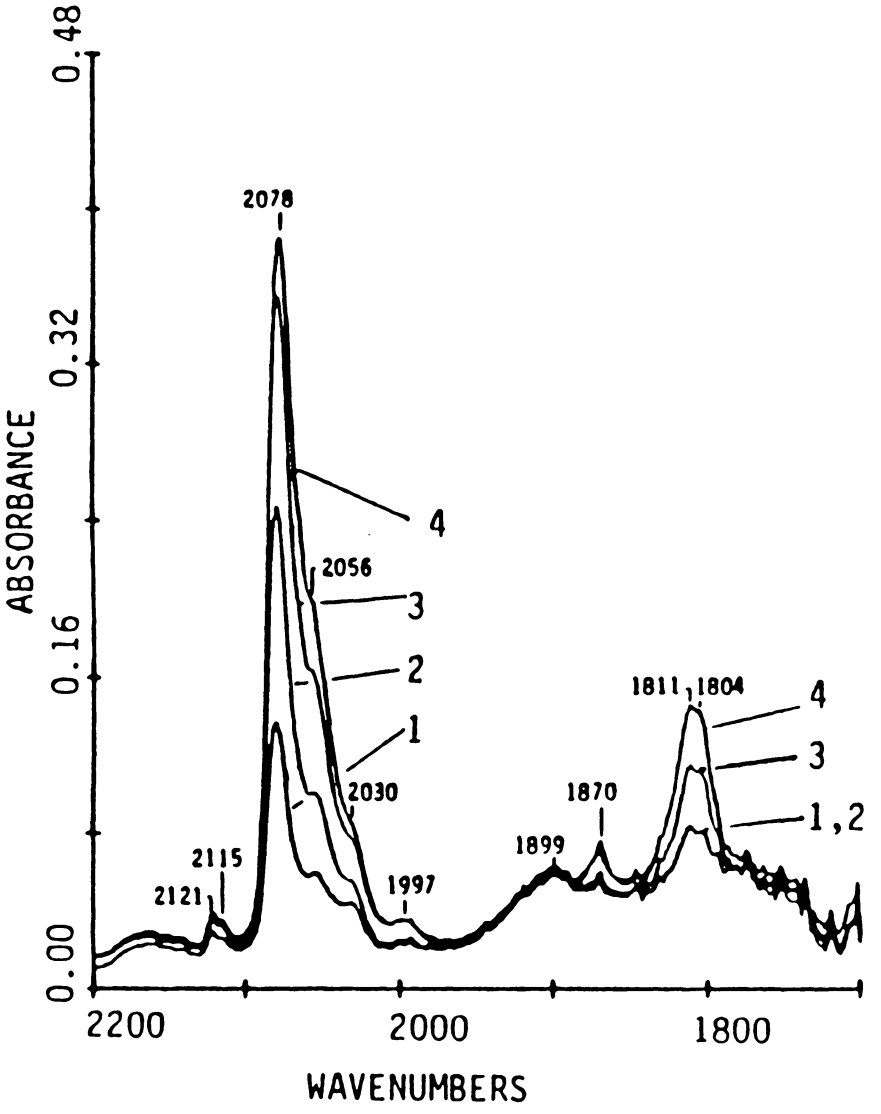

Figure 3.3. IR spectra obtained by four consecutive immersions of NaY pellet into $Co_4(CO)_{12}$/pentane solution; (1) first immersion, (2) second immersion, (3) third immersion, (4) fourth immersion.

Table 3.1

System	Carbonyl Stretching Frequencies (cm^{-1})											
Solution												
$Co_2(CO)_8$/pentane	2112w	2071s	2045s	2031s	2024s	2001w			1867m	1858m		
$Co_4(CO)_{12}$/pentane		2064s	2056s	2036w	2025w				1867m			
$[Co(CO)_3(PEt_3)_2]$ $[Co(CO)_4]$/THF						2008s	1995s		1885s,br			
$Co_2(CO)_8$/NaY Batch (nujol mull)	2122w	2078s	2050m	2030m		2007m	1940m	1913m	1893m	1860w		1817m
In Situ												
$Co_2(CO)_8$/NaY	2122w	2079	2062	2029		2010	1943	1914	1885			1809m
$Co_2(CO)_8$/NaX	2127w	2090	2069	2042	2026		1934		1894	1870		1805
$Co_4(CO)_{12}$/NaY	2121w	2115w	2078s	2056sh	2030sh		1997w		1899w	1870w	1811m	1804m
$Co_4(CO)_{12}$/NaX	2108w	2064s	2055s	2040m	2029m		1989w		1902s,br	1868s	1833w	
$Co_2(CO)_8$/HY	2119		2056	2031					1898	1856		1815

Table 3.2

System	Carbonyl Stretching Frequencies (cm^{-1})											
In Situ												
PEt_3/NaY, $Co_2(CO)_8$						2003	1989		1884	1869		
PEt_3/NaX, $Co_2(CO)_8$						2003	1989		1884	1869		
$Co_2(CO)_8/NaY$, PEt_3		2080sh	2060w		2012m	1995m	1966m	1912sh	1890s	1876sh		
$Co_2(CO)_8/NaX$, PEt_3	2127w	2090w	2069w		2026w			1920sh	1894s			
$Co_4(CO)_{12}/NaY$, PEt_3			2070w	1980m	1964m	1944	1925sh	1918sh	1905s	1870m	1846w	
$Co_4(CO)_{12}/NaY$, $P(t\text{-}Bu)_3$									1902s,br			
$Co_2(CO)_8/NaY$,MeOH		2070	2045	2026				1906				
MeOH/NaY, $Co_2(CO)_8$			2054		2022	2008sh			1903			
$Co_2(CO)_8/NaY$, H_2O	2115	2068		2045	2024			1915	1908		1835	
H_2O/NaY, $Co_2(CO)_8$								1919				
$Co_2(CO)_8/NaY$, Pyr	2119,	2074		2049	2025		1931		1896	1880		1816

for the cluster to reside within the zeolite structure. This cannot be the case for adsorption of $Co_4(CO)_{12}$, however, since this cluster is too large to pass through the 7.4 Å channels of NaY zeolite. Reaction with large and small phosphines confirms this expectation as will be discussed in section 3.4.

Adsorption of $Co_4(CO)_{12}$ on NaX gives a distinctly different infrared spectrum, as seen from Figure 3.4. The set of bands at 2064s, 2055s, 2040w, 2029w and 1868s cm^{-1} are nearly superimposable on the spectrum of $Co_4(CO)_{12}$ in pentane. The only other infrared band resulting from adsorption of $Co_4(CO)_{12}$ on NaX is a broad adsorption at 1902 cm^{-1}, which may be due to $Co(CO)_4^-$ stemming from disproportionation of the cluster. Thus the surfaces of faujasites NaX and NaY appear to have different types of sites for adsorption of $Co_4(CO)_{12}$.

Tables 3.1 and 3.2 summarize the results of the experiments discussed above and others to be discussed later. Table 3.3 gives the proposed assignments for the various carbonyl stretching frequencies.

3.3 $Co_2(CO)_8$ SUPPORTED ON HY ZEOLITE

When a pentane solution of $Co_2(CO)_8$ is slurried with HY zeolite, less than 0.5 weight % Co is adsorbed on the support. It is likely that $Co_2(CO)_8$ is only adsorbed on the surface of the zeolite crystallites which would account for the low Co weight % loadings which can be achieved with this support. During thermal treatment of the support prior to the addition of $Co_2(CO)_8$, some dealumination with concurrent pore closure may occur which could account for the surface adsorption of $Co_2(CO)_8$ on HY zeolite.

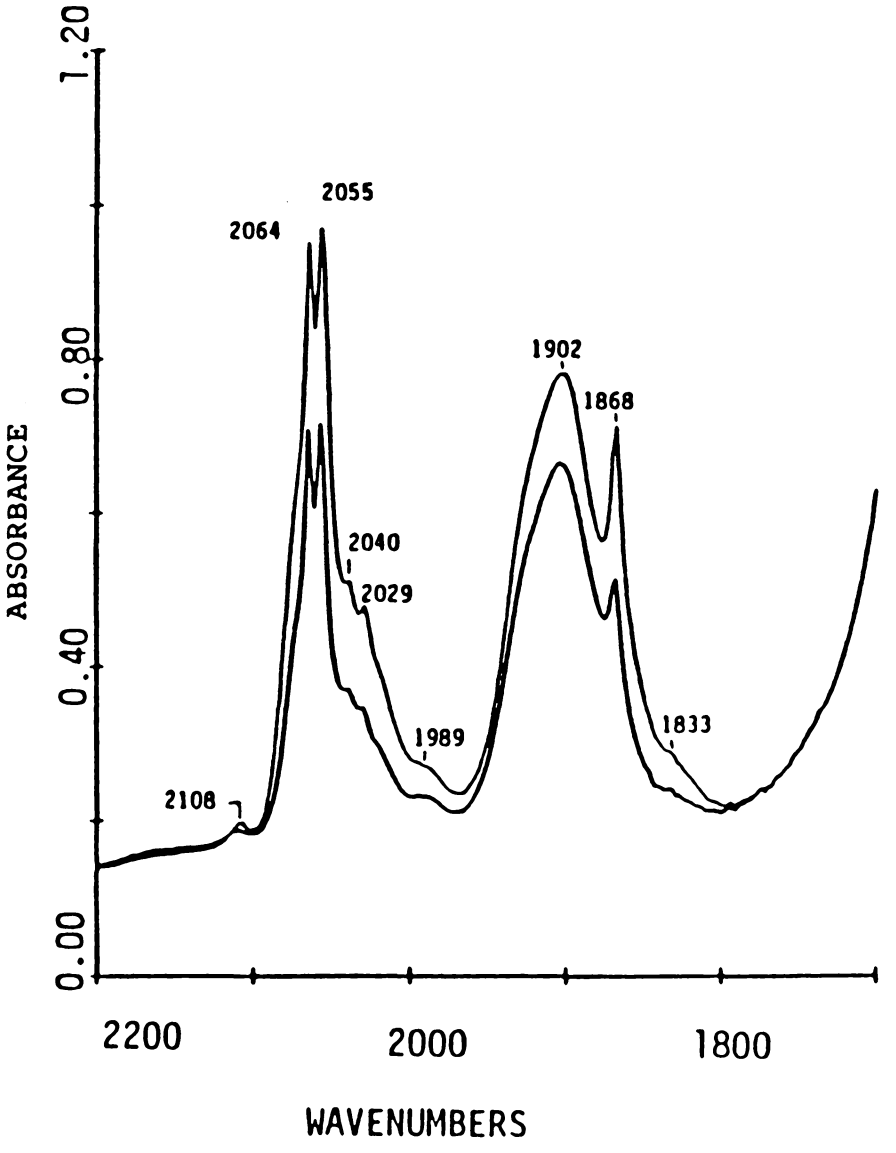

Figure 3.4. Adsorption of $Co_4(CO)_{12}$ on NaX; top spectrum is immediately after immersion of pellet into solution, lower spectrum is 3 min after immersion.

Table 3.3

Assignment of Carbonyl Stretching Frequencies (cm^{-1})

Support	Complex	Assigned Frequencies
NaY	$Co_2(CO)_8$	2062, 2030, 1846, 1802
	$Co_4(CO)_{12}$	2121, 2079, 2054, 1812
	$Co(CO)_3L_2^+$	2008
	$Co(CO)_4^-$	1902, 1885
	$Co_x(CO)_y$	1943
NaX[a]	$Co_4(CO)_{12}$ (surface)	2108, 2064, 2055, 2040, 2029, 1989, 1869, 1833
	$Co(CO)_3L_2^+$	2026
	$Co(CO)_4^-$	1902, 1894

[a] Many of the carbonyl bands observed upon adsorption of $Co_2(CO)_8$ and NaX are left unassigned at this time. These may be due to species $Co_x(CO)_y$.

When the acid form of Y zeolite is immersed in a pentane solution of $Co_2(CO)_8$, initially an IR spectrum is obtained which contains several sharp bands. The peaks at 2112w, 2071s and 2044s cm^{-1} in Figure 3.5 may be assigned to terminal carbonyls in the bridged form of $Co_2(CO)_8$ while the bands at 1865 and 1857 cm^{-1} probably arise from bridging carbonyls as they are very close to those for $Co_2(CO)_8$ in solution. The peaks at 2032s and 2024s cm^{-1} may be due to a non-bridged form of $Co_2(CO)_8$ since they coincide with bands reported by Braterman[69] for the non-bridged structure. The carbonyl stretching in $Co_4(CO)_{12}$ may give rise to the band at 2057 cm^{-1}. Other bands arising from the tetramer may be hidden by the strong absorption of $Co_2(CO)_8$.

As the adsorption of $Co_2(CO)_8$ on HY zeolite is followed with time, the sharp bands in the spectrum of the initially impregnated pellet rapidly broaden. The broadening of the bands may be due to $Co_2(CO)_8$ adsorbing in various environments provided by the zeolite support. A striking difference between the HY support and the NaY and NaX supports is the slight propensity of $Co_2(CO)_8$ to disproportionate on HY zeolite. No strong absorption band in the vicinity of 1900 cm^{-1} is observed in the spectrum as the absorption is followed with time indicating only slight formation of $Co(CO)_4^-$. Another observation on the adsorption of $Co_2(CO)_8$ on HY is that the carbonyl stretching frequencies remain close to the bands reported for $Co_2(CO)_8$ in solution. It appears that HY is much less capable of activating $Co_2(CO)_8$ toward disproportionation and other chemical pathways than are NaY and NaX zeolites. Formation of the complex $NaCo(CO)_4$ is known to occur when $Co_2(CO)_8$ is reacted with a base such as NaOH in a polar solvent [87] at room temperature. It has also

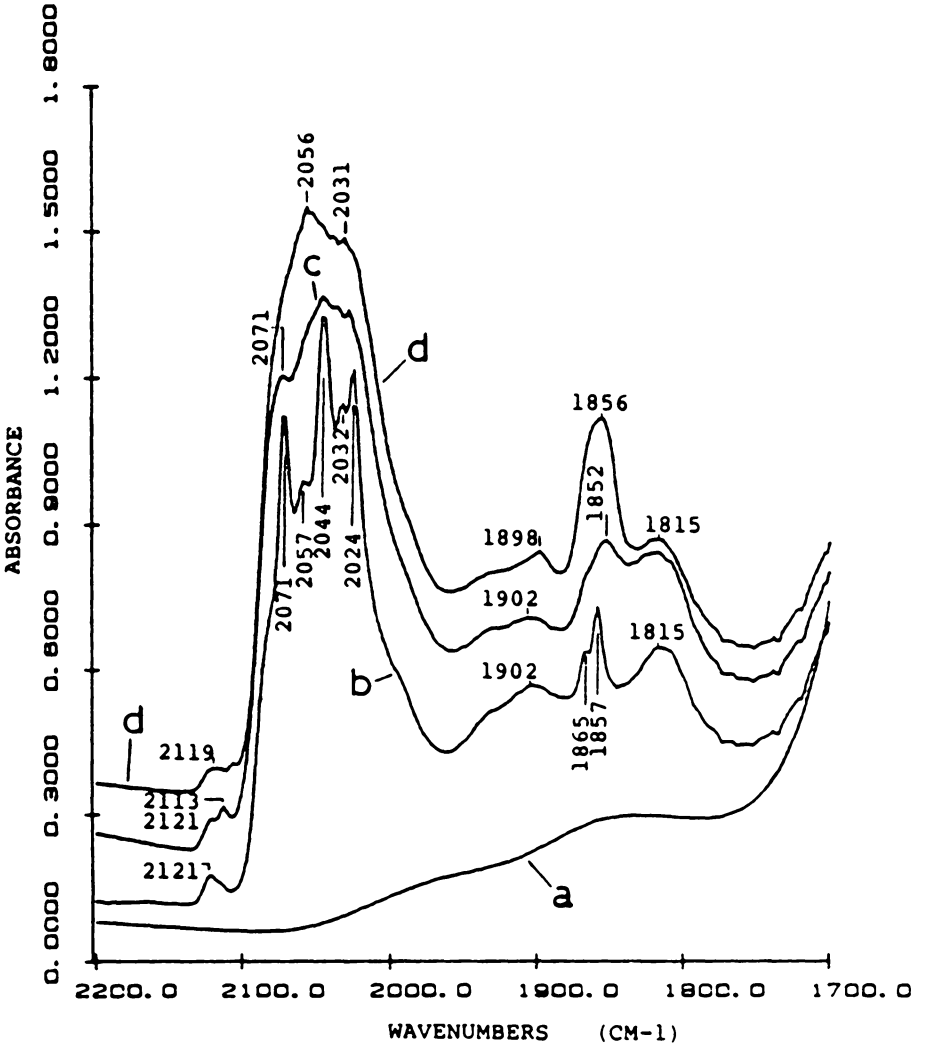

Figure 3.5. $Co_2(CO)_8$ supported on HY zeolite; (a) HY pellet; (b) immediately after immersion of pellet into $Co_2(CO)_8$/pentane solution; (c) 3 min after immersion; (d) 6 min after immersion.

been observed that univalent cation forms of some zeolites such as NaX do not contain a total exchange equivalency as based on chemical analysis. The deficiency in the metal cation balance has been attributed to partial hydrolysis of the cation and replacement by hydronium ions.[88,89] The hydrolysis[5] may be represented by eq. 3.1

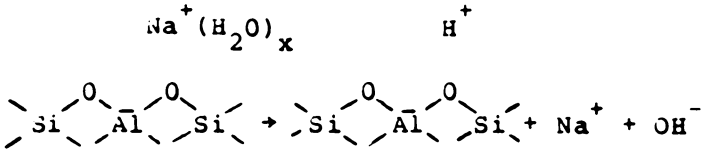

(eq. 3.1)

The formation of hydroxyl groups via cation hydrolysis may induce the disproportionation of $Co_2(CO)_8$ on NaX and NaY zeolites whereas cation hydrolysis and subsequent disproportionation of $Co_2(CO)_8$ on the acid form of Y zeolite would not be expected.

3.4 SUPPORTED COBALT CARBONYLS REACTED WITH PHOSPHINES

The identity of the adsorbed cobalt carbonyls may be assigned, in principle, on the basis of their reactivity with phosphines. Brown[61] studied the kinetics of the reactions of basic phosphines with $Co_2(CO)_8$ in hexane solution and found $[Co(CO)_3(PR_3)_2][Co(CO)_4]$ to be the major product which results from disproportionation of the dimer. The reaction is inhibited by traces of oxygen and a radical chain mechanism was proposed to account for this observation. Key steps in the radical chain involve an electron-transfer process of the form $Co(CO)_3L^{\bullet} + Co_2(CO)_8 \rightarrow Co(CO)_3L^{+} + Co_2(CO)_8^{-}$; rapid dissociation of the radical anion to yield $Co(CO)_4^{-}$ and $Co(CO)_4^{\bullet}$ and rapid substitution of $Co(CO)_4^{\bullet}$ by L to form $Co(CO)_3L^{\bullet}$. Tri-tert-butylphosphine and tri-ethylphosphine were therefore chosen to probe the surface chemistry of cobalt carbonyls.

therefore chosen to probe the surface chemistry of cobalt carbonyls. Also the tetramer, $Co_4(CO)_{12}$, is well-known to react with simple phosphines to yield neutral substituted clusters of the type $Co_4(CO)_{12-x}(PR_3)_x$.[38,62] In two experiments $P(Et)_3$ was preadsorbed onto a wafer of NaX or NaY zeolite. A solution of $Co_2(CO)_8$ was then syringed onto the wafer and the infrared spectrum recorded. The resulting spectrum on NaY zeolite is shown in Figure 3.6; the spectrum on NaX is identical. The spectrum is completely consistent with $[Co(CO)_3(PEt_3)_2][Co(CO)_4]$ as expected. The anion has a strong absorption at 1885cm^{-1}, which gives evidence for the previous assignment of this species. The cation bands are seen at 2003 and 1990 cm^{-1}. If, as suggested earlier, the terminal bands observed at 2029 and 2010 cm^{-1} are due to a complex of the type $[Co(CO)_3L_2]^+$ when L is a framework oxide, then the bands are shifted to higher wavenumber compared to the present example where L is $P(Et)_3$.

Figure 3.7 shows the infrared spectrum obtained upon addition of $P(Et)_3$ onto a NaY wafer which had been reacted previously with $Co_2(CO)_8$. The spectra shown in Figures 3.7 and 3.1 are of similarly prepared samples. The spectrum given in 3.8 is after addition of $P(Et)_3$. The most obvious feature of this spectrum is the band which occurs at 1891 cm^{-1}. Thus nearly all of the supported cobalt carbonyl reacts with $P(Et)_3$ to yield $Co(CO)_4^-$, including adsorbed $Co_4(CO)_{12}$ since the bands assigned to this species nearly disappear. No evidence is observed for phosphine-substituted tetracobalt clusters except for a very weak bridging band at 1756 cm^{-1}. All other terminal bands also diminish in intensity as the 1891 cm^{-1} band increases. Thus $P(Et)_3$ reacts with the adsorbed cobalt carbonyls by further disproportionation. Bands assigned to $[Co(CO)_3(PEt_3)_2]^+$ in Figure 3.8, 2012 and 1995 cm^{-1}, are relatively

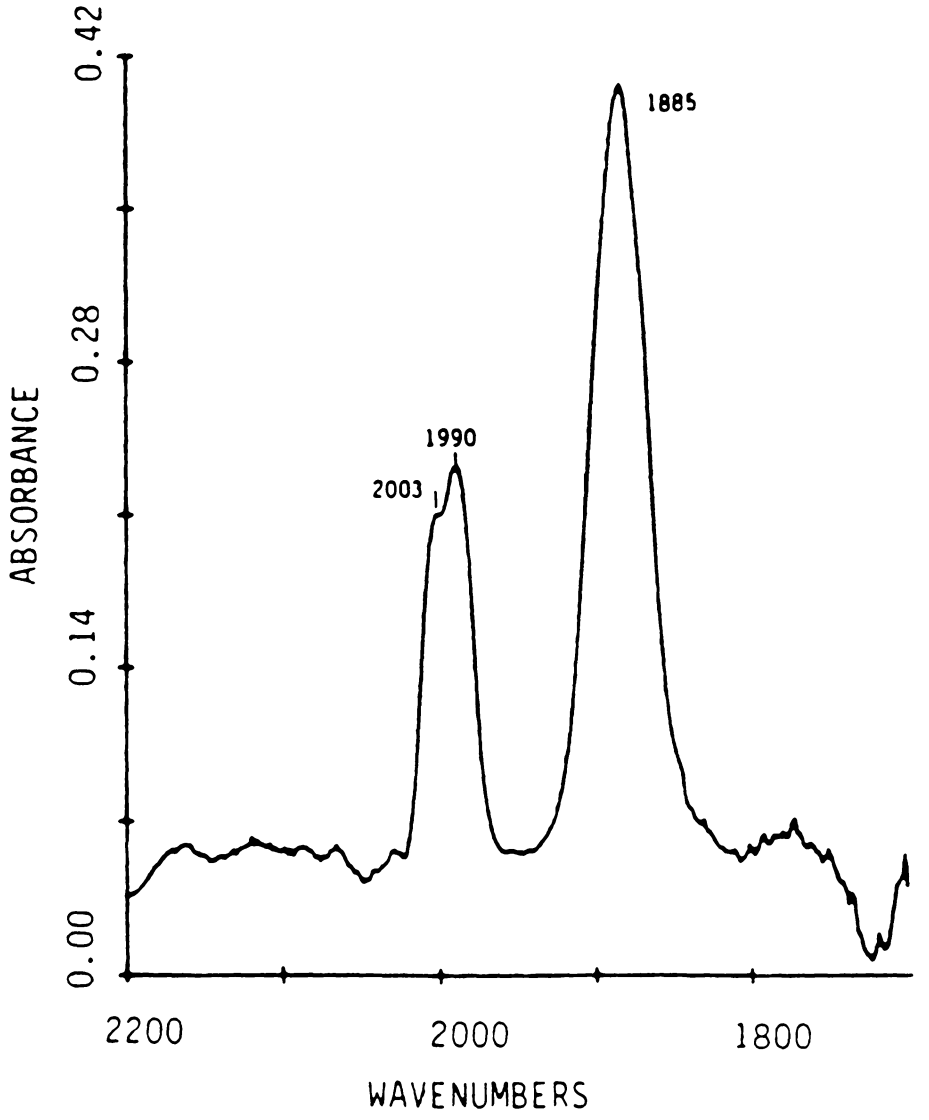

Figure 3.6. Triethylphosphine adsorbed on NaY followed by addition of $Co_2(CO)_8$.

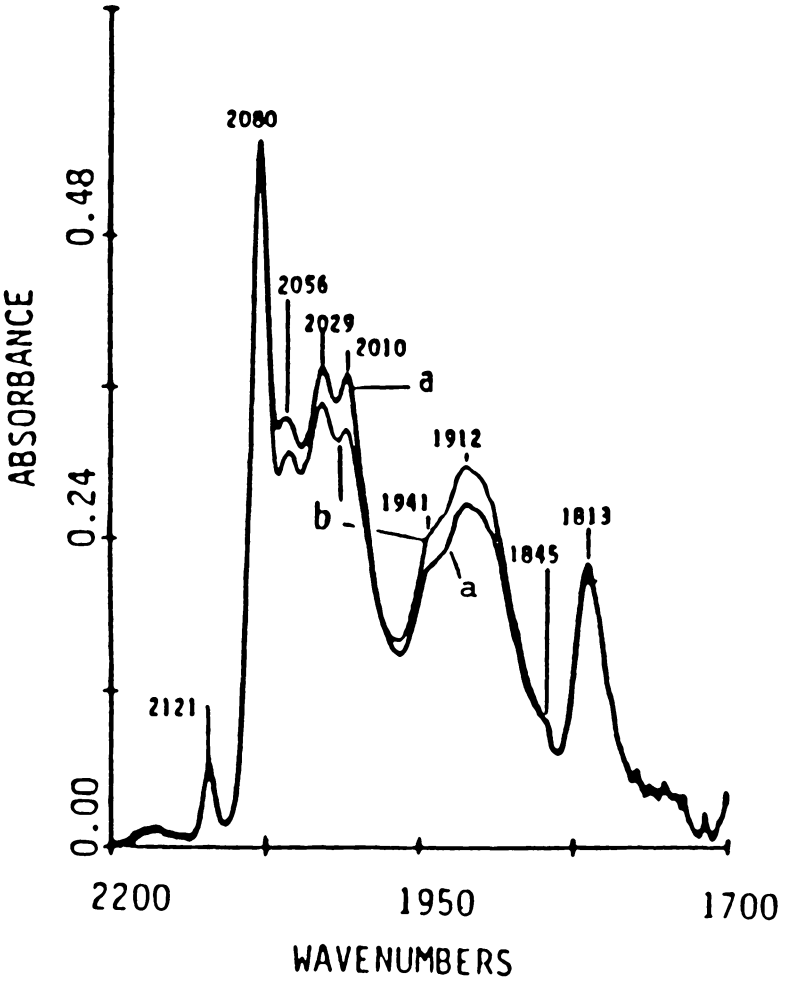

Figure 3.7. $Co_2(CO)_8$ adsorbed on NaY; (a) immediately after immersion of the pellet into solution (b) 2.5 min after immersion.

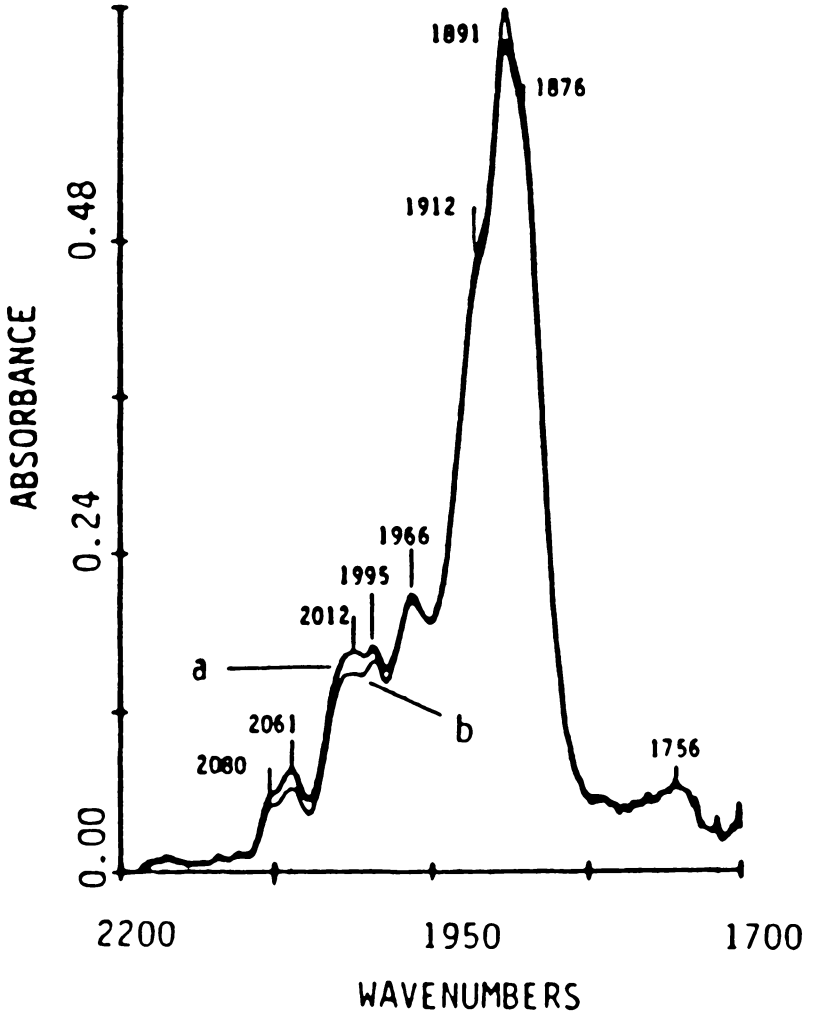

Figure 3.8. Addition of $P(Et)_3$ to $Co_2(CO)_8$ adsorbed on NaY shown in trace (a); (b) 3 min after additon of $P(Et)_3$.

weak. The reactions of cobalt carbonyls on oxide surfaces may be explained by analogies to known solution reactions. Wender[90] proposed a general reaction of $Co_2(CO)_8$ with bases. Basic ligands (B) are required to stabilize the cobalt cations formed according to eq. 3.2.

$$3Co_2(CO)_8 + nB \rightarrow 2[CoB_n][Co(CO)_4]_2 + 8\ CO \qquad \text{(eq. 3.2)}$$

The reaction is thought to consist of several steps, including the initial development of an unstable base-complexed metal carbonyl cation $[BCo(CO)_4]^+$. It is possible that the cation formed is $Co(PEt_3)_6^{2+}$, which obviously will not give a carbonyl stretch in the infrared spectrum. When the same experiment is performed on NaX, a similar infrared spectrum is generated in that nearly all of the carbonyl intensity is in the 1890 cm^{-1} peak.

The adsorbed tetracarbonyl cluster formed directly from the $Co_4(CO)_{12}$ also reacts with $P(Et)_3$ to yield an intense band at approximately 1900 cm^{-1}. Disproportionation of $Co_4(CO)_{12}$ in solution has been observed upon reaction with nitrogen- and oxygen- containing bases such as pyridine.[63] With phosphines, simple ligand substitution reactions are observed with $Co_4(CO)_{12}$.[62] Thus this cluster is activated toward disproportionation when adsorbed onto a faujasite.

Figures 3.9 and 3.10 compare the reactions of supported cobalt carbonyls from $Co_2(CO)_8$ and $Co_4(CO)_{12}$ with the large phosphine, $P(t\text{-}Bu)_3$. From molecular models it is estimated that $P(t\text{-}Bu)_3$ has a cross sectional diameter of ca. 8.3 Å. This is slightly larger than the kinetic pore diameter of NaY zeolite, ca. 8.1 Å.[5] Thus this phosphine is too large to penetrate the pores of the zeolite at a reasonable rate at room temperature and can only react with surface carbonyls.

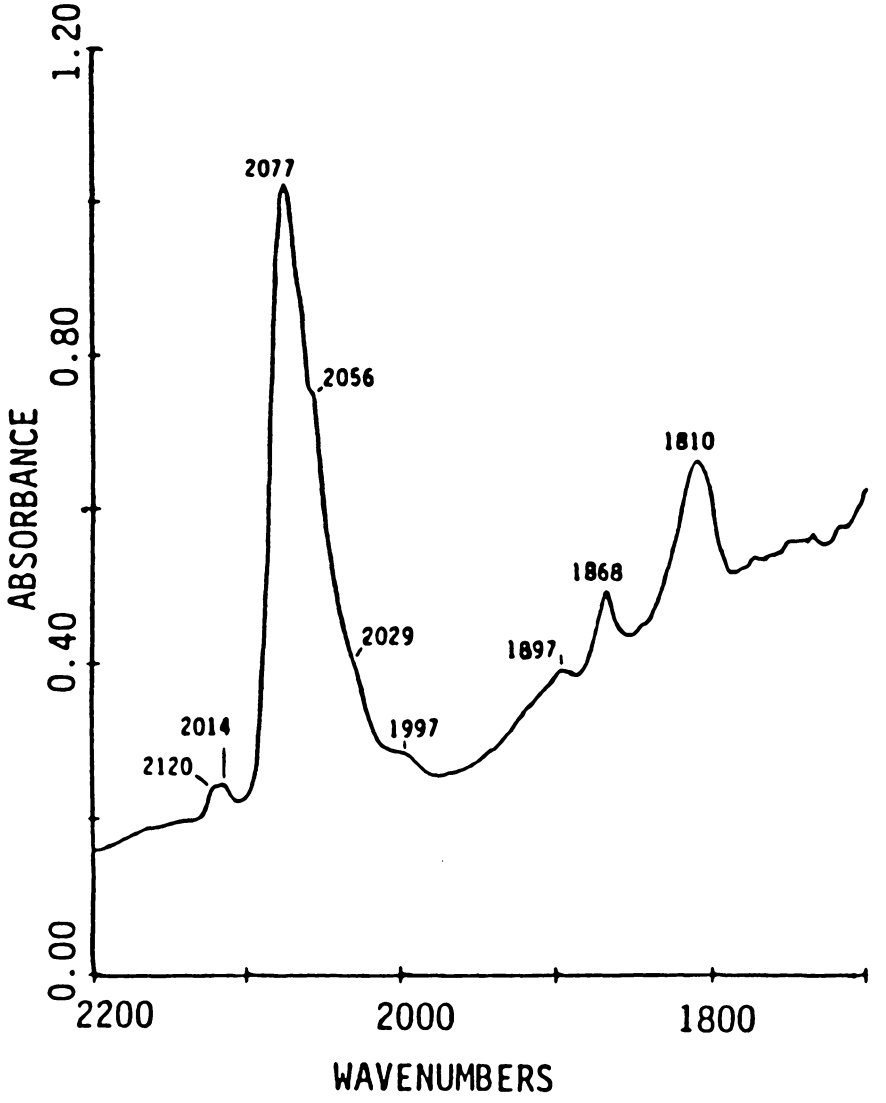

Figure 3.9. $Co_4(CO)_{12}$ adsorbed on NaY.

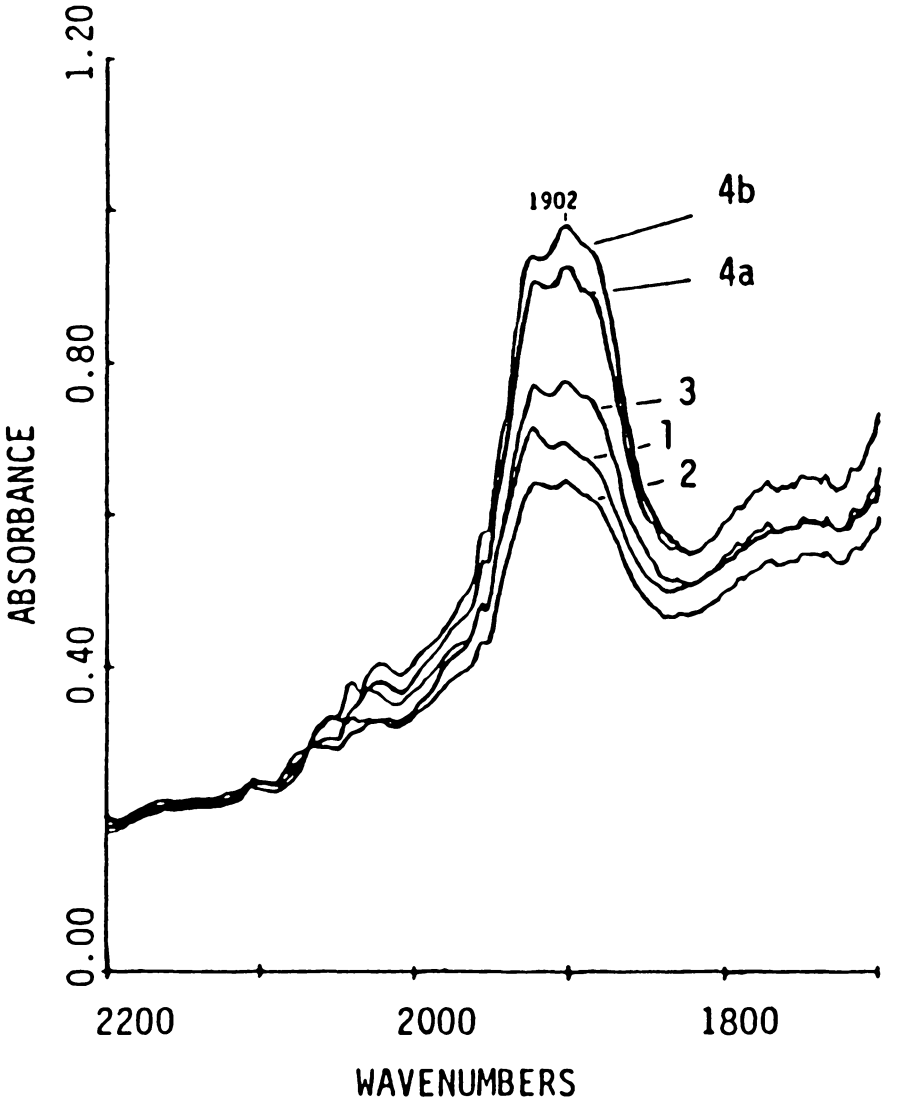

Figure 3.10. Addition of $P(t\text{-}Bu)_3$ to NaY wafer with adsorbed $Co_4(CO)_{12}$ absorbed on NaY shown in trace (1); (2) after immersion into $Co_4(CO)_{12}$ solution; (3) after second immersion; (4a) after addition of $Co_4(CO)_{12}$ solution by syringe; (4b) 5 min after addition of $Co_4(CO)_{12}$ from syringe.

In the set of spectra labeled 3.9 and 3.10, the reaction of $Co_4(CO)_{12}$ (ads), generated from $Co_4(CO)_{12}$, with $P(t\text{-}Bu)_3$ is shown. Clearly all the bands associated with the adsorbed carbonyl cluster disappear when $P(t\text{-}Bu)_3$ is added. These are replaced by a set of three bands centered at 1902 cm^{-1}. The reaction therefore appears to yield $Co(CO)_4^-$. This reaction confirms that $Co_4(CO)_{12}$ (ads) generated from $Co_4(CO)_{12}$ in solution lies on the surface.

The spectra labeled 3.11 and 3.12 represent the results from the analogous experiment represented in spectra 3.9 and 3.10 performed with the adsorbed carbonyls generated from $Co_2(CO)_8$ on NaY. (The spectra shown in Figure 3.11 are from a sample prepared similarly to the compounds whose spectra are shown in Figures 3.1 and 3.7. The spectra shown in Figures 3.1, 3.7 and 3.11 give an indication of the reproducibility of the infrared experiment.) The spectra shown in Figure 3.12 were obtained after addition of $P(t\text{-}Bu)_3$. Clearly very little of the adsorbed carbonyls react with this phosphine. Thus the majority of the chemistry with $Co_2(CO)_8$ takes place within the channels and/or cages of the faujasite.

3.5 SUPPORTED COBALT CARBONYLS REACTED WITH VARIOUS LIGANDS

The spectrum obtained by the addition of methanol to $Co_2(CO)_8$ supported on NaY zeolite is shown in Figure 3.13b. In trace 3.13a, bands at 2121 and 2078 cm^{-1} can be assigned to terminal carbonyl stretching frequencies of $Co_4(CO)_{12}$ while the band at 1813 cm^{-1} is due to a bridging carbonyl of the tetramer. The broad band at 2024 cm^{-1} may be due to a non-bridged form of $Co_2(CO)_8$. The 1895 cm^{-1} peak in

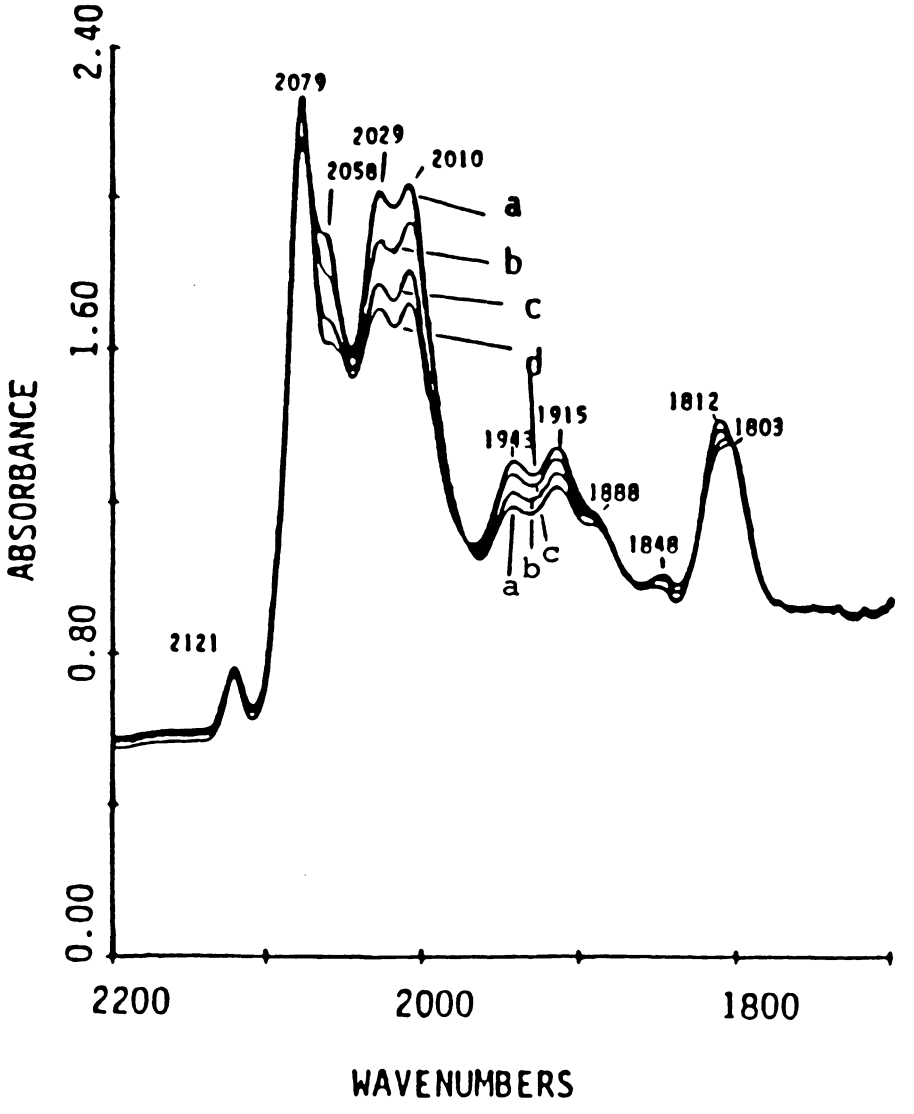

Figure 3.11. $Co_2(CO)_8$ adsorbed on NaY; (a) immediately after immersion of the pellet into $Co_2(CO)_8$ solution; (b) 2.5 min after immersion; (c) 5 min after immersion; (d) 7.5 min after immersion.

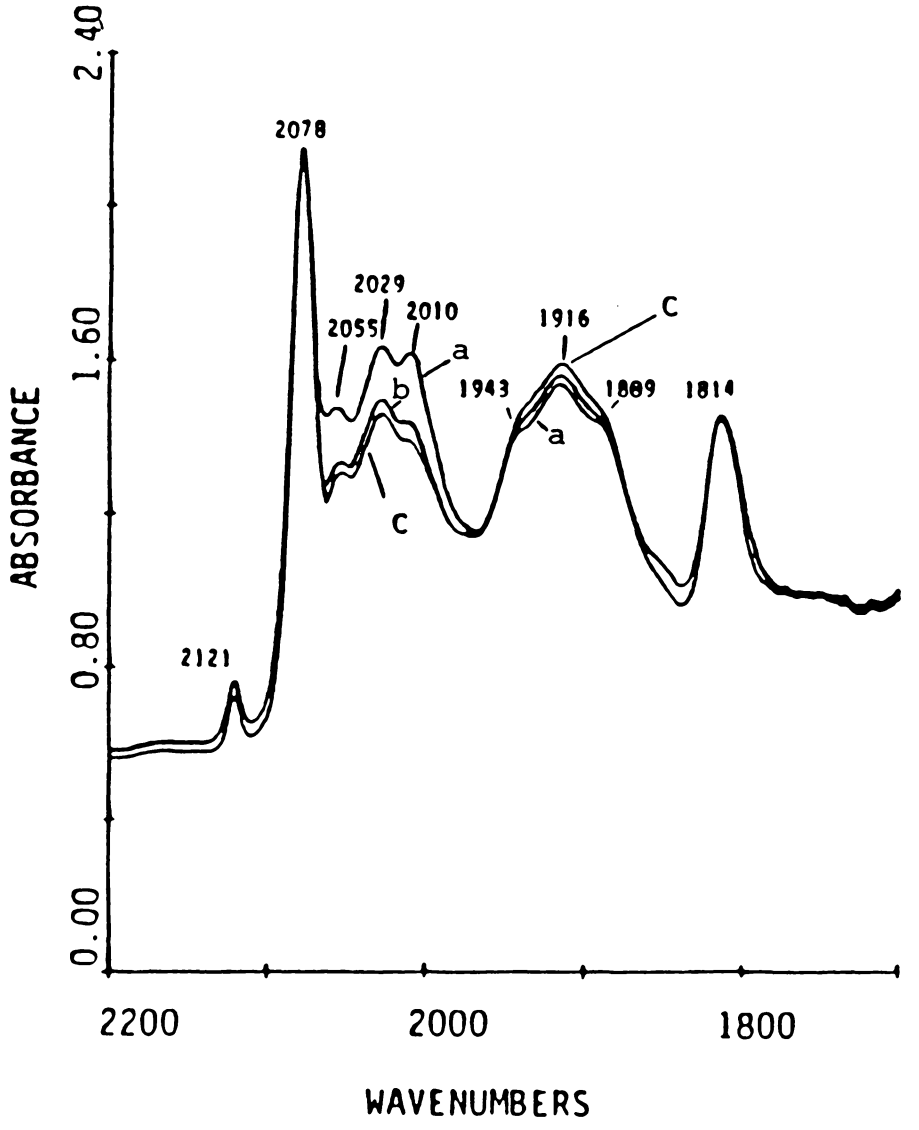

Figure 3.12. $Co_2(CO)_8$ adsorbed on NaY 10 min after immersion of the pellet into solution (trace a); (b) addition of $P(t\text{-}Bu)_3$ from syringe onto pellet; (c) 5 min after addition of $P(t\text{-}Bu)_3$.

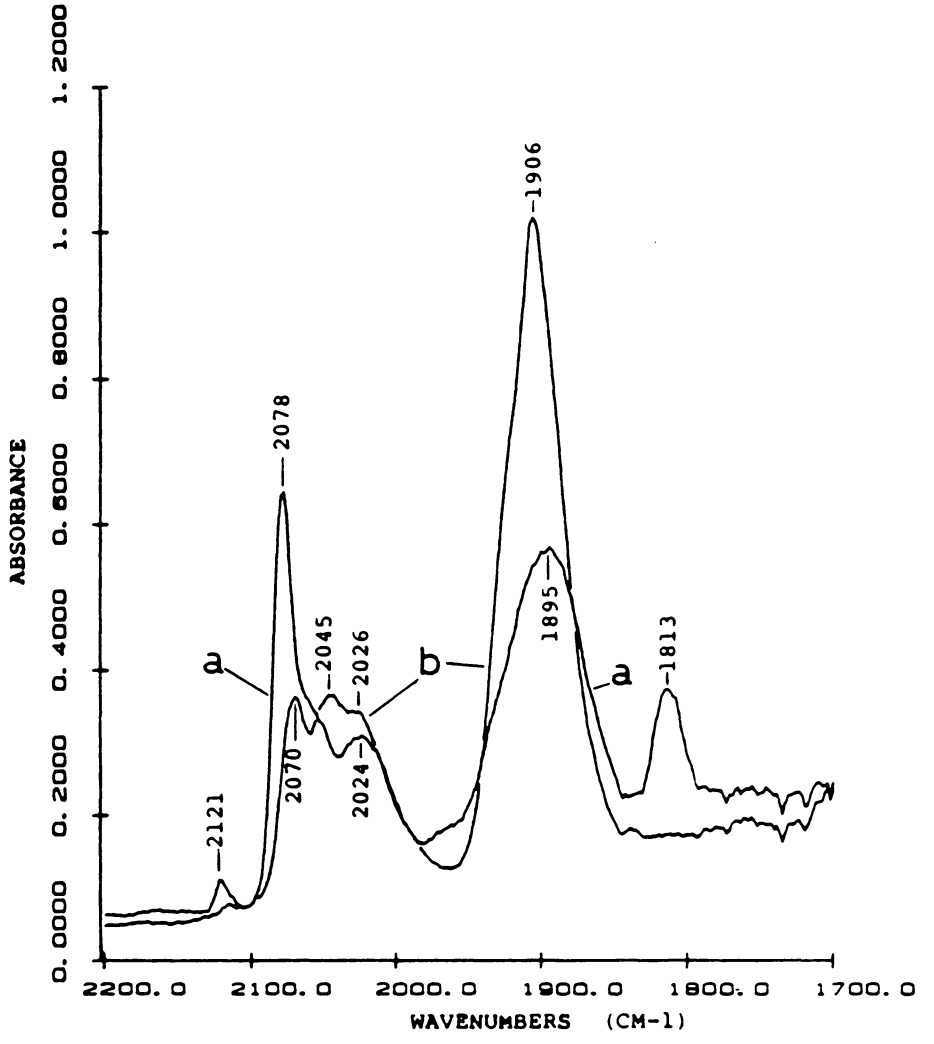

Figure 3.13. $Co_2(CO)_8$ supported on NaY 30 min after immersion of the pellet into solution (a) and addition of methanol by syringe onto pellet (b).

spectrum 3:13a arises from the anion, $Co(CO)_4^-$.

When methanol is syringed on the impregnated pellet, depicted in trace 3.13b, a dramatic increase in the region around 1900 cm^{-1} occurs due to the absorption of the anion, $Co(CO)_4^-$, with a concurrent loss in intensity of the peaks at 2121, 2078 and 1812 cm^{-1}. This indicates disproportionation of $Co_2(CO)_8$ and $Co_4(CO)_{12}$ induced by methanol to give $Co(CO)_4^-$ and an associated cation. The bands at 2070, 2045 and 2026 cm^{-1} in spectrum 3.13b may be due to a cation such as $[Co(CO)_3(MeOH)_2]^+$. The set of spectra in Figure 3.14 indicate the transformations which ensue when a NaY pellet wet with methanol is loaded with $Co_2(CO)_8$. Trace 3.14a illustrates the NaY pellet with methanol syringed onto its surface. Only one slight absorption is observed at 2044 cm^{-1}. Spectrum 3.14b shows the same pellet immediately after a pentane solution of $Co_2(CO)_8$ has been syringed on it. The absorbance bands at 2115, 2073, and 2042 cm^{-1} are be assigned to terminal carbonyls of $Co_2(CO)_8$ and the 1848 cm^{-1} peak originates from a bridging carbonyl of the dimer. The shoulder at 2026 cm^{-1} probably arises from a terminal carbonyl of $Co_4(CO)_{12}$. The band at 1903 cm^{-1} present in spectrum 3.14b which increases greatly in intensity in spectrum 3.14c can be assigned to $Co(CO)_4^-$. The terminal and bridging bands present in spectrum 3.14b are not apparent in trace c. The band at 2054 cm^{-1} in trace c may be due to $Co_4(CO)_{12}$ which has not undergone disproportionation. The 2022 cm^{-1} peak is assigned to a non-bridged form of $Co_2(CO)_8$ which may be more resistant to disproportionation than the bridged form. A cation such as $[Co(CO)_3(MeOH)_2]^+$ associated with the anion, $[Co(CO)_4]^-$, probably accounts for the absorption at 2008 cm^{-1} in trace 3.14c. The spectra

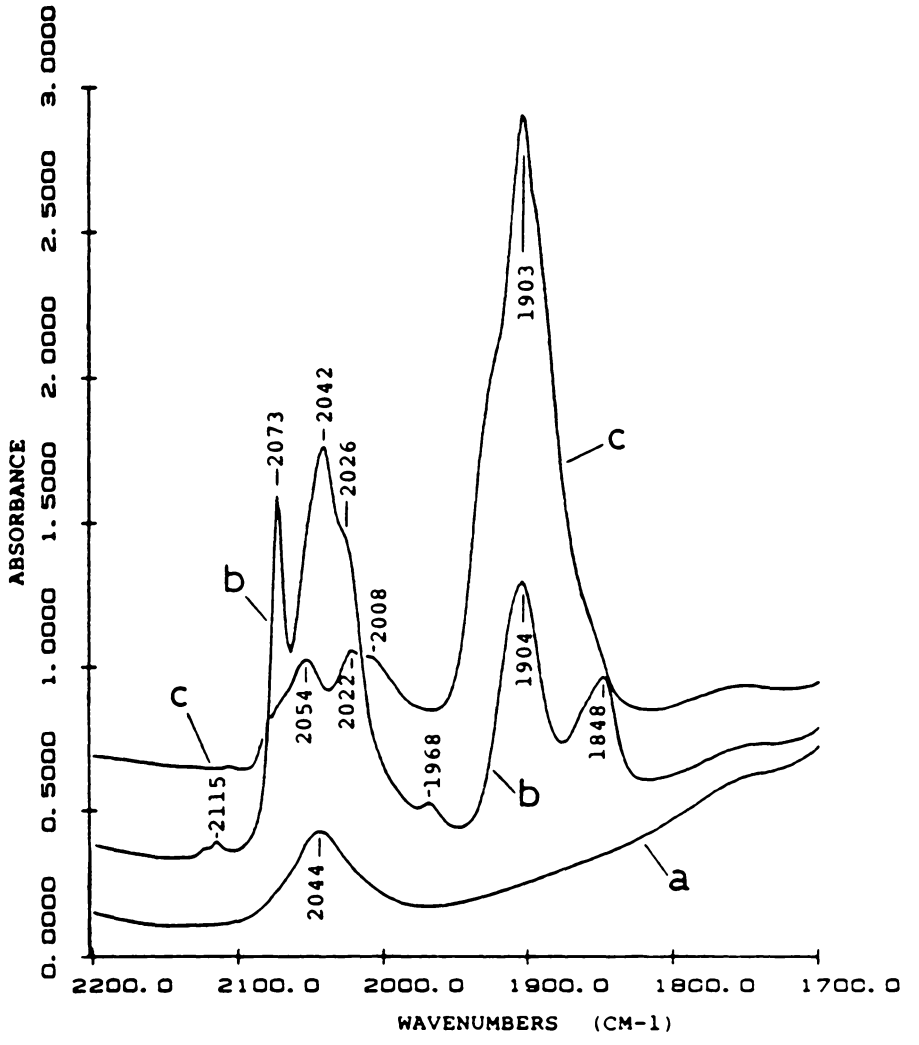

Figure 3.14. Methanol adsorbed on NaY (a), immersion of pellet into $Co_2(CO)_8$ solution (b) and 1.5 min after immersion of pellet (c).

3.13b and 3.14c are fairly similar in appearance. This suggests that the chemistry which occurs is similar whether $Co_2(CO)_8$ is supported and methanol is then added to the supported complex or whether the zeolite is impregnated with methanol prior to the addition of $Co_2(CO)_8$. In both cases it is readily apparent that methanol induces the disproportionation of cobalt carbonyl compounds to yield the anion, $Co(CO)_4^-$.

Figures 3.15a and 3.15b show the spectrum of $Co_2(CO)_8$ supported on NaY zeolite and the pellet after the addition of water, respectively. Terminal carbonyl bands at 2121, 2078, 2064, 2028 and 2020 cm^{-1} in trace a are removed from the spectrum upon the addition of water as is a bridging carbonyl band at 1815 cm-1. The terminal carbonyl bands which appear upon addition of water in trace b occur at 2115, 2068, 2045 and 2024 cm^{-1}. The 2115, 2068 and 2045 cm^{-1} peaks in Figure 3.15b can be assigned to terminal carbonyls of the bridged form of $Co_2(CO)_8$ while the band at 2024 cm^{-1} may be assigned to an all terminal carbonyl form of $Co_2(CO)_8$ or a cation such as $[Co(CO)_3(H_2O)_2]^+$. The weak band at 1835 cm^{-1} may be due to a bridging carbonyl of $Co_4(CO)_{12}$. Terminal bands of the tetramer may be hidden under bands arising from absorptions of $Co_2(CO)_8$. The most apparent difference between traces 3.15a and b is the increased intensity and splitting of the band at 1909 cm^{-1} in trace a which becomes the 1915 and 1908 cm^{-1} bands in trace b. The increase in intensity of the bands in the 1900 cm^{-1} region arises from the formation of $Co(CO)_4^-$ produced by the disporportionation of $Co_2(CO)_8$ and $Co_4(CO)_{12}$. Water appears to react less vigorously than methanol with the supported cobalt carbonyls. Certain species seem to be resistant to disproportionation induced by water although when methanol is reacted

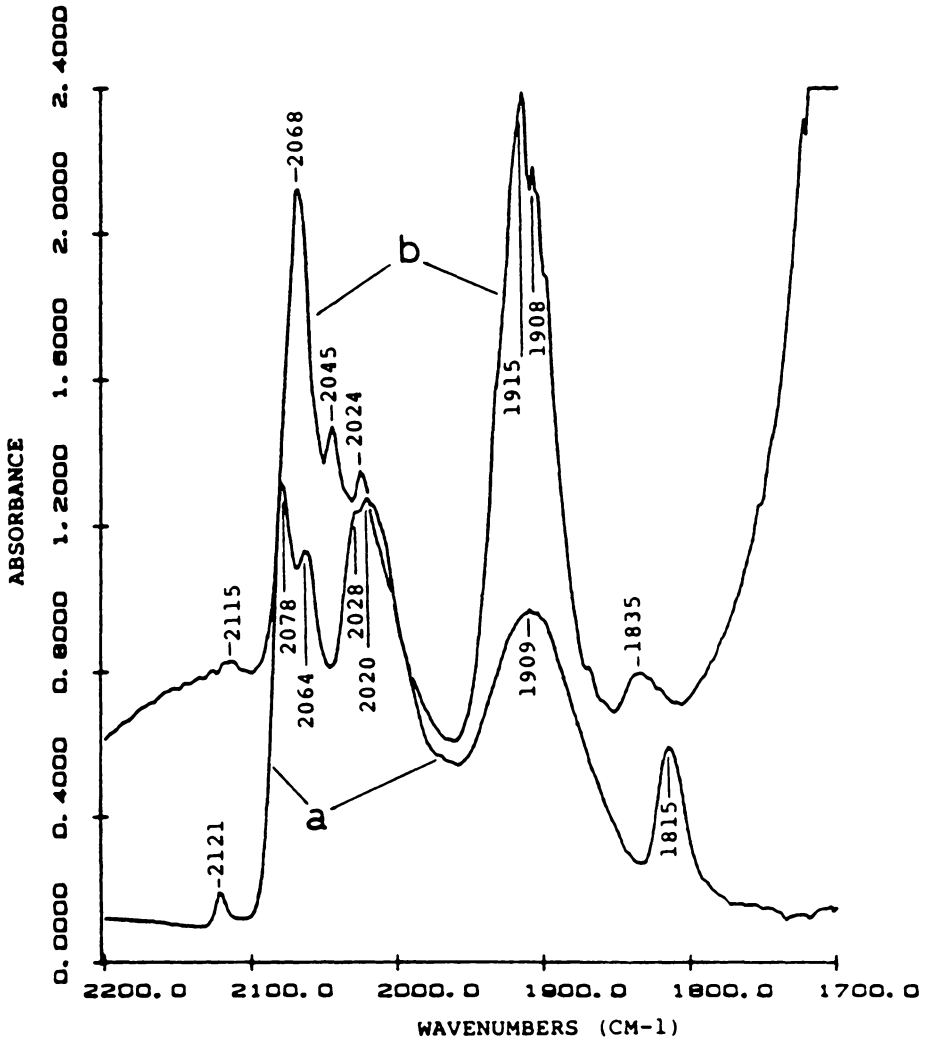

Figure 3.15. $Co_2(CO)_8$ supported on NaY (a) and after addition of water by syringe (b).

with the supported cobalt carbonyl, nearly all of the carbonyl intensity assigned to $Co_2(CO)_8$ and $Co_4(CO)_{12}$ is removed from the spectrum.

Traces a, b and c in Figure 3.16 depict a NaY zeolite wafer wet with water, the same pellet with a solution of $Co_2(CO)_8$ syringed onto it and the pellet after standing for one minute after the addition of $Co_2(CO)_8$, respectively. The very strong absorption below 1800 cm^{-1} in all three spectra is due to water present on the zeolite. When $Co_2(CO)_8$ is loaded on hydrated NaY, a spectrum is obtained which is quite different from the spectrum obtained when $Co_2(CO)_8$ is adsorbed on dry NaY. A broad band centered at 2033 cm^{-1} is observed in the terminal carbonyl region and two bands of medium intensity at 1845 and 1829 cm^{-1} are seen in the region where bridging carbonyls are located. This set of bands may be assigned to $Co_2(CO)_8$. The band at 1919 cm^{-1} in trace b is due to the anion $Co(CO)_4^-$. In a very short time, within one minute, the carbonyl bands in the terminal and bridging regions are lost leaving only one band at 1919 cm^{-1} assigned to $Co(CO)_4^-$ which increases in intensity in trace c.

The presence of water on NaY zeolite appears to affect the adsorption process and induces the disproportionation of $Co_2(CO)_8$. The results of adsorbing $Co_2(CO)_8$ and then adding water differ from the case when water is first adsorbed on the zeolite and $Co_2(CO)_8$ is then loaded on the support. When $Co_2(CO)_8$ is added to NaY wet with water, this appears to yield disproportionation as the major reaction. In the case where $Co_2(CO)_8$ is preadsorbed and water is then added, several carbonyl bands seem to be resistant to disproportionation. These two results differ from the analogous experiments performed with methanol. The

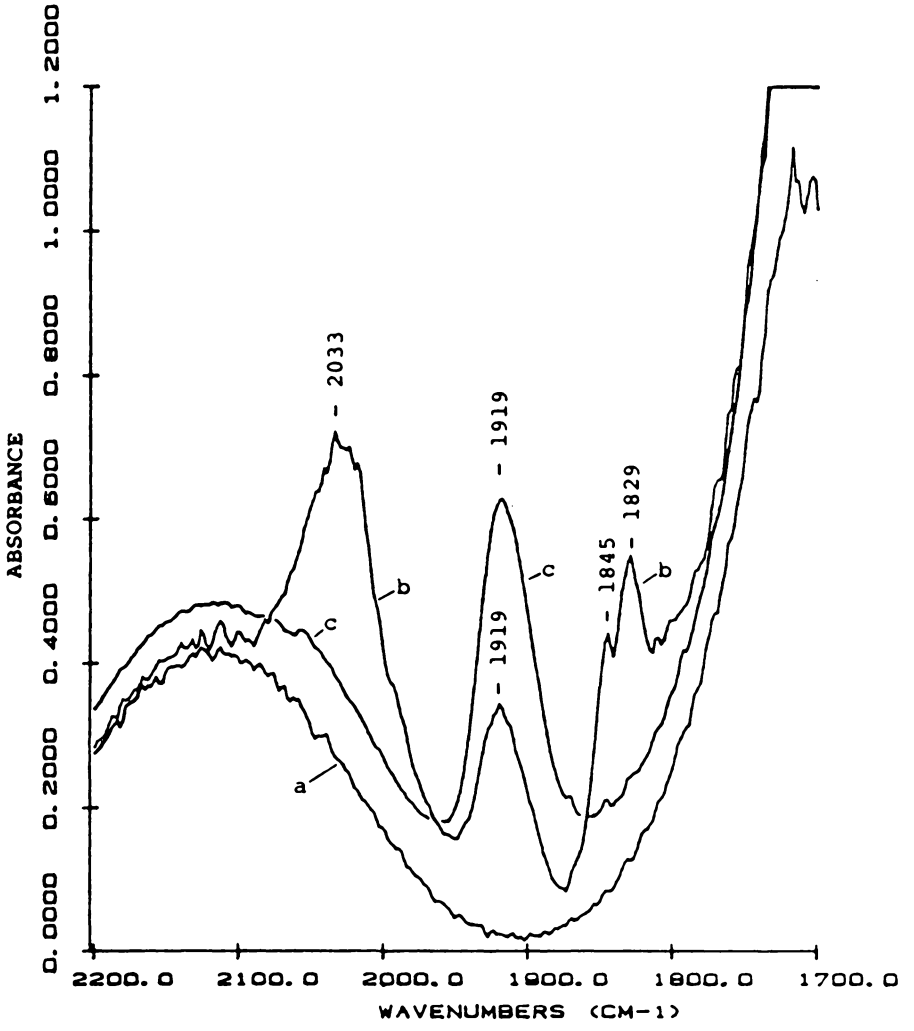

Figure 3.16. Wacer adsorbed on NaY (a), (b) addtion of $Co_2(CO)_8$ solution by syringe and (c) 1 min after addition of $Co_2(CO)_8$.

final spectrum with a strong band assigned to $Co(CO)_4^-$ indicated disproportionation results whether methanol is added to $Co_2(CO)_8$ supported on NaY or if $Co_2(CO)_8$ is added to NaY with preadsorbed methanol. The differences observed for the reactivity of supported cobalt carbonyls with water and methanol may result from the variation in size of the two ligands. Water, having a kinetic diameter of 2.65Å[5] can readily enter the small sodalite cages. Methanol and $Co_2(CO)_8$ have much larger diameters and are prohibited from entering the sodalite cages due to their larger proportions. For the adsorption experiments involving methanol, whether its addition precedes or follows the addition of $Co_2(CO)_8$ the results are expected to be similar since both molecules will adsorbed into the α-cages. In the analogous experiments conducted with water it appears that water may be adsorbed into both cage types when it is added prior to adsorption of the dimer and induces disproportionation of $Co_2(CO)_8$. When the addition of water follows adsorption of $Co_2(CO)_8$, water may preferentially diffuse into the sodalite cages and only limited disproportionation is observed.

Figure 3.17 shows a fairly heavy loading of $Co_2(CO)_8$ adsorbed on an NaY wafer 35 min after immersion of the pellet into the pentane solution in the spectrum labeled a and in the spectrum labeled b the same pellet after the addition of pyridine. Several changes occur upon addition of pyridine to the sample. In the terminal carbonyl region the band at 2121 cm^{-1} in trace a splits into two bands at 2119 and 2104 cm^{-1} upon addition of pyridine. Also, the band at 2080 cm^{-1} is lost leaving only a strong adsorption at 2074 cm^{-1} in trace b. The 2050 cm^{-1} peak in trace a sharpens on addition of pyridine being centered at 2049 cm^{-1} in

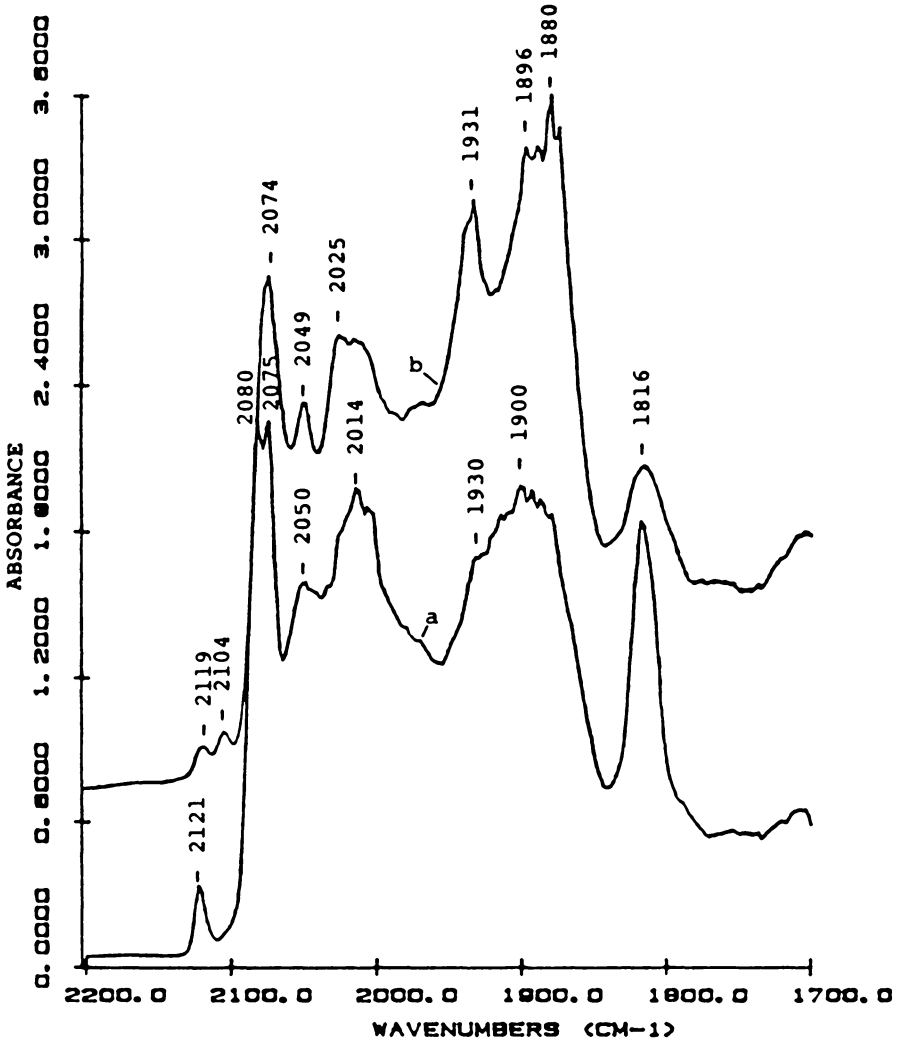

Figure 3.17. 35 min after immersion of NaY pellet into $Co_2(CO)_8$ solution (a) and (b) after addition of pyridine by syringe onto pellet.

trace b. The broad region centered at 2014 cm^{-1} in spectrum a shifts with the maxima occurring at 2025 cm^{-1} in 3.17b. In the next region where strong carbonyl absorptions occur, a broad band centered at 1900 cm^{-1} with a shoulder at 1930 cm^{-1} becomes more defined in trace b with a concurrent increase in intensity. In trace b a sharp band becomes apparent at 1931 cm^{-1} and a broad band centered at 1880 cm^{-1} with a shoulder occurring at 1896 cm^{-1}. The bridging carbonyl band at 1816 cm^{-1} looses intensity and broadens in trace b.

Pyridine appears to induce disproportionation to a slight extent as seen by the increase in intensity of the carbonyl bands in the 1900 cm^{-1} region assigned to the anion, $Co(CO)_4^-$ and the concurrent decrease in intensity of the terminal and bridging carbonyl bands. Ligand substitution may be a more important reaction pathway of supported $Co_2(CO)_8$ with pyridine. Substituted dimers and tetramers of cobalt may be the major products of cobalt carbonyl on NaY with pyridine which is a quite different result than is obtained when supported cobalt carbonyl is reacted with methanol or water.

3.6 THERMOLYSIS OF SUPPORTED COBALT CARBONYL COMPLEXES

The infrared spectrum of adsorbed $Co_2(CO)_8$ on NaY zeolite was monitored as a function of temperature. The starting point for this experiment was the steady state spectrum after adsorption of $Co_2(CO)_8$ similar to the traces in Figures 3.1, 3.7 and 3.11.

Heating slowly to 60°C causes the bands at 2028 and 2008 cm^{-1} to decrease in intensity while the bands at 1941, 1910, and 1890 cm^{-1} increase slightly. Thus additional disproportionation may take place.

The bands assigned to $Co_4(CO)_{12}$ are unaffected at 60°C. When the temperature is raised to 80°C, the $Co_4(CO)_{12}$ bands disappear rapidly. New bands appear and disappear at 2052 and 2025 cm^{-1} during the course of this experiment. At 80°C, the most intense peak is a broad absorption centered at 1918 cm^{-1}. Also, there are at least five overlapping bands between 1786 and 1701 cm^{-1}. Further heating to 100°C decreases the overall intensity of the spectrum; two broad bands remain at 1918 and 1740 cm^{-1}. The samples become black during the heat treatment so it is possible that large clusters or cobalt metal is formed during thermolysis.

3.7 CARBON MONOXIDE EVOLUTION

Dry NaX and NaY zeolites react with pentane solutions of $Co_2(CO)_8$ to completely remove the cobalt complex from solution with concurrent evolution of carbon monoxide. Many experiments were performed to quantify the evolution of carbon monoxide during the adsorption of $Co_2(CO)_8$. The quantity of CO evolved is very sensitive to reaction conditions. Up to 2 equivalents of $CO/Co_2(CO)_8$ are observed if the adsorption is conducted in a closed vessel. The time allowed for adsorption (stirring time) in the closed vessel was varied while the carbon monoxide evolved during the process was followed. The results of this experiment are given in Figure 3.18. Approximately one equivalent of $CO/Co_2(CO)_8$ is evolved fairly rapidly, within the initial 15 min of adsorption, while the second equivalent of CO is evolved more gradually. This correlates with in situ IR studies of the adsorption of $Co_2(CO)_8$ on NaY. The most dramatic changes occur in the spectrum during the first

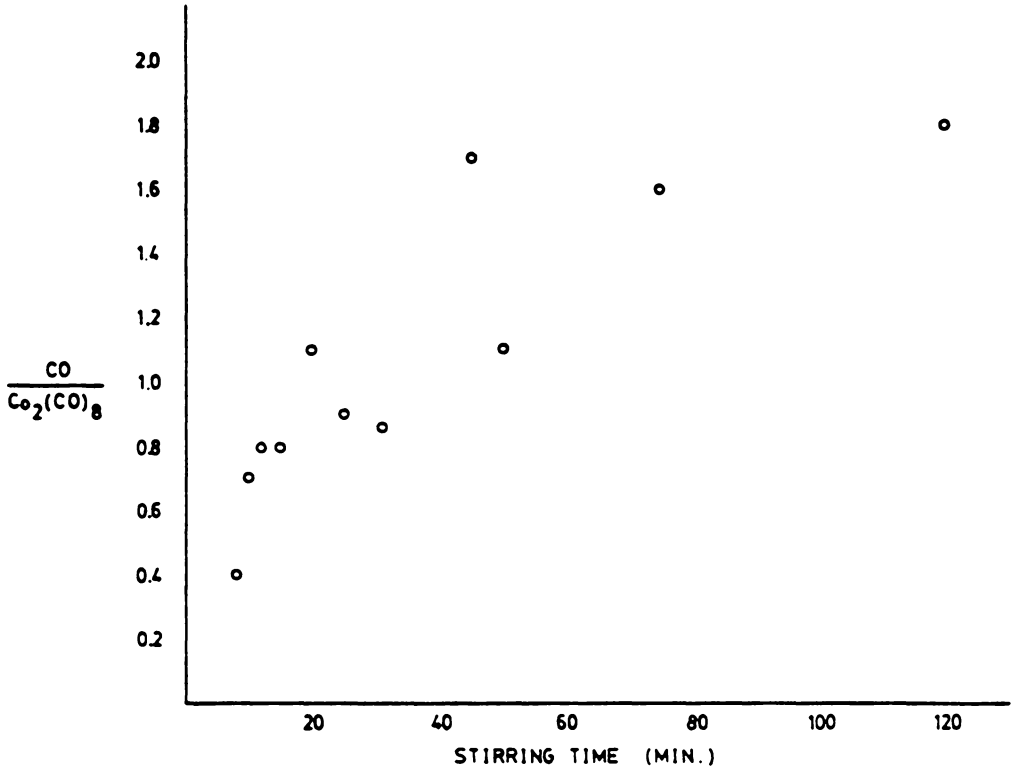

Figure 3.18. Carbon Monoxide Evolved vs. Stirring Time (Adsorption Time).

TABLE 3.4

EQUIVALENTS CO EVOLVED/$Co_2(CO)_8$ UNDER VARIOUS ADSORPTION CONDITIONS

CO / $Co_2(CO)_8$ Evolved	Conditions	Average Empirical Formula
up to 2	Static	$Co(CO)_3$ $Co_4(CO)_{12}$, $Co(CO)_4^-$
up to 4	Helium Flow	$Co(CO)_2$
up to 6	Helium Flow, 150°C	$Co(CO)$

15 min of adsorption.

When a helium purge through the vessel accompanies the adsorption, up to 4 moles of CO/mole $Co_2(CO)_8$ are evolved at 25°C. Thermolysis of adsorbed $Co_2(CO)_8$ on NaY at 150°C for 1 hour yields a total of 6 moles of CO/mole $Co_2(CO)_8$. The results of the CO evolution experiments are compiled in Table 3.4. The above experiments indicate that $Co_2(CO)_8$ is very reactive toward faujasitic zeolites. The lack of a clear cut, stoichiometric evolution of CO is consistent with the IR spectrum in that the reaction of $Co_2(CO)_8$ with NaY does not proceed by a single pathway.

The tetramer, $Co_4(CO)_{12}$ is only slightly adsorbed on NaY and probably only on the surface of the crystallites. Virtually no carbon monoxide is evolved when $Co_4(CO)_{12}$ is impregnated on NaY. In several experiments the quantity of CO evolved during adsorption of $Co_4(CO)_{12}$ was always less than 0.2 equivalents of $CO/Co_4(CO)_{12}$. Thus $Co_4(CO)_{12}$ appears to be simply physisorbed on NaY zeolite.

3.8 DISCUSSION OF INFRARED SPECTROSCOPY AND CO EVOLUTION RESULTS

The cation-exchange capacity of zeolites is well established.[5] Cobalt(II), for example, will readily replace 77% of the sodium ions in NaY zeolite.[64] Modified ZSM-5 materials may exchange cations beyond the value calculated from elemental analysis.[65] The added capacity is associated with silicate sites within the structure. Other complexes may react directly with protons on the zeolite. Also, it is known that $Rh(allyl)_3$ reacts with protonated faujasites to yield a supported rhodium complex.[66,67]

Dicobaltoctacarbonyl is adsorbed onto faujasites by chemical reaction although protons are not required for the reaction. Dry NaX and NaY zeolites react directly with pentane solutions of $Co_2(CO)_8$ to completely remove the cobalt complex from solution with concomitant evolution of carbon monoxide. Extremely high weight percent loadings of cobalt may be achieved in this fashion without precipitation of the complex onto the zeolite surface. In one experiment a 4.8 weight % loading of cobalt was obtained in which all of the $Co_2(CO)_8$ was removed spontaneously from solution. This corresponds to approximately 1.5 cobalt atoms per supercage. At low cobalt loadings (0.6-1.0 weight % cobalt) the zeolite powder is reddish-brown in color. At high weight % loadings as was sometimes achieved in the in situ IR studies the samples become black.

The tetramer, $Co_4(CO)_{12}$, reacts in a much different manner with faujasites. Only a slight quantity of $Co_4(CO)_{12}$ is extracted from pentane solution. The maximum weight percent loading obtained from the spontaneous extraction of $Co_4(CO)_{12}$ from pentane was 0.08 weight % of cobalt. This is approximately two orders of magnitude less than the amount of $Co_2(CO)_8$ adsorbed under similar conditions. Furthermore, virtually no carbon monoxide is evolved during the adsorption of $Co_4(CO)_{12}$. Thus the tetramer appears to be simply physisorbed on NaY zeolite.

These results are consistent with the fact that $Co_4(CO)_{12}$ is too large to penetrate the channels of the faujasite and therefore must be located on the surface. The dimer, $Co_2(CO)_8$, is small enough to penetrate the channels. This may account for the large capacity of

faujasites to adsorb this molecule.

The assignments proposed for various cobalt carbonyl complexes generated on NaY, NaX and HY when the supports are impregnated with $Co_2(CO)_8$ in pentane are consistent with the data of Watters et.al.[43] and Ballivet-Tkatchenko et.al.[45] which were obtained by subliming $Co_2(CO)_8$ onto these supports. The similarity of the results is somewhat unexpected since the methods of cobalt impregnation are quite different.

The bridging carbonyl band of the supported cobalt complexes is shifted to lower wavenumber compared to the complex in solution. This has been observed for $Fe_3(CO)_{12}$ on HY,[68] for carbonyl clusters on alumina[47] and for carbonyl complexes in solution with Lewis acids.[70,71] The stronger the acid-base interaction, the more pronounced is the downward shift. This may be due to hydrogen bonding of the zeolite supports to the basic oxygens of the bridging carbonyls of the cobalt complexes. The shift of the terminal carbonyl bands to higher wavenumbers may be due to movement of electron density away from the metal toward the bridging carbonyls H-bond formation, allowing less $M(d\Pi)\rightarrow CO(\Pi^*)$ back-bonding to occur with the terminal carbonyl ligands. The shifting of the terminal and bridging bands assigned to $Co_4(CO)_{12}$ was noted by Watters et.al. and from this evidence it was concluded that the tetramer must reside within the supercage of the zeolite where the Lewis acid-base interactions would be greatest. The results of this study indicate that identical spectra can be obtained for $Co_4(CO)_{12}$ adsorbed directly on the zeolite surface and for the cluster generated in situ. Therefore the IR spectrum alone indicating Lewis acid-base interaction can not be used as conclusive evidence to locate the cobalt

carbonyl cluster.

The observation of identical spectra for $Co_4(CO)_{12}$ adsorbed on the surface and on the interior of NaY is unexpected. For $Rh_6(CO)_{16}$ adsorbed on the surface of a zeolite, a different IR spectrum is observed compared to that for $Rh_6(CO)_{16}$ that is postulated to occur within the zeolite.[50,56] In the case of $Co_4(CO)_{12}$ similar sites for adsorption must exist on the surface and in the interior of NaY zeolite. It has been postulated that a site of 3-fold symmetry can be found in the supercage.[43] This allows the C_{3v} structure of $Co_4(CO)_{12}$ to retain its symmetry upon adsorption. Certainly sites of 3-fold symmetry will also exist on the surface of the zeolite crystals. This is easily seen from models of the faujasite structure; the α-cage may be terminated in such a fashion to give the β-cages in a chair conformation that has 3-fold symmetry.

The spectrum of $Co_4(CO)_{12}$ adsorbed on NaY is significantly simpler than that observed in solution. This is indicated in Table 3.1. In solution, three intense adsorptions are observed for $Co_4(CO)_{12}$ at 2062, 2054 and 1868 cm^{-1}. The adsorbed specie gives only one intense band at ~2079 cm^{-1} and a weak band at 2056 cm^{-1}. An intriguing possibility is that the cluster adopts a structure different from the C_{3v} structure observed in solution. One possibility is the D_{2d} structure with four bridging carbonyls suggested by Cotton.[72]

It is clear that NaX, NaY and HY zeolites stabilize different cobalt carbonyl moieties. On NaX, $Co_2(CO)_8$ is observed to give substantially more disproportionation to $Co(CO)_4^-$ than on NaY or HY. Also the cluster $Co_4(CO)_{12}$ adsorbed on the surface of NaX gives a

spectrum identical to its spectrum in hydrocarbon solution. When $Co_2(CO)_8$ is supported on HY, very little disproportionation occurs and the dimer appears to be stabilized on the acid form of Y zeolite. The sites for $Co_4(CO)_{12}$ and $Co_2(CO)_8$ adsorption must vary on NaX, NaY and HY zeolites. Another possibility is that the structure of $Co_4(CO)_{12}$ varies depending upon the support on which it resides.

Two independent reaction pathways appear to function for $Co_2(CO)_8$ as it is adsorbed on faujasites. These are given in equations 3.3 and 3.3 where L is used to refer to a framework oxygen of the zeolite.

$$2\ Co_2(CO)_8 \rightarrow Co_4(CO)_{12} + 4\ CO \qquad \text{(eq. 3.3)}$$

$$Co_2(CO)_8 + 2\ L \rightarrow [Co(CO)_3L_2]^+ + [Co(CO)_4]^- + CO \qquad \text{(eq. 3.4)}$$

At least one additional pathway is required to generate the species giving rise to the 1943 cm^{-1} band on NaY denoted as $Co_x(CO)_y$ in Table 3.4. Further disproportionation may occur to yield cobalt(II) salts according to equation 3.5.

$$Co_2(CO)_8 + 2\ [Co(CO)_3L_2]^+ + 8\ L \rightarrow 2\ [Co(L)_6]^{2+} + 2\ [Co(CO)_4]^- + 6\ CO \qquad \text{(eq. 3.5)}$$

Equations 3.3 and 3.4 are sufficient to explain most of the IR spectra obtained for $Co_2(CO)_8$ adsorbed on NaY and HY. On NaX the infrared absorption due to the anion is far more intense than the terminal bands in the region 2100-2000 cm^{-1} therefore it is likely that reaction of the type given by 3.5 is an important pathway on NaX zeolite.

The observations for the reaction between supported cobalt carbonyls with phosphines, methanol, water and pyridine may be explained by equations 3.6-3.9 where L' refers to the ligands mentioned.

$3\ Co_4(CO)_{12} + 24\ L' \rightarrow 4[Co(L')_6]^{2+} + 8\ [Co(CO)_4]^- + 4\ CO$ (eq. 3.6)

$Co_4(CO)_{12} + [Co(CO)_3L_2]^+ + 12\ L' \rightarrow 2\ [Co(L')_6]^{2+} + 3\ [Co(CO)_4]^- + 3\ CO$ (eq. 3.7)

$[Co(CO)_3L_2]^+ + 2\ L' \rightarrow [Co(CO)_3(L')_2]^+$ (eq. 3.8)

$Co_4(CO)_{12} + X\ L' \rightarrow Co_4(CO)_{12-x}(L')_x + x\ CO \quad x = 1\text{-}4$ (eq. 3.9)

Reactions 3.6 and 3.7 show the formation of six coordinate cobalt(II) complexes. It is possible that one or more of the added ligands denoted by L′ should be replaced by a zeolite oxygen.

The disproportionation of $Co_4(CO)_{12}$ appears to take place for the cluster both inside and on the surface as judged by its reactions with phosphines. The disproportionation of adsorbed $Co_4(CO)_{12}$ with phosphines represents a departure from the expected chemistry of this cluster although disproportionation of the cluster is known to occur with oxygen- and nitrogen-containing ligands.[63] It is apparent that the adsorbed tetramer is activated toward disproportionation.

When the supported cobalt carbonyl complexes on NaY are heated, bands assigned to $Co_4(CO)_{12}$ loose intensity while new bands at 2052, 2025 cm^{-1} and several bands between 1786 and 1701-1 become observable. The occurrence of bands in the 1700 cm^{-1} region may suggest μ^3-CO ligands and therefore a cluster of high nuclearity, possibly $Co_6(CO)_{15}^{2-}$. This anion decomposes in solution at 135-185°C. Reactions which account for the production of the hexacobalt cluster are given in equations 3.10 and 3.11.

$7\ [Co(L)_6][Co(CO)_4]_2 \rightarrow 3\ [CoL_6][Co_6(CO)_{15}] + 11\ CO$ (eq. 3.10)

$5\ [CoL_6][Co(CO)_4]_2 + 6\ L' \rightarrow [CoL_6'][Co_6(CO)_{15}] + 2\ Co_4(CO)_{12}$ (eq. 3.11)

The cluster, $Co_6(CO)_{15}^{2-}$, is too large to reside within the α-cage of

the zeolite. If indeed this cluster is formed it must reside on the surface of the crystallites.

CHAPTER IV.

METHANOL CARBONYLATION

4.1 INTRODUCTION AND LITERATURE SURVEY ON METHANOL CARBONYLATION

Recently, a great deal of effort has been directed toward the synthesis of a heterogeneous rhodium-based methanol carbonylation catalyst.[3,73-80] Rhodium has been supported on polymer carriers,[76] activated carbon,[77] alumina,[78] and zeolites.[3,73-75,79,80] Rates for conversion of methanol reported for many of the insoluble catalyst systems investigated are much lower than those found for the homogeneous case. Some zeolite incapsulated rhodium complexes display catalytic activity which approaches that of the homogeneous catalyst.[75] Another difficulty found with the heterogeneous catalysts is leaching of the metal from the support. The expense of rhodium metal prohibits use of a supported catalyst where leaching is a significant problem.

Very little research has been conducted concerning the investigation of a heterogeneous cobalt based methanol carbonylation catalyst. The major disadvantages of the cobalt catalyst are its lower selectivity and activity compared with the rhodium system. The disadvantages of cobalt may be compensated by its much lower cost relative to rhodium.

Mirbach[94,95] studied the reaction of $Co_2(CO)_8$ in methanol in the presence of potassium iodide under pressure of synthesis gas. IR and UV spectroscopy and polarography indicated that $[Co(MeOH)_6][Co(CO)_4]_2$ was the sole product observed in solution resulting from the disproportionation of $Co_2(CO)_8$. From IR spectroscopy conducted in this work which was discussed in Chapter 3, it appears that similar chemistry is also observed for zeolite supported cobalt carbonyls. The disproportion-

ation product of $Co_2(CO)_8$ may be the active specie or a precursor to the methanol carbonylation catalyst.

The results to be discussed refer to the catalyst designed by supporting $Co_2(CO)_8$ on NaY zeolite which was applied to the methanol carbonylation reaction. The reactivity of the cobalt system displays significant differences from the rhodium system with respect to reactivity and selectivity. The supported cobalt catalyst is observed to possess greater activity than the homogeneous cobalt complex. Thus the zeolite in conjunction with the supported cobalt carbonyls appears to enhance the activity in the carbonylation process.

4.2 METHANOL CARBONYLATION CONDUCTED IN A BATCH REACTOR

Zeolite supported $Co_2(CO)_8$ is an active catalyst for the carbonylation of methanol. The supported cobalt system demonstrates significant differences from reported rhodium systems.[73-76, 78] The major products observed in the carbonylation of methanol using $Co_2(CO)_8$ supported on NaY are methyl acetate, CH_3COOCH_3, and acetaldehyde dimethyl acetal, $CH_3CH(OCH_3)_2$, with the minor products being dimethyl ether and water. Acetic acid is not observed as a product. Any acetic acid which may form is assumed to be converted rapidly to methyl acetate in view of the large excess of methanol present in the system. The major product reported for methanol carbonylation using a supported rhodium catalyst is methyl acetate with the minor products being acetic acid, dimethyl ether and water. No reports of the formation of acetaldehyde dimethyl acetal have been found. This may be due to the

high partial pressure of hydrogen used in conducting the methanol carbonylation with the cobalt carbonyl catalyst.

Table 4.1 compares a methanol carbonylations experiment performed with $Co_2(CO)_8$ in a homogeneous fashion to an average of three runs with the supported $Co_2(CO)_8$/NaY catalyst conducted under identical conditions of temperature, partial pressures of CO and H_2 and total $Co_2(CO)_8$ concentration. Several significant points should be noted. The activity denoted by the turnover based on methyl acetate production, N_{MA} and based on the combined production of methyl acetate and acetaldehyde dimethyl acetal, N_{TOT} and the rate of the reaction indicated by the turnover numbers based on methyl acetate and the combined production of the two major products, N^*_{MA} and N^*_{TOT}, respectively, is greater for the heterogeneous catalyst than for the homogeneous case. This result is unusual since supporting a homogeneous catalyst generally decreases its activity. The zeolite in conjunction with the cobalt carbonyls appears to facilitate the catalysis. The selectivity for methyl acetate is somewhat greater in the homogeneous reaction being about 80% selective while in the heterogeneous case the selectivity is about 65%. Also, in the homogeneous reaction the formation of the byproducts dimethyl ether and water is about twice as great as is their production in the heterogeneous reaction. Ethanol is a minor product in the homogeneous catalysis whereas this is not observed under heterogeneous conditions.

The supported cobalt carbonyl catalyst is sensitive to the reaction temperature and the partial pressure of hydrogen. Table 4.2 gives a comparison of the methanol carbonylation reaction as the temperature and partial pressure of hydrogen is varied. The results of

TABLE 4.1

HOMOGENEOUS CATALYST VS. HETEROGENEOUS CATALYST ACTIVITY

System	N_{MA}	N^*_{MA} (hr^{-1})	N_{TOT}	N^*_{TOT} (hr^{-1})	MA/DA
Homogeneous	57	3.5	70	4.4	4.3
Heterogeneous	74 ± 4	4.7 ± 0.2	101 ± 10	8.3 ± 3.5	2.1 ± 0.4

$$N_{MA} = \frac{\text{moles methyl acetate (MA) produced}}{\text{moles Co}}$$

N^*_{MA} = N_{MA}/duration of batch reaction (hr)

$$N_{TOT} = \frac{\text{moles methyl acetate + acetaldehyde dimethyl acetal (DA)}}{\text{moles Co}}$$

N^*_{TOT} = N_{TOT}/duration of batch reaction (hr)

MA/DA = moles MA / moles DA produced

TABLE 4.2

METHANOL CARBONYLATION CATALYST ACTIVITY UNDER VARIOUS CONDITIONS

P(psi) CO	P(psi) H_2	T (°C)	Rate [a] (hr^{-1})	M.A./D.A.
600	200	200	5.7	1.6
600	---	200	0.3	16.0
600	400	100	0.5	1.0
600	---	100	---	---

a) Rate based on methyl acetate production

the two runs conducted at 100°C with and without hydrogen present indicates that the activity is low at this temperature but increases in the presence of hydrogen. Comparing these results to those for the reaction conducted at 200°C, it can be seen that the rate of the reaction is much greater at 200°C and the presence of hydrogen appears to be required for significant production of acetaldehyde dimethyl acetal.

Table 4.3 compares the cobalt carbonyl/zeolite catalyst to several supported rhodium catalysts. The selectivity of the heterogeneous cobalt system is similar to the selectivity observed for the rhodium catalysts. The activity of the cobalt system is similar to the rates observed for the supported rhodium system conducted under mild conditions namely the $RhCl(CO)(Pp)_2$ where Pp refers to a phosphinated polymer support and $Rh(CO)Cl(PPh_3)_2/Al_2O_3$ catalysts. Comparing the cobalt system to the rhodium catalysts used under more severe conditions, specifically the [Si]-ORh(allyl)H and the [Z-X]-ORh(allyl)H catalysts, it can be seen that the cobalt catalyst is much less active. The lower activity of the cobalt system may be compensated by its much lower cost when compared with rhodium.

4.3 DISCUSSION OF METHANOL CARBONYLATION RESULTS

Several conclusions can be made concerning the results of the methanol carbonylation conducted with the cobalt carbonyl/NaY catalyst. The zeolite appears to facilitate the catalysis since the rate of the reaction increases and the production of acetaldehyde dimethyl acetal is greater with its inclusion in the system. Some cobalt leaches from the

TABLE 4.3

COBALT-BASED CATALYST VS. RHODIUM-BASED CATALYSTS

Methanol Carbonylation

Catalyst	P (psi)	T (°C)	Rate[b] (hr^{-1})	Selectivity[b] (%)
$Co_2(CO)_8$/NaY [a]	800	200	5.7	60
$RhCl(CO)(P_p)_2$ [c]	15	100	11	40
$Rh(CO)Cl(PPh_3)_2$/Al_2O_3 [d]	15	200	55	76
[Si]-ORh(allyl)H [e]	500	200	133	52
[Z-X]-ORh(allyl)H [e]	1000	200	1090	89

a) 1.8 wt % Co on NaY, 25 ml CH_3OH, 80 ul CH_3I, 600 psi CO, 200 psi H_2

b) Rate and selectivity are based on methyl acetate production

c) B. C. Gates, J. Catal. 40(1975) 255.

d) A.Krzywicki and G. Pannetier, Bull. Soc. Chim. Fr. (1975) 1093.

e) Hai-Nang Huang, Jeffrey Schwartz and Nobumasa Kitajima, J. Mol. Catal., 22 (1984) 389.

zeolite, 12 ± 2%, during the reaction as indicated by DCP conducted on samples of the reaction products. The cobalt leached into solution however is not active in catalyzing the carbonylation. Product solutions filtered from the catalyst under nitrogen exhibited no further synthesis of methyl acetate or acetaldehyde dimethyl acetal when run under conditions necessary for the reaction though these solutions did exhibit a 25% conversion of acetaldehyde dimethyl acetal to methyl acetate. Hydrogen appears to hold a key role in the catalysis by increasing the formation of acetaldehyde dimethyl acetal. Hydrogen may be necessary in stabilizing cobalt in its low oxidation state and may be required to reduce an intermediate leading to the formation of acetaldehyde dimethyl acetal. Temperature is also important as a 100°C increase in temperature enhances the rate of the reaction significantly. The zeolite alone is inactive in catalyzing the reaction as was shown by conducting the reactions with a clean NaY sample with no metal carbonyl present. The rate of the reaction decreases with time. The catalyst displays an overall turnover number of 9.0 ± 0.3 hr^{-1} during the initial 3 hours of a run which then declines to 4.7 ± 0.2 hr^{-1} after 16 hours. The catalysts are inactive and can not be reused after one 16 hour run indicating that deactivation has taken place. When attempts were made to reuse the catalysts, no product formation was observed. Initially the catalysts are light brown in color but become pink after a catalytic run. This may suggest that a change in the oxidation state of cobalt occurs during the reaction which might account for the deactivation of the catalyst.

CHAPTER V.

ZEOLITE SUPPORTED COBALT AS A CATALYST FOR FISCHER-TROPSCH SYNTHESIS

5.1. INTRODUCTION AND LITERATURE SURVEY OF COBALT CATALYZED FISCHER-TROPSCH SYNTHESIS

Cobalt containing zeolites have been reported to exhibit interesting properties for the catalytic reduction of CO with H_2.[41,83-85] Cobalt exchanged zeolites reduced with cadmium atoms show a high selectivity of the synthesis of alkenes with propylene as the major product.[83] Cobalt faujasites from either $Co(CO_3)(NO)$[84] or cobalt atoms display well defined cutoffs in hydrocarbon chain length for the Fischer-Tropsch synthesis of hydrocarbons. Sublimation of $Co_2(CO)_8$ onto NaY zeolite followed by thermal decarbonylation produces a mixture of cobalt species in high and very low oxidation states which when applied to the reduction of CO exhibits formation of hydrocarbons having fairly short chain-length.[41]

Impregnation of faujasitic zeolites by adsorption of $Co_2(CO)_8$ from non-aqueous solution followed by thermal decomposition yields highly disperse supported cobalt metal. These materials are active heterogeneous Fischer-Tropsch catalysts selective in forming linear hydrocarbons of low molecular weight under relatively mild conditions. The catalysts are characterized by gas adsorption, gas evolution, XPS, x-ray powder diffraction and F-T activity under both batch and flow conditions.

5.2. CHARACTERIZATION BY GAS EVOLUTION AND GAS ADSORPTION

A light brown material is produced when $Co_2(CO)_8$ is adsorbed on the zeolite support which becomes slightly darker during thermal treatment at 200°C. After thermal treatment at 200°C for one hour in flowing helium no IR absorption appears in the carbonyl stretching region of the spectrum indicating complete decarbonylation of the supported cobalt carbonyl. The catalyst produced in this manner is air sensitive and exposure to air yields a light blue material which is inactive for Fischer-Tropsch synthesis. The blue material remains inactive even after attempting to reduce the cobalt with H_2 or $CO:H_2$ mixtures at 900 psi and 200°C.

The evolution of hydrogen was not detected either during the adsorption of cobalt carbonyl or during the thermal decomposition to yield cobalt metal. It appears that little or no oxidation of cobalt metal by residual protons occurs. This suggests that very few protons remain on the zeolite after sodium exchange and calcination pretreatments.

Irreversible oxygen titration conducted in a pulsed microreactor indicated that 0.38 moles O_2 were adsorbed per mole cobalt. Under similar conditions neither H_2 nor CO was irreversibly adsorbed. Under the assumption that one oxygen atom is absorbed per cobalt, 76% of the cobalt atoms are accessible to oxygen. Alternatively, if all the cobalt atoms are accessible to oxygen but only those in the zero oxidation state react then an average oxidation of 0.48 may be calculated. The former interpretation seems more probable in view of the fact that no H_2 is evolved during thermal decomposition of the cobalt carbonyl.

Reuel and Bartholomew[40] have reported hydrogen adsorption for alumina supported cobalt metal. For zeolite supported cobalt prepared from cobalt carbonyl, no adsorption occurs at 25°C or at 150°C under a static pressure of hydrogen. Thus the dispersion based on hydrogen adsorption at ambient or elevated temperature cannot be calculated. Hydrogen adsorption was also studied at -196°C. The adsorption isotherm for the cobalt impregnated zeolite relative to the zeolite support without metal is given in Figure 5.1. The adsorption due to cobalt is approximately 3 torr throughout the range of the isotherm. In accordance with the hydrogen adsorption stoichiometry given by Reuel and Bartholomew[40], this indicates that 0.78 mole of hydrogen atoms are adsorbed per cobalt atom. This result is in agreement with the oxygen adsorption data indicating that the cobalt is approximately 80% disperse or that about 80% of the cobalt present is available to adsorb hydrogen. Table 5.1 summarizes the results of the gas adsorption experiments.

5.3. CHARACTERIZATION BY X-RAY POWDER DIFFRACTION, SCANNING ELECTRON MICROSCOPY AND X-RAY PHOTOELECTRON SPECTROSCOPY

A signal was not observed for cobalt metal or cobalt oxide in the x-ray powder diffraction spectrum on cobalt/zeolite samples prior to or after catalysis. This evidence suggests that cobalt particles greater than 50 Å are not present on the zeolite. A similar result was obtained when SEM was applied to the cobalt zeolite samples prior to and after catalysis. With the maximum resolution used, no indication of cobalt metal or cobalt oxide was apparent. A typical scanning election micrograph is given in Figure 5.2.

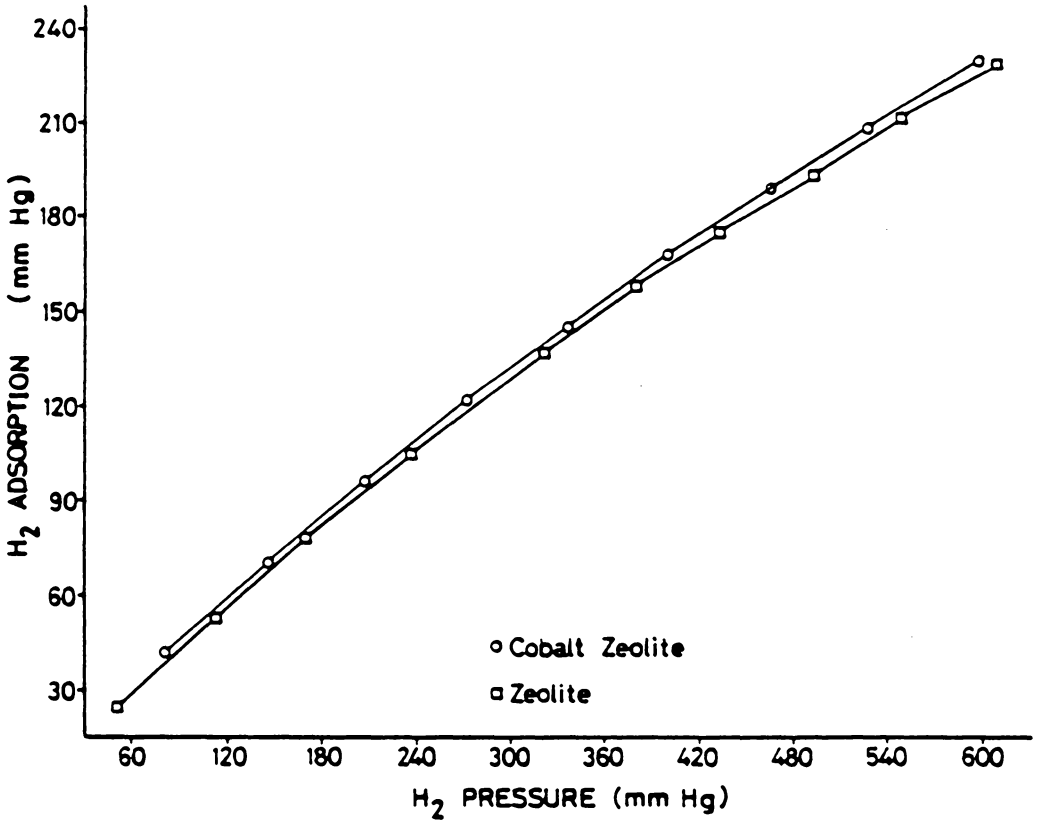

Figure 5.1. Adsorption isotherms for zeolite support and cobalt impregnated zeolite at -196°C.

TABLE 5.1

GAS ADSORPTION BY PULSE TECHNIQUE ON COBALT/ZEOLITE CATALYST

Gas	Moles adsorbed/ Mole Co	Oxidation State	Accessible Metal
O_2	0.38	0.48	76 %
CO	0	----	--
H_2	0	----	--

25000x

Figure 5.2. Scanning electron micrograph of cobalt zeolite catalyst. (Bar is equivalent to 0.5 μ)

The weight percent of metal calculated from XPS data and from actual loading shows fairly good agreement of samples prior to catalysis, 0.078 and 0.032 weight % cobalt, respectively. XPS spectra are shown in Figures 5.3 and 5.4 for a 3.4 weight % cobalt sample. Figure 5.4 represents the sample following 50 min. of argon ion sputtering. Peaks at 779.1 and 794.0 eV are indicative of Co° while peaks at 783.2, 797.6 and 804.1 eV arise from Co^{2+}.[97] The concentration of Co° appears to increase following argon ion sputtering. This may be an artifact of reduction of Co^{2+} by argon ion sputtering. Exposure to air encountered in transferring the samples to the XPS instrument may account for the presence of the high concentration of Co^{2+} in the materials.

5.4. FISCHER-TROPSCH SYNTHESIS CONDUCTED IN A BATCH REACTOR

For Fischer-Tropsch synthesis conducted in the batch reactor, results were obtained for cobalt loadings between 1.0-1.5 and 2.0-2.5 weight % metal. All catalysts were found to be inactive below 200°C. Only those catalysts which had been subjected to thermal decomposition at 200°C were found to exhibit activity. Catalyst samples that were not thermally decomposed prior to exposure to the synthesis gas gave no production of hydrocarbon products at 200°C. Cobalt metal supported on NaX was found to be virtually inactive. Only cobalt supported on NaY displayed significant activity for Fischer-Tropsch synthesis. When octane slurries of the catalysts were used no activity was observed.

The product distribution is similar to the Schulz-Flory pattern of light hydrocarbons with a minimum at C_2 when the 2.0-2.5 weight %

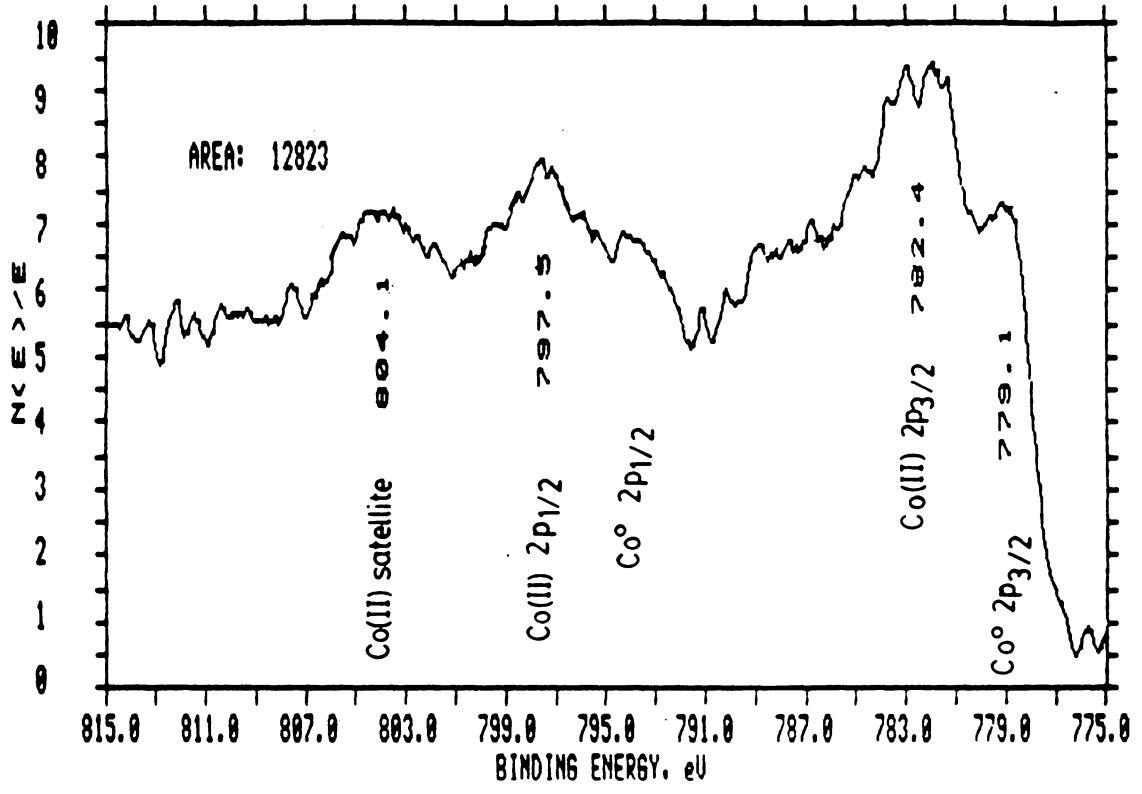

Figure 5.3. ESCA spectrum of thermally decomposed Co/zeolite Fischer-Tropsch catalyst.

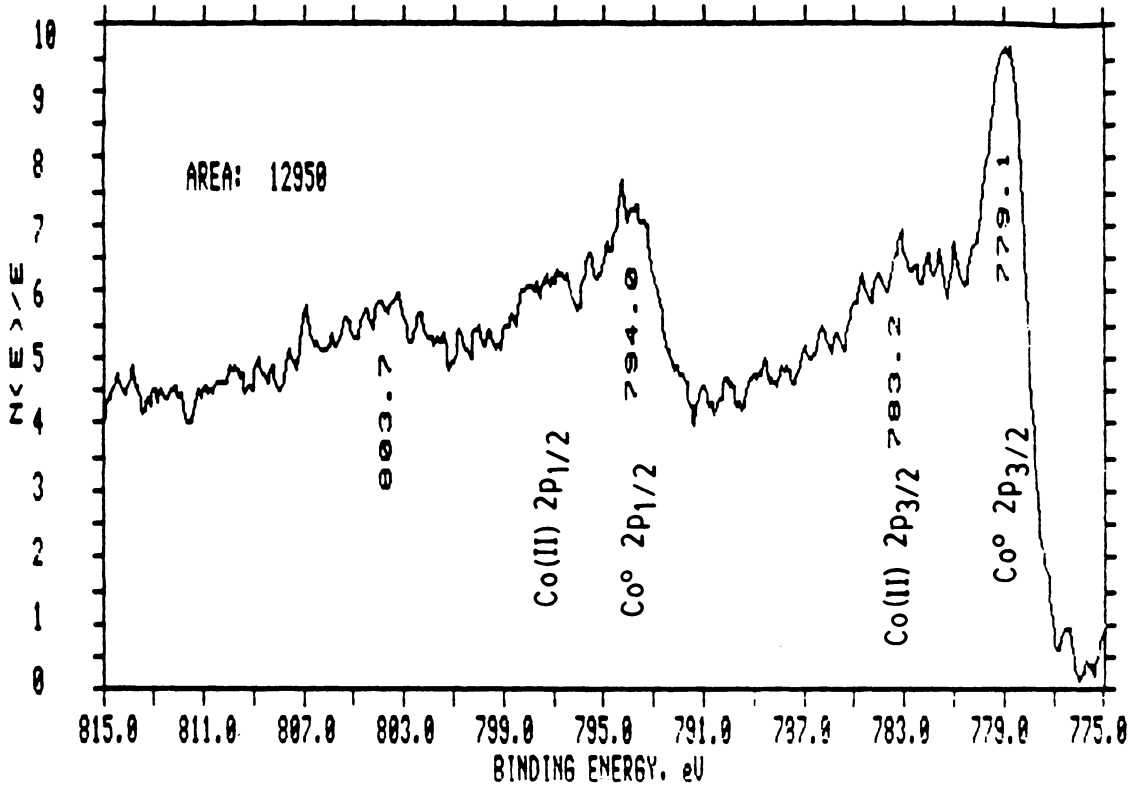

Figure 5.4. ESCA spectrum of sample shown in Figure 5.3 following 50 min of argon ion sputtering.

catalyst was used (Figure 5.5). The catalyst was selective in producing only linear alkanes. Products in the C_1-C_9 range were analyzed by venting the bomb and sampling the product stream after the run had been conducted for 16-18 hours. A pentane extraction of the catalyst indicated production of heavy olefins with a maximum at C_{12}.

The vented gas stream for the Fischer-Tropsch synthesis using the 1.0-1.5 weight % catalyst indicated linear hydrocarbon production up to C_5 with a minimum at C_4. The product distribution is similar to the Schulz-Flory pattern. Pentane extraction of the catalyst indicated production of linear hydrocarbons from C_6-C_9. Various alkali halide salts were either dry mixed or ball milled with the catalyst in an attempt to modify or enhance its activity. The product distribution remained unchanged when the salts were added to the catalyst.

Figure 5.6 displays the total CH_4 production as a function of time using a 2.0-2.5 weight % cobalt catalyst. The activity of the catalyst is constant for the first two hours of the run and then declines. After 20 hours, the catalyst is inactive. The production of other light hydrocarbons follows a similar pattern though the activity of the catalyst decreases as the chain length of the product increases. The turnover number based on CH_4 production in the first two hours is 6.2 hr^{-1}.

5.5. FISCHER-TROPSCH SYNTHESIS CONDUCTED IN A DIFFERENTIAL REACTOR

When the Fischer-Tropsch synthesis was conducted in a high pressure flow system, the catalyst was again selective for linear hydrocarbons. Only light hydrocarbons, C_1-C_4, were observed in the product stream.

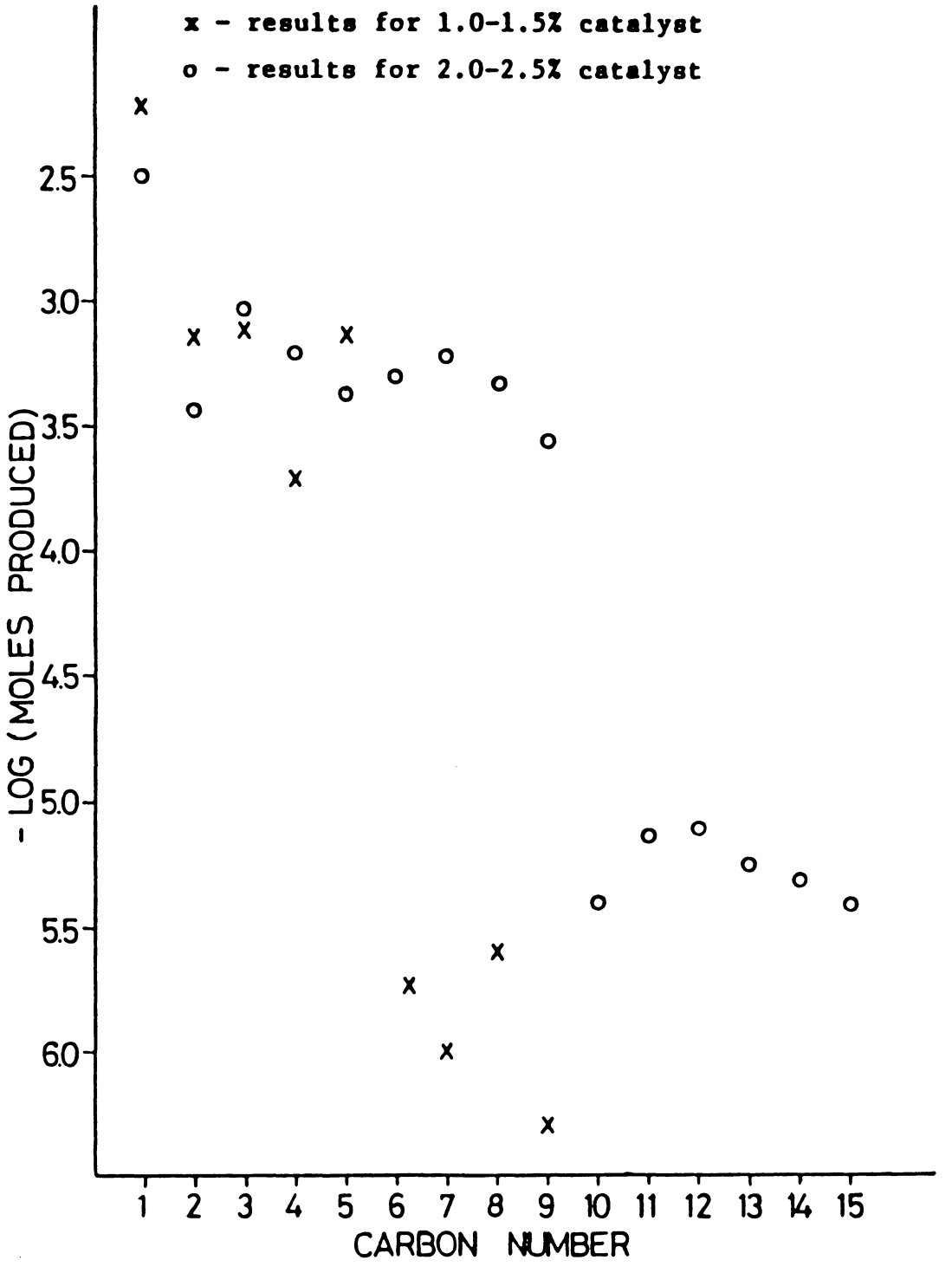

Figure 5.5. Total hydrocarbon production vs. carbon number conducted in a batch reaction.

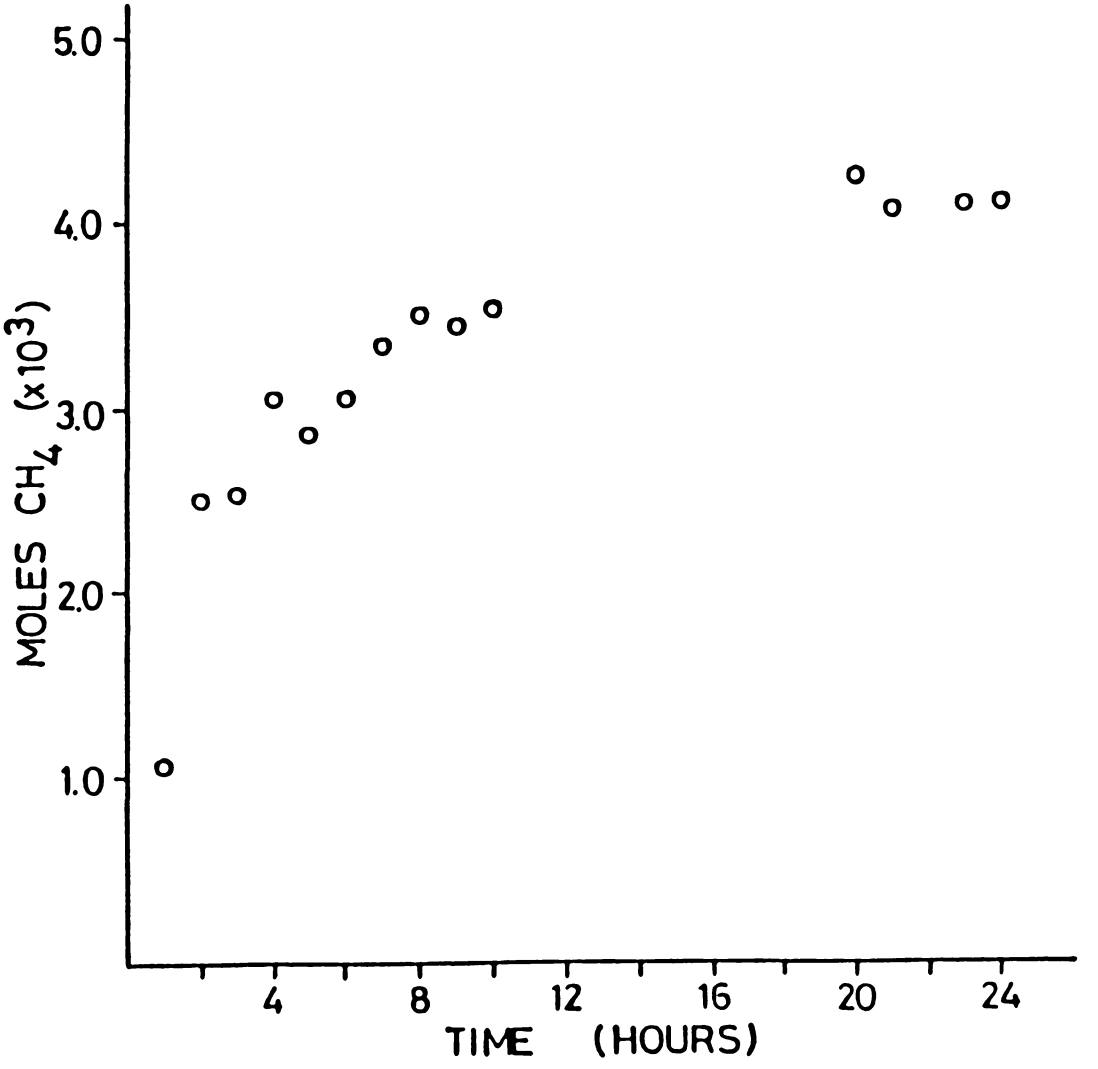

Figure 5.6. Methane production as a function of time for F-T synthesis conducted with 2.1 wt% catalyst in a batch reactor.

When the catalyst from the flow reactor was extracted with pentane, heavier hydrocarbons were not observed. Figure 5.7 displays the total moles of products formed as a function of time. The catalytic activity appears to decline after about 10 hours with an initial induction period of 2 hours for CH_4 production. Hydrocarbon production is observed for over 260 hours. The induction period for production of ethane and propane is somewhat longer, 4 and 10 hours, respectively. Production of C_2 and C_3 hydrocarbons is very similar and the activity for their production remains fairly constant throughout the run. Butane is not observed until over 30 hours into the run and in very low yields.

Figure 5.8 shows hydrocarbon production throughout the Fischer-Tropsch run at various points in time. Activity for CH_4 approaches a maximum at about 8 hours into the run and then declines. Sites responsible for CH_4 production may undergo poisoning to account for the loss in activity. The activity for C_2-C_4 hydrocarbons remains fairly constant throughout the run though the catalyst is much less active for C_2-C_4 production than for CH_4 production.

5.6. DISCUSSION OF FISCHER-TROPSCH RESULTS

Cobalt faujasites generated from cobalt carbonyl contain highly dispersed cobalt metal and are active for Fischer-Tropsch synthesis under mild conditions. Using $Co_2(CO)_8$ as the source of cobalt eliminates the necessity of reducing the cobalt as in ion-exchange methods. The presence of metallic cobalt on the zeolite is consistent with the lack of hydrogen evolution during cobalt deposition or thermal treatment. The XPS spectrum gives evidence for the presence of cobalt

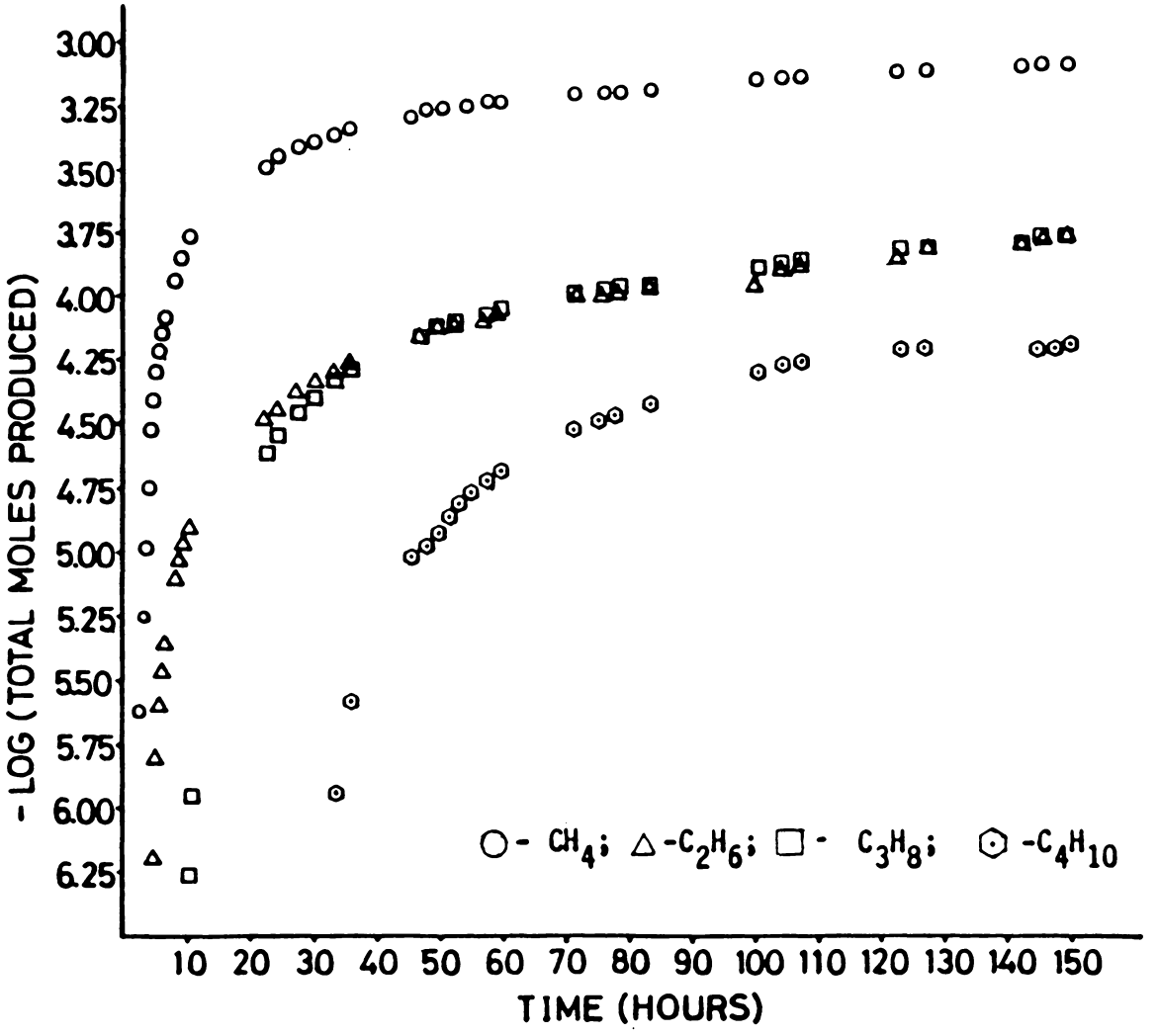

Figure 5.7. Total hydrocarbon production as a function of time for the F-T synthesis conducted in a differential reactor.

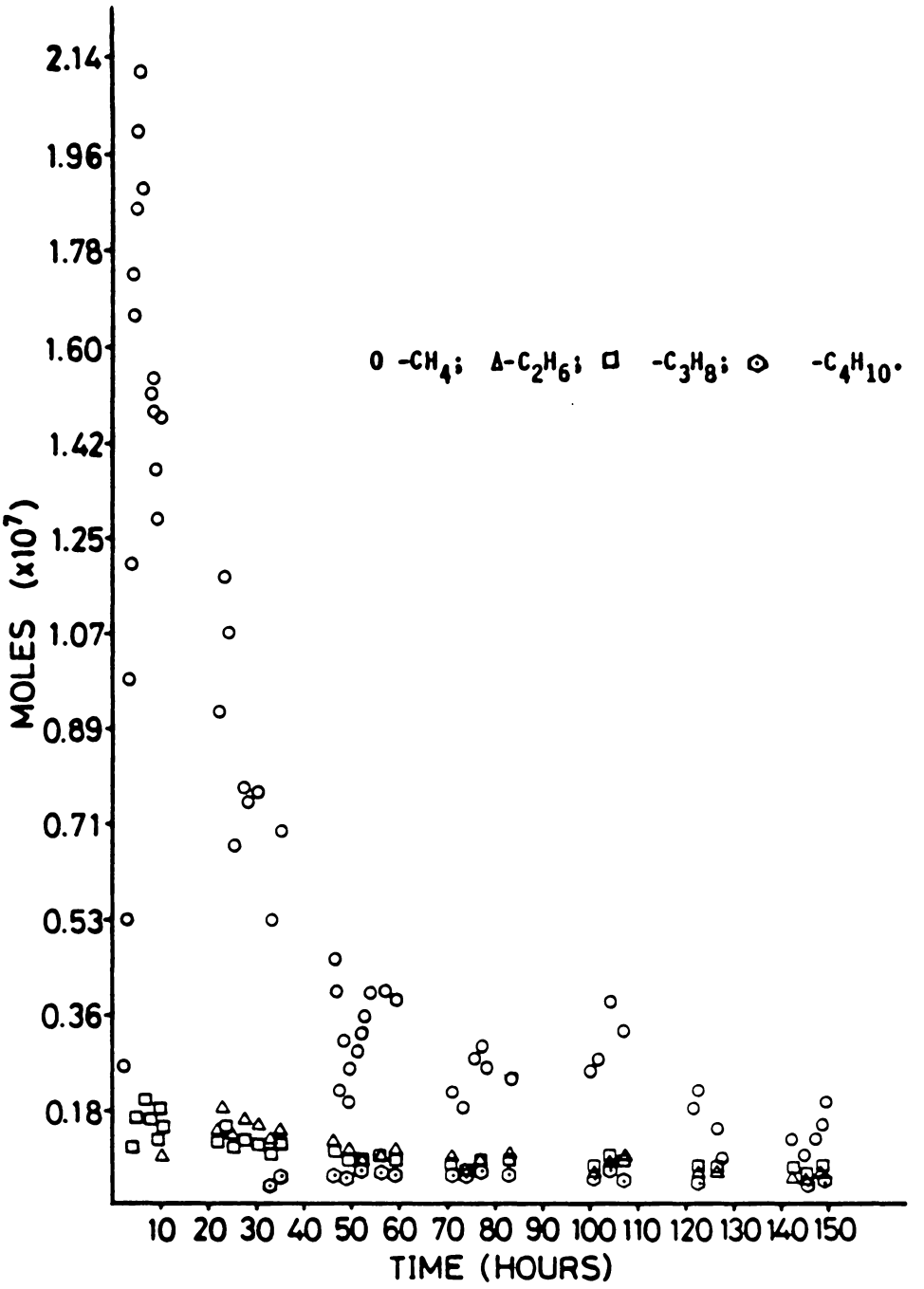

Figure 5.8 Hydrocarbon production at various time intervals for the F-T synthesis conducted in a differential reactor.

metal. Titration of the supported cobalt with oxygen in flowing helium shows that at least 70% of the cobalt irreversibly adsorbs oxygen at 25°C. If the reaction stoichiometry is such that the end product for adsorption is CoO, the most probable cobalt oxide to form under the conditions used for oxygen adsorption, then 24% of the cobalt present initially is either already oxidized or is unavailable for reaction with oxygen.

Decarbonylation of cobalt carbonyl on NaY zeolite to yield cobalt metal is an irreversible process hence no CO is readsorbed under flowing conditions after thermal treatment at 200°C. The lack of hydrogen adsorption at room temperature under dynamic conditions is also consistent with the presence of metallic cobalt. It has been shown by Reuel and Bartholomew[40] that very little hydrogen is irreversibly adsorbed by supported cobalt metal at room temperature. Cobalt metal supported on aluminum oxide reversibly adsorbs H_2 at 25°C; however, no evidence for reversible adsorption is seen on the NaY supported cobalt. The nature of the support may be important in determining hydrogen adsorption.

X-ray photoelection spectroscopy data is consistent with adsorption of $Co_2(CO)_8$ yielding an initially homogeneous distribution of the metal on the zeolite and that this method can be used to reproducibly generate well dispersed materials. The lack of observable signal for cobalt or cobalt oxide in the X-ray powder diffraction pattern is also consistent with a disperse non-crystalline metal on the support. This evidence suggests that crystalline aggregates greater than 50 Å are not present on the zeolite. Results from the SEM experiments are also consistent

with this observation in that evidence for cobalt aggregates greater than 50 Å were not observed.

Results from the Fischer-Tropsch synthesis conducted in the batch reactor indicate that the catalysts are inactive below 200°C and must undergo thermal decomposition prior to catalysis. Generation of a catalytic species directly from the supported cobalt carbonyl is not possible at 200°C. Thus the irreversible loss of CO during thermal decomposition appears to be essential for generating an active catalyst. It is likely that cobalt carbonyls are stabilized at high CO pressures and do not decompose in situ. When NaX is used as the support, an active catalyst is not generated. This may be due to degradation of the zeolite structure during thermal treatment. Octane slurries of the catalyst were also found to be inactive. The octane may prevent or inhibit diffusion of synthesis gas to the active sites.

The product distribution appears to be dependent on the weight percent loading of cobalt. Chain growth appears to be enhanced at higher metal loadings. Thus sites responsible for chain growth are more concentrated on the 2.0-2.5 weight % catalyst than on the 1.0-1.5 weight % catalyst.

In a batch reactor the catalyst deactivates after a 16 hour run. Heavy products adhering strongly to the zeolite which are removed by extraction may account for blocking active sites and deactivation of the catalyst. Another possibility may be oxidation of the cobalt by water formed during the Fischer-Tropsch process which may initiate hydronium ion formation on the zeolite surface. The catalysts, in fact, are blue after all batch reactions which is consistent with oxidation of the

cobalt. Activity in the batch process is highest during the first two hours of the run. Deactivation must begin after this point resulting in a slower rate of product formation as seen from Figure 5.6.

Alkali salts added to the catalyst by dry methods were not found to modify the activity of the catalyst. This may suggest that active sites do not lie on the surface but exist further into the zeolitic crystallites. The selectivity of the catalyst for small, linear hydrocarbons is also consistent with this interpretation.

When the Fischer-Tropsch process was conducted in the flow system, selectivity for small hydrocarbons C_1-C_4, was observed. The greater selectivity in the flow system can probably be accounted for by the lower contact time of the reactants with the catalyst. The enhanced lifetime of the catalyst may be connected with the shorter contact time. Less formation of heavy products and the removal of water from the catalyst may aid in lengthening the life of the catalyst in the flow system.

An induction period for production of all hydrocarbons is observed in the flow reactor. This is shortest for methane (2 h) and longest for butane production (over 30 h). The induction period observed may be related to a migration process or site reformation process associated with the active catalyst. A decline in activity for CH_4 production is observed as the formation of heavier products begins. This may be due to conversion of methanation sites to sites that favor chain growth as the run proceeds. Selective poisoning of the methanation sites may also account for the decline in CH_4 production with time.

Cobalt faujasites generated from cobalt carbonyls are different in some important aspects from previously reported materials. A high selectivity for alkenes and especially propylene is reported for cadmuim reduced cobalt zeolites. The nitrosyl complex $Co(CO)_3NO$ also leads to a supported catalyst which shows high alkene production.[84] The nitrosyl also shows extremely high activity for formation of light hydrocarbons. The cobalt faujasites reported here show lower conversions and turnover numbers than the nitrosyl materials. It has been postulated that activity for Fischer-Tropsch synthesis over cobalt catalysts is inversely proportional to the particle size of the metal.[85] The low activity of the materials generated from $Co_2(CO)_8$ may be due to the presence of extremely small cobalt particles, which by comparison of the catalytic activity the cobalt/zeolite samples used in this work to those prepared by other investigators [40,41,96] may be on the order of 25 Å in diameter or less.

CHAPTER VI.

CONCLUSIONS

The adsorption of $Co_2(CO)_8$ on faujasitic zeolites is a complex process as indicated by in situ IR spectroscopy and carbon monoxide evolution. The major products observed to form are $Co_4(CO)_{12}$ and $Co(CO)_4^-$ resulting from condensation and disproportionation of the cobalt carbonyl dimer, respectively. Disproportionation of the supported cobalt carbonyl moieties can be further induced by the addition of phosphines and oxygen-containing ligands. Cobalt deposition from solution occurs mainly within the pores and cages of the zeolite structure. The cobalt adsorbed on the zeolite by this process retains a low oxidation state without the necessity of induced reduction of the metal.

Preliminary studies with $Co_2(CO)_8$ adsorbed on Y-type zeolites revealed that the carbonyl containing species were not strongly chemisorbed on the support and measures were needed to prevent leaching of the metal if heterogeneous solution phase catalysis was to be conducted. Two methods have been used to stabilize cobalt on a zeolite support, namely formation of ionic cobalt complexes via addition of reagents which induce disproportionation of supported cobalt carbonyl moieties and thermal decarbonylation of carbonyl species thus generating cobalt metal on the faujasite. The first method has been applied in designing an active catalyst for the carbonylation of methanol. A catalyst which is active for the Fischer-Tropsch synthesis is generated using the second method of stabilization.

The material formed by the first method is an active methanol carbonylation catalyst. The active species may form via the oxidative addition of CH_3I to $Co(CO)_4^-$ generating a species similar to the catalyst proposed in the mechanism proposed for rhodium-based system. The zeolite supported cobalt catalyst exhibits good selectivity for the production of methyl acetate under relatively mild conditions. The cobalt catalyst displays significant differences from the rhodium based systems with regard to activity and product formation. Formation of acetaldehyde dimethyl acetal is observed when the supported cobalt catalyst is employed with a high partial pressure of hydrogen as well as production of methyl acetate in methanol carbonylation. The supported cobalt catalyst exhibits significant sensitivity to the partial pressure of hydrogen and the temperature employed during the carbonylation reaction. The heterogeneous catalyst exhibits greater activity than $Co_2(CO)_8$ for the reaction carried out in a homogeneous fashion. Some leaching of cobalt from the zeolite occurs during the reaction though the leached metal does not show activity for the carbonylation. A disadvantageous of the cobalt carbonyl/zeolite catalyst is deactivation and short lifetime which probably results by oxidation of the active species.

Thermal decomposition of cobalt carbonyl on NaY produces a material containing cobalt in a low oxidation state active in catalyzing the Fischer-Tropsch synthesis of hydrocarbons. Gas evolution and gas adsorption experiments revealed that this technique yields highly disperse cobalt metal in a reproducible manner. The supported cobalt material is selective in forming linear hydrocarbons and the product

distribution does not strictly adhere to the Schultz-Flory pattern. The propensity toward chain growth is sensitive to the metal loading and is enhanced at the higher metal loadings studied. Reagents such as alkali halide salts added to the surface of the catalyst do not significantly alter the activity of the catalyst suggesting that active sites reside within the pores and cages of the zeolite. The life of the catalyst can be maximized by conducting the F-T reaction in a flow system relative to a batch process. Use of a differential reactor also increases the selectivity for short-chain hydrocarbons due at least in part to a lower contact time of the reactants with the catalyst.

REFERENCES

1. Adkins, H.; Krsek, G. J. Am. Chem. Soc. **1948**, 70, 343.

2. Evans, D.; Osborn, J. A.; Wilkinson, G. J. Chem. Soc. A **1968**, 133.

3. Yamanis, J.; Lien, K. C.; Caracotsios, M.; Powers, M. E. Chem. Eng. Comm. **1981**, 11, 355.

4. Herron, N.; Stucky, G. D.; Tolman, C. A. Inorg. Chem. Acta. **1985**, 100, 135.

5. Breck, D. W. "Zeolite Molecular Sieves"; Wiley-Interscience: New York, 1974.

6. Derouane, E. G. Zeolites: Science and Technology; F. R. Ribeiro, A. E. Rodriques, L. D. Rollman, C. Naccache, Eds.; Martinus Nijhoff: The Hague **1984**.

7. Howe, R. F. "Tailored Metal Catalysts"; Y. Iwasawa, Ed. D. Reidel Publishing Company: Dordrecht, Holland, 1986.

8. Forster, D. "Advances in Organometallic Chemsitry"; vol. 17, p. 255, F.G.A. Stone and R. West eds. Academic Press: New York, San Francisco, London, 1979.

9. von Kutepow, N.; Hinnele, W.; Hohenschutz, H. Chem. Ing. Tech. **1965**, 37, 383.

10. Hohenschutz, H.; von Kutepow, N.; Himmele, W. Hydrocarbon Process **1966**, 45, 141.

11. Paulik, F. E.; Roth, J. F. Chem. Commun. **1968**, 1578.

12. Roth, J. F.; Craddock, J. H.; Hershman, A.; Paulik, F. E. Chem. Technol., **1971**, 600.

13. Falbe, J. "Carbon Monoxide in Organic Synthesis"; Springer-Verlag Berlin and New York, 1970.

14. Forster, D. Inorg. Chem. **1969**, 8, 2556.

15. James, B. R.; Rempel, G. L. Chem. Commun. **1967**, 158.

16. Wender, I. Catal. Rev. - Sci. Eng. **1976**, 14, 97.

17. Schultz, R. G.; Montgomery, P. D. J. Catal. **1969**, 13, 105 .

18. Robinson, K. K.; Hershman, A.; Craddock, J. H.; Roth, J. F. J. Catal. 1972, 27, 389 .

19. Jarrell, M. S.; Gates, B. C. J. Catal. 1975, 40, 255.

20. Webber, K. M.; Gates, B. C.; Drenth, W. J. Mol. Catal. 1977, 3, 1.

21. Masters, C; Adv. Organometallic Chem. F.G.A. Stone, R. West, Eds. Academic Press, New York 1979, 17, 61.

22. Cochran, N. P. Sci. Am. 1976, 234, 24.

23. Sabatier, P.; Senderens, J. B. Hebd. Seances. Acad. Sci. 1902, 134, 514.

24. Badische and Soda Fabrik, German Patents 293, 787 (1913).

25. Fischer, F.; Tropsch, H. Brennst. Chem. 1923, 4, 276.

26. Fischer, F.; Tropsch, H. German Patent 484, 337 (1925).

27. Pichler, H. H.; Hector, A. Kirk-Othmer Encycl. Chem. Technol. 2nd. Ed., 1969, 4, 446.

28. Frohning, C. D.; Cornels, B. Hydrocarbon Process. 1976, 53, 143.

29. Schulz, G. V. Z. Phys. Chem. B 1935, 30, 379.

30. Flory, P. J. J. Am. Chem. Soc. 1936, 58, 1877.

31. Jacobs, P. A.; Van Wouwe, D. J. Mol. Catal. 1982, 17, 145.

32. Fischer, F.; Tropsch, H. Brennst. Chem. 1926, 7, 97.

33. Craxford, S. R.; Rideal, E. K. J. Chem. Soc. 1939, 1604.

34. Storch, H. H.; Golumbic, N.; Anderson, R. B. "The Fischer Tropsch and Related Synthesis," Wiley, New York, 1951.

35. Pichler, H.; Schulz, H. Chem. Ing. Tech. 1970, 42, 1162.

36. Burwell, R. L., Jr.; Brenner, A. J. J. Mol. Catal. 1975, 1, 77.

37. Brenner, A. Ph.D Thesis, Northwestern University, 1975.

38. Chini, P.; Heaton, B. T. Top. Curr. Chem. 1977, 71, 53.

39. Bartholomew, C. H.; Pannell, R. B. J. Catal. 1980, 65, 390.

40. Reuel, R. C.; Bartholomew, C. H. J. Catal. 1984, 85, 63.

41. Ballivet-Tkatchenki, D.; Coudurier, G.; Duc-Chau, N. "Metal Microstructures in Zeolites", P. a. Jacobs, et.al. Eds., Elsevier 1982, 123.

42. Lisitayn, A. S.; Golovin, A. V.; Kuznetoov, V. L.; Yermakov, Yu I. J. Catal. 1985, 95, 527.

43. Schneider, R.; Howe, R. F.; Watters, K. L. Inorg. Chem. 1984, 23, 4600.

44. Schneider, R.; Howe, R. F.; Watters, K. L. Inorg. Chem. 1984, 23, 4593.

45. Alves, R.; Ballivet-Tkatchenko, D.; Coudurier, G.; Duc Chou, N.; Santia, M.; B. S. Chim. Fr. 1985, 3, 386.

46. Schneider, R. L.; Howe, R. F.; Watters, K. L. J. Catal. 1983, 79, 298.

47. Tessier-Younge, C.; Correa, F.; Pioch, D.; Burwell, R. L., Jr.; Shriver, D. F. Organometallics 1983, 2, 898.

48. Hicks, R. F.; Keller, C. S.; Savatsky, F. J.; Hecker, W. C.; Bell, A. T. J. Catal. 1971, 71, 216.

49. Yates, J. T., Jr.; Duncan, T. M.; Vaughan, R. W. J. Chem. Phsy. 1979, 71, 2908.

50. Rode, E.; Davis, M. E.; Hanson, B. E. J. Catal. 1985, 96, 574.

51. Connaway, M. C.; Hanson, B. E. Inorg. Chem. 1986, 25, 1445.

52. Hanson, B. E.; Bergmeister, J. J.; Petty, J. T.; Connaway, M. C. Inorg. Chem. 1986, 25, 3089.

53. Hanson, B. E.; Wagner, G. W.; Davis, R.; Motell, E. Inorg. Chem. 1984, 23, 385.

54. Toscano, P. J.; Marks, T. J. J. Am. Chem. Soc. 1985, 107, 653.

55. McKenna, W. P.; Eyring, E. M. J. Mol. Catal. 1985, 29, 363.

56. Falconer, J. L.; Schwartz, J. A. Catal. Rev. Sci. Eng. 1983, 25, 141.

57. Beringhelli, T.; Gervasimi, A.; Morazzoni, F.; Strumbolo, D. J. Chem. Soc., Faraday Trans. 1, 1984, 80, 1479.

58. He, M. Y.; Xeong, G.; Toscano, P. J.; Burwell, R. L., Jr.; Marks, T. J. J. Am. Chem. Soc. 1985, 107, 641.

59. Ceriotti, A.; Martinengo, S.; Zanderighi, L. J. Chem. Soc., Faraday Trans. 1, **1984**, 80, 1605.

60. Vanhove, D.; Zhuyoung, Z.; Makanlo, L.; Blanchard, M. App. Catal. **1984**, 9, 327.

61. Absi-Halabi, M.; Atwood, J. D.; Forbus, N. P.; Brown, T. L. J. Am. Chem. Soc. **1980**, 102, 6248.

62. Darensbourg, D. J.; Incorvia, M. J. Inorg. Chem. **1981**, 20, 1911.

63. Nichols, D. "Comprehensive Inorganic Chemistry". Barlar, J. C., Jr., Emeleus, H. J., Nyholm, R., Frotman-Dickenson, A. F., Eds.; Pergammon: Oxford, England., 1973; Vol. 3, Chapter 41, p. 1062.

64. Windhorst, K. A.; Lundsford, J. H. J. Am. Chem. Soc. **1975**, 97, 1407.

65. Chester, A. W.; Chu, Y. F.; Dessau, R. M.; Kerr, G. T.; Kresege, C. T. J. Chem. Soc., Chem. Commun. **1985**, 289.

66. Huang, T. N.; Schwartz, J. J. Mol. Catal. **1984**, 22, 389.

67. Huang, T. N.; Schwartz, J. J. Mol. Catal. **1982**, 104, 524.

68. Praliaud, H.; Coudurier, G.; BenTaarit, Y. J. Chem. Soc. Faraday Trans. I, **1978**, 74, 3000.

69. Braterman, P. S. "Metal Carbonyl Spectra" P. M. Maitlis, F.G.A. Stone, R. West Eds. Academic Press: London, New York San Franciso, 1975.

70. Kristoff, J. S.; Shriver, D. F. Inorg. Chem. **1974**, 13, 499.

71. Alich, A.; Nelson, N. J.; Strope, D.; Shriver, D. F. Inorg. Chem. **1972**, 11, 2976.

72. Cotton, F. A. Inorg. Chem. **1966**, 5, 1083.

73. Yashima, T.; Onikasa, Y.; Takahashi, N.; Hara, N. J. Catal. **1979**, 59, 53.

74. Takahashi, N.; Orikasa, Y.; Yashima, T. J. Catal. **1979**, 59, 61.

75. Huang, T. N.; Schwartz, J. J. Mol. Catal. **1984**, 22, 389.

76. Jarrell, M. S.; Gates, B. C. J. Catal. **1975**, 40, 255.

77. Schulz, R. G.; Montgomery, P. D. J. Catal. **1969**, 13, 105.

78. Krzywicki, A.; Pannetier, G. Bull. Soc. Chim. Fr. **1975**, 1093.

79. Christensen, B.; Scurrel, M. S. J. Chem. Soc. Faraday Trans. I, 1977, 2036.

80. Gelen, P.; Lefelvre, F.; Elleuch, B.; Naccache, C.; Ben Taasit, Y. A.C.S Symp. Ser. 1983, 218, 455.

81. Gates, B. C. J. Catal. 1975, 40, 255.

82. Huang, H.; Schwartz, J.; Kitajima, N. J. Mol. Catal. 1984, 22, 389.

83. Frankel, D.; Gates, B.C. J. Am. Chem. Soc. 1980, 102, 2478.

84. Ungar, R. K.; Baird, M. C. J. Chem. Soc., Chem. Comm. 1986, 643.

85. Nozar, L. F.; Ozin, G. A.; Huguer, F.; Godber, J.; Rancourt, D. Angew. Chem., Int. Ed. Eng. 1983, 22, 624.

86. Mantovani, E.; Palladin, N.; Zanoli, A. J. Mol. Catal. 1977, 3, 285.

87. Edgell, W. F.; Lyford, J., IV Inorg. Chem. 1970, 9, 1932.

88. Angell, C. L.; Schaffer, P. C. J. Phys. Chem., 1965, 69, 3463.

89. Ward, J. W. J. Catal. 1968, 10, 34.

90. Wender, I.; Steinberg, H. W.; Orchin, M. J. J. Am. Chem. Soc. 1952 74, 1216.

91. Bor, G. Spectrochim. Acta. 1963, 19, 2065.

92. Noack, K. Spectrochim. Acta. 1963, 19, 1925.

93. Purcell, K. F.; Kotz, J. C. "Inorganic Chemistry": W. B. Saunders Co.: Philadelphia, PA., 1977. p. 858.

94. Mirbach, M. F.; Mirbach, J. J. Mol. Catal. 1985, 32, 59.

95. Mirbach, M. F.; Mirbach, J. J. Mol. Catal. 1985, 33, 23.

96. Anderson, J. R.; Mainwaring, D. E. J. Catal. 1974, 35, 162.

97. Wagner, C. D.; Riggs, W. M.; Davis, L. E.; Moulden, J. F. "Handbook of X-ray Photoelectron Spectroscopy" G. E. Muilenberg Ed. Perkin-Elmer Corp. Eden Prarie, Minnesota, 1979.

APPENDIX I.

GAS FLOW SYSTEM

The gas flow system used for catalyst preparation, gas evolution quantification and pulsed gas adsorption experiments is illustrated in Figure A.1 and is similar in design to that of Brenner and Burwell's apparatus.[36,37] The gas line was constructed of 1/4" soft copper tubing with Swagelok fittings at all junctions. All 2- and 3-way valves, bellows valves and unions were obtained from Dibert Valve and Supply Company. Gases (1) which were used on line were hydrogen (a) (99.995%), helium (b) (99.999%), carbon monoxide (c) (99.99%), oxygen (e) or another gas of choice (d). The gas used was conducted through a purification tube (2) (with exception of oxygen) to remove oxygen and water which contained 20 weight % MnO_2 supported on silica gel. Flow meters (3) and a second purification tube (4) followed. The next piece of equipment consisted of a gas sampling valve (5) used in quanification of evolved gas and pulse gas adsorption followed by a hydrator (6) containing distilled water. The glass vessel used for catalyst preparation described in Chapter 2 was then connected in line at position (7) followed by a glass condenser (8) held at -196°C used for trapping solvents removed from the catalyst. Two traps followed, the first contained silica gel (Davisil 62 from Davison Chemical) (9) and the second contained 60 mesh 5A molecular sieve, both of which had been dried at 200°C in vacuum. The SiO_2 trap held at -196°C was used to trap condensable gases such as CO and O_2. The 5A molecular sieve trap held at -196°C could be used to capture H_2. Position (11) contained a quartz

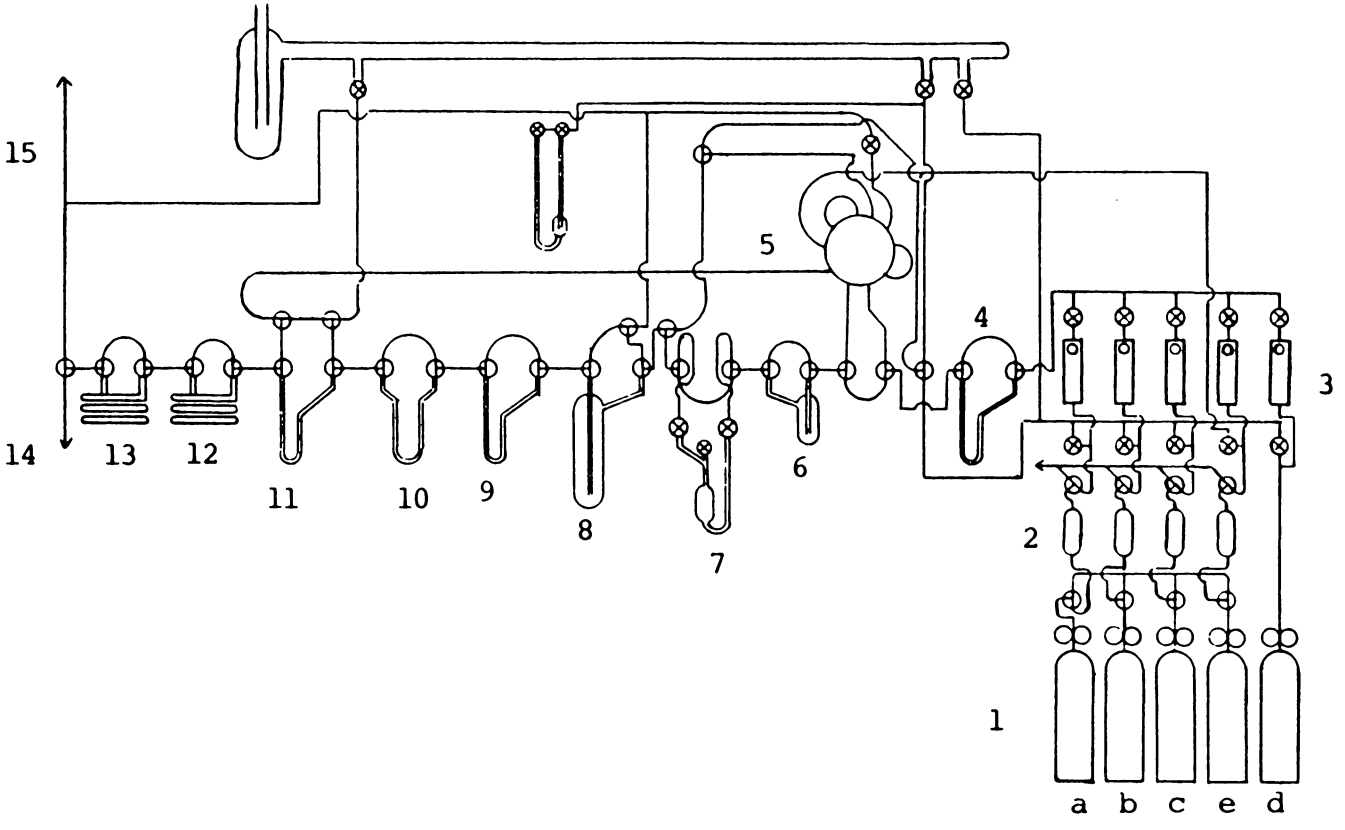

Figure A.1. Schematic representations of gas flow system.

tube of CuO which when heated to 500°C was used to convert H_2 to H_2O which gives a greater response on the thermal conductivity detector. Two gas chromatography columns occupied the following two positions. The first was a 6 ft. column containing 60 mesh 5A molecular sieve (12) used to separate condensable gases and the second was a 6 ft column containing 60 mesh 13X molecular sieve (13) used to separate hydrocarbons. Each column was activated at 150°C for 2 hours in flowing helium prior to use. Separations were carried out at ambient temperature. The gas flow was then conducted to either a Gow Mac thermal conductivity detector (14) for gas analysis or vented to a fume hood (15).

The vita has been removed from the scanned document